Trace element and isotope measurement on artificially precipitated calcium carbonate

Dissertation

zur Erlangung des Doktorgrades

Dr. rer. nat.

der Mathematisch-Naturwissenschaftlichen Fakultät

der Christian-Albrechts-Universität zu Kiel

vorgelegt von

Mahmoud Alkhatib

Master-Chem., Al-Quds University-Palestine

Kiel 2016

1. Gutachter und Betreuer: Prof. Dr. Anton Eisenhauer

2. Gutachter: Prof. Dr. Klaus Wallmann

Eingereicht am: 13.07.2016

Datum der Disputation: 12.07.2016

Zum Druck genehmigt: 23.05.2016

Der Dekan

I certify that I have created this dissertation independently and only with the help of sources and aids stated. I also assure you that the content of this document in present or modified form was not submitted to any other department or institution under an examination procedure. I further certify that this work has been developed in compliance with the rules of good scientific practice of the “Deutsche Forschungsgemeinschaft”.

Kiel, 23 May 2016

Mahmoud Alkhatib

Contents

Abstract

Trace elements incorporation of certain trace elements like strontium (Sr) and magnesium (Mg) among others and their isotope composition in different $CaCO_3$ polymorphs (e.g. calcite and aragonite) as archives provide valuable for proxy information, that can be used as important tools for reconstructing the paleo- environmental conditions of the oceans throughout time. However, data on Sr incorporation into inorganic precipitated $CaCO_3$ (calcite and aragonite), Mg incorporation into aragonite and Sr isotopic fractionation during minerals formation are still very rare. In addition, literature values available concerning Ca isotopic fractionation between calcite and aqueous solution are discrepant to a certain extent, while on the other hand the data available concerning Ca isotopic fractionation between inorganic precipitated aragonite and aqueous solution are also scarce. In order to overcome this lag of information in this study calcite and aragonite were precipitated at three different temperatures (12.5, 25.0 and 37.5±0.2 °C), different precipitation rates (R*) and solution composition by diffusing NH_3 and CO_2 gases into aqueous solutions containing trace elements and NH_3 ions. For the kinetic study we used the initial rate method to solve the rate equations (rate law) with R* values in the range between 2.5 to 4.5 $\mu mol/m^2 \cdot h$. We find that both calcite and aragonite have exactly the same order of reaction only differing in their activation energy (114 kJ/mol for calcite and 149 kJ/mol for aragonite) and rate constants at 25 °C ($80.6*10^{-4}$ for calcite and $17.3*10^{-4}$ $mM^{-2} \cdot h^{-1}$ for aragonite). The order of reaction with respect to Ca^{2+} ions is ≈ 1 and temperature dependent, while the order of reaction with respect to HCO_3^- ions is temperature dependent decreasing from 3 via 2 to 1 as temperature increases from 12.5 via 25.0 to 37.5°C, respectively. Calcium isotope fractionation for both calcite and aragonite ($\Delta^{44/40}Ca$) was found to be R* and temperature dependent. For 12.5 and 25.0 °C we observe a general increase of the $\Delta^{44/40}Ca$ values as a function of R*, whereas at 37.5 °C decreasing $\Delta^{44/40}Ca$ values are observed relative to increasing R*. It is suggested that the temperature triggered change from a Ca^{2+}-NH_3-aquacomplex covalent controlled bonding to a Ca^{2+}-H_2O-aquacomplex van-der-Waals controlled bonding caused the change in sign of the R* - $\Delta^{44/40}Ca$ slope due to the switch of an equilibrium type of isotope fractionation related to the covalent bonding during lower temperatures to a kinetic type of isotope fractionation at higher temperatures. This behavior of Ca is in sharp contrast to the Sr isotopes which do not show any change of its fractionation behaviour as a function of complexation in the liquid phase. For both polymorphs of $CaCO_3$ as a function of increasing R* the $\Delta^{88/86}Sr$-values become more negative

and as temperature increases the $\Delta^{88/86}$Sr values also increase at constant rate. However effect oft R* on the $\Delta^{88/86}$Sr values is more significant in calcite than in aragonite. Magnesium incorporated into aragonite (expressed as D_{Mg}= [Mg/Ca] $_{aragonite}$/ [Mg/Ca] $_{solution}$) increases with decreasing temperature and also increases with increasing R* and as temperature increases the R* effect decreases. Later behavior is opposite to Mg in calcite (as temperature increases D_{Mg} also increases) as already known from earlier studies. Strontium incorporated into both calcite and aragonite (expressed as D_{Sr}= [Sr/Ca] $_{solid}$/ [Sr/Ca] $_{solution}$) was found to be R* and temperature dependent. Rate effect is more dominant over temperature effect in calcite, while on the other hand temperature effect is more dominant over rate effect in the case of aragonite. In calcite D_{Sr} increases with increasing R* and decreasing temperature. In aragonite also D_{Sr} increases with decreasing temperature. However concerning R* it responds differently: at 37.5°C D_{Sr} as R* increases D_{Sr} values increase, but decrease at 12.5°C. At 25.0°C, both behaviors are detected depending on the molar [Sr]/[Ca] ratio of the reacting solution (0.005 or 0.01). In the frame of a qualitative model to explain our trace element and isotope observations we speculate that increasing Mg^{2+} -concentrations control the material flux back (R^*_{detach}) from the crystal to the solution to a large extend. As a consequence R* values for aragonite tend to be lower than for calcite as observed from our data. Hence, Sr incorporation into aragonite is affected as function of temperature to a higher degree when compared to the R* effect. This is also reflect on the $\Delta^{88/86}$Sr values and decreasing the R* effect when compared to the temperature effect. Moreover concerning Ca isotope fractionation, the switch of direction in Ca isotope fractionation above ~25°C may be either due to the Mg^{2+} blocking effect or due to the switch of complexation from NH_3 at and below 25 °C to H_2O complexation at 37.5 °C. Plotting D_{Sr} versus $\Delta^{88/86}$Sr may be used as a proxy to reconstruct precipitation rates of calcite and of precipitation temperature of inorganic aragonite. Latter correlation may also have important implications for the verification of $CaCO_3$ diagenesis.

Zusammenfassung

Durch Einlagerung von Spurenelementen und die isotopische Zusammensetzung bieten die polymorphen Formen (Calcit und Aragonit) von Calciumcarbonat ($CaCO_3$) wertvolle Archive für die Anwendung von Paleoproxies zur Rekonstruktion der Umweltbedingungen der Ozeane. Experimentelle Daten über die Einlagerung von Sr in anorganisch ausgefälltes $CaCO_3$, die Einlagerung von Magnesium in Aragonit und die isotopische Fraktionierung von Sr während der Ausbildung von Mineralen sind immer noch sehr selten. Auch zeigen die verfügbaren Literaturwerte in Bezug auf die isotopische Fraktionierung zwischen festem Calcit und der wässrigen Lösung eine gewisse Diskrepanz, während die Datenlage in Bezug auf die Isotopenfraktionierung bei der Präzipitation von anorganischem Aragonit ebenfalls sehr knapp bemessen ist. Im Laufe dieser Studie wurden Präzipitationsexperimente von Calcit und Aragonit unter verschiedenen Temperaturen (12.5, 25.0 und 37.5±0.2 °C), Präzipitationsraten (R*) und der Variation der Zusammensetzung der Lösungen durch die Diffusion von unterschiedlichen Mengen von gasförmigem NH_3 und CO_2. Für die kinetischen Untersuchungen wurde die Methode der Anfangsgeschwindigkeit verwendet, um die verschiedenen Ratengleichungen zu lösen. Die Bildung von Calcit und Aragonit zeigte dieselbe Reaktionsordnung und unterschied sich lediglich in Aktivierungsenergie und Geschwindigkeitskonstante. In Bezug auf die Konzentration der Ca^{2+} Ionen war die Reaktionsordnung ≈ 1 und temperaturabhängig, während die Reaktionsordnung in Bezug auf die Konzentration der HCO_3^- Ionen sich als ebenfalls temperaturabhängig zeigte, allerdings mit steigender Temperatur (12.5 - 37.5°C) graduell von 3 nach 1 abnahm. Die Aktivierungsenergie für die Präzipitation von Calcit betrug 114 und für Aragonit 149 kJ/Mol. Die Isotopenfraktionierung für sowohl Calcit, als auch für Aragonit ($\Delta^{44/40}Ca$) war abhängig von R* und Temperatur. Während sich bei den niedrigeren Temperaturen (12.5 und 25.0 °C) eine positive Korrelation zwischen zwischen $\Delta^{44/40}Ca$ und R* zeigte, war die Korrelation bei 37.5 °C signifikant negative, abhängig von der Art der molekularen Wechselwirkung zwischen den Ca^{2+} Ionen und den verschiedenen anderen Spezies in wässriger Lösung. Der Wechsel zwischen positiver und negativer R* - $\Delta^{44/40}Ca$ - Korrelation lässt sich durch einen temperaturabhängigen Wechsel zwischen einem kovalent gebundenem Ca^{2+}-NH_3-aquacomplex zu einem van-der-Waals gebundenem Ca^{2+}-H_2O-aquacomplex erklären (Wechsel zwischen aufgrund der kovalenten Bindungen thermodynamisch kontrollierter zu kinetisch kontrollierter Isotopenfraktionierung unter höheren Temperaturen). Dies steht im

Kontrast zur Fraktionierung der Sr Isotope, die keinerlei Änderung im Fraktionierungsverhalten als Funktion der Komplexierung innerhalb der flüssigen Phase zeigt. Für beide untersuchten polymorphen Formen von $CaCO_3$ zeigte $\Delta^{88/86}Sr$ eine negative Korrelation zu R* und eine positive Korrelation zur Temperatur. Der Effekt von R* auf $\Delta^{88/86}Sr$ war signifikanter bei der Präzipitation von Calcit ans bei Aragonit. Die Einlagerung von Mg in Aragonit (D_{Mg}= [Mg/Ca] $_{aragonite}$/ [Mg/Ca] $_{solution}$) war negativ korreliert zur Temperatur und positiv korreliert zur R*, wobei der Effekt von R* mit steigender Temperatur abnahm. Dieses Verhalten steht im genauen Gegensatz zur Einlagerung von Mg in Calcit (positive Korrelation zwischen D_{Mg} und Temperatur). Auch ist der Einfluss von R* dominanter bei der Formation von Calcit im Gegensatz zu Aragonit. Die Einlagerung von Strontium (D_{Sr}) in Calcit wiederum ist positive korreliert zu R* und negativ zur Temperatur, während in Aragonit D_{Sr} ebenfalls mit steigender Temperatur abnimmt. In Bezug auf die Präzipitation verhält sich R* unterschiedlich: 37.5 °C – positive Korrelation zwischen D_{Sr} und R*; 12.5 °C negative Korrelation zwischen R* und D_{Sr}. Bei einer Temperatur von 25°C wurden beide Phänomene beobachtet in Abhängigkeit des molaren [Sr]/[Ca] Verhältnisses der Reaktionslösung (0.005 oder 0.01). Vermutlich wird der Rückfluss von Materie vom Kristall zur Lösung (R^*_{detach}) zu einem großen Teil von der Mg^{2+} - Konzentration kontrolliert. Konsequenterweise ist R* typischerweise niedriger für Aragonit als für Calcit und Sr Einlagerung in Aragonit wird stärker beeinflusst durch Temperatur als durch R*. Dieser Effekt würde sich auch in Bezug auf $\Delta^{88/86}Sr$ wiederspiegeln und den Einfluss von R* im Verhältnis zum Einfluss der Temperatur vermindern. Ferne lässt sich der Wechsel in Bezug auf die Richtung der Ca Isotopenfraktionierung über 25°C entweder durch den blockierenden Effekt der Mg^{2+} Ionen oder zwischen NH_3 und H_2O Komplexierung erklären. Diese Daten zeigen, dass die parallele Bestimmung von D_{Sr} und $\Delta^{88/86}Sr$ sich als wertvoller Proxy erweisen kann zur Rekonstruktion von Präzipitationsraten von Calcit (sowohl anorganischem als auch biogenem) und zur Rekonstruktion der Temperatur während der Bildung von Aragonit. Weiter könnte letztere Korrelation als wichtiger Nachweis der Diagenese von $CaCO_3$ verwendet werden.

Chapter 1

Introduction

Calcium carbonate ($CaCO_3$) is one of the most abundant and reactive mineral in the natural environment and is among others a dominant component of marine sediments (Morse and Mackenzie (1990)). For this reason, precipitation, crystallization and dissolution of $CaCO_3$ in aqueous solution has attracted the interest of many investigators in a wide variety of marine disciplines like geochemistry paleo-oceanography, sedimentology and marine biology (e.g. Leeder (1982) Crowley (1983) Farrell and Prell (1989) Milliman (1993) Enmar et al. (2000)).

Living calcifying organisms (uni- and multicellular especially in the photic zone) are the main source of marine $CaCO_3$, while inorganic precipitation is the minor one (Morse and Mackenzie (1990)). Calcium carbonate exists in crystalline form (the most abundant and thermodynamic stable) and amorphous phases (Brecevic and Nielsen (1989)). In general the solubility of all pure carbonates decreases with increasing temperature and is ordered: amorphous calcium carbonate (ACC) > vaterite > aragonite > calcite (Brecevic and Nielsen (1989)). At 25 °C the solubility product ksp equals $3.3*10^{-9}$, $4.6*10^{-9}$ and $1.2*10^{-8}$ for calcite, aragonite and vaterite, respectively (Plummer and Busenberg (1982), Radha et al. (2010)). Among all $CaCO_3$ polymorphs Calcite is the most abundant and thermodynamically most stable one and the least soluble polymorph (Plummer and Busenberg (1982)). The crystalline structure of calcite is hexagonal, Point Group: 3 2/m. Density = 2.71 g/cm^3 Anthony et al. (2003). In contrast Mg-calcite is more soluble than pure calcite, as content of Mg increases in calcite solubility also increases (Morse and Mackenzie (1990)). At ~20 mol% $MgCO_3$ ksp for both biogenic and inorganic magnesium calcite ~ $8.3* 10^{-9}$ Davis et al. (2000).

In the present day ocean inorganic precipitated Mg-free calcite in the marine environment is not observed due to the inhibition effect of Mg ions (c.f. Morse et al. (2007)). Inorganic Mg-calcite consists as a very minor component of total sedimentary carbonate minerals and may occur in voids found in biogenic carbonates (Morse and Mackenzie (1990). In contrast to the inorganic marine carbonates the majority of sedimentary calcites are the skeletal remains of

coccolithophores and foraminifera (Morse et al. (2007)) which are composed of low-Mg calcite (>99% $CaCO_3$).

The second abundant $CaCO_3$ polymorph is aragonite. It is less stable and more soluble than calcite (Plummer and Busenberg (1982)). The crystalline structure of aragonite is orthorhombic and pseudo hexagonal. The point Group is: 2/m 2/m 2/m and its density correspond to 2.93 g/cm^3 (Anthony et al. (2003)). Aragonite sediments are primarily produced by the disintegration of the skeletons of calcifying organisms, such as corals, echinoids, molluscs, pteropods and coralline algae (Morse and Mackenzie (1990)). In the present day ocean aragonite is the main constitute of the inorganic marine sediments (cements and ooids) in modern seawater ((c.f. Morse et al. (2007)). However, observations of ancient sediments indicate that at times in the past, when the Mg/Ca ratios was low, calcite was favourably precipitated over aragonite especially in cold waters (c.f. Morse et al. (1997)). It has been observed that time of favourable aragonite precipitation (aragonite seas) alternated with times of favourable calcite precipitation (calcite seas) as a function of the Mg/Ca ratio in seawater (Hardie (1996)). The cement mineralogy is also controlled by carbonate ion concentration (Given and Wilkison (1985)) and temperature (c.f. Chave (1954), Schlager and James (1978), Füchtbauer and Hardie (1976)). These authors also suggested that the general sequence of precipitation is from low-Mg via high-Mg calcite to aragonite as a function of both increasing temperature and carbonate ion concentrations.

Vaterite is metastable with respect to calcite and aragonite and limited to a minor biogenic occurrence (Morse et al. (2007)), as in fish otoliths, mollusc shells and human gallstones. It is less dense and more soluble than both calcite and aragonite. Vaterite is not easy to precipitate but in a recent study by Niedermayr et al. (2013) Vaterite was experimentally precipitated in the presence of poly aspartic acid.

Hydrated $CaCO_3$ phases (e.g., ikaite $CaCO_3 \cdot 6H_2O$) are usually found only in very low temperature but high-pressure environments. Ikaite is also crystalline but less dense (1.77 g/cm^3) than other polymorphs of $CaCO_3$ (Bischoff et al. 1992 and Marland 1975).

Amorphous calcium carbonate (ACC) is present in exoskeletons of crustaceans, ascidians and calcareous sponge (Lowenstam and Weiner (1989)). Certain proteins and Mg ions cooperate in the stabilization of thermodynamically and kinetically unstable ACC in vivo (Aizenberg et al. (1996)). When formed in vitro as a result of excessive supersaturation in the solution, ACC is rapidly transformed into calcite (Aizenberg et al. (2002)). However stabilization can be achieved

by adding special additives which inhibit the formation of nuclei of crystallization, e.g. hydroxy-containing molecules, certain proteins and some polymers as poly-(propylene imine) dendrimers (c.f. Aizenberg et al. (1996) and Aizenberg et al. (2002)).

Calcium carbonate minerals are not pure (c.f. Garrels and Christ, (1965)) rather contain a variety of trace elements mostly alkaline-earth elements like magnesium (Mg), Strontium (Sr), Barium (Ba), but also other elements like Lithium (Li), Boron (B), Cadmium (Cd), Uranium (U), Thorium (Th) and others (e.g. Ortega et al. (2005)). The enrichment of these trace elements in biogenic and inorganic $CaCO_3$ relative to Ca reflects certain environmental conditions (temperature, growth rate, pH, salinity and the composition of seawater) at their time of formation (e.g. Morse and Bender (1990), Lopez et al. (2009) and Tang et al. (2012)). In case of biogenic origin it also affected by the individual species dependent metabolism and calcification mechanism known as the "vital effect" (Weber and Woodhead (1970), Weber and Woodhead (1972), Elderfield et al. (1996) and Lea et al. (1999)). In this regards the trace element to calcium ratios of biogenic and inorganic $CaCO_3$ providing a valuable proxy information of oceanographic data, (e.g. Stoll et al. (2002), Gaetani and Cohen (2006) and Gaetani et al. (2011)). For example Mg enrichment in inorganic precipitated calcite is linearly increasing with temperature (Mucci (1987)) serving as a paleo-temperature proxy (c.f. Nürnberg et al. (1996), Dekens et al. (2002)) using mostly foraminifera as archive. Furthermore, Sr/Ca ratios are applied ad temperature proxy in corals (c.f. Beck et al. 1992). However, being thermodynamically less stable Sr/Ca based temperature reconstructions are less reliable due to diagenetic alterations and recrystallization to calcite (DeVilliers et al (1994)).

Environmental conditions and vital effects are not only affecting the trace elements to Ca ratios in biogenic and inorganic precipitated $CaCO_3$ but also the isotopic composition of different elements (e.g. Böhm et al. (2012) and Tang et al.(2008b)). Isotope analysis has a wide range of applications in many fields, as in forensic science (C, O, H, N and S isotope systems) (Benson et al. (2006)), in environmental science (e.g Cl isotopes) (Michener and Lathja (2007)), in chemical analysis (H, C and P isotope systems) (nuclear magnetic resonance spectroscopy), in industry (radioisotopes Am and Cf), in medicine (radioisotopes I, H and C) and in ecology (H, C, N and O) (Newsome et al. (2010)), as geographic proxy to determine the origin of food ((H,C, N,O and Sr isotope systems, Kellya et al. (2005)), in geochemistry (C, O, Ca, Sr, B and others isotope systems) geology (Sr isotope system), biogeochemistry (Hg isotope system) , paleoceanography

(the main parent-daughter pairs used are Rb–Sr, Th–U–Pb, Sm–Nd, Lu–Hf, and Re–Os, as summarized in Goldstein and Hermming (2003)). Isotope data from biogenic and inorganic $CaCO_3$ have been used as independent and as multi environmental proxies of calcification and precipitation processes. For instance, the analysis of the ratio of stable oxygen isotopes in calcium carbonate, secreted by organisms like foraminifera and buried in deep-sea sediments, has permitted the reconstruction of paleo-temperatures for the last 150 million years or so (Zeebe and Wolf-Gladrow (2003)). Oxygen-isotope fractionation in carbonates is not only temperature dependent but also affected by seawater salinity, pH and the change in the volume of polar and continental ice sheet McCrea (1950), Usdowski et al. (1991), Zeebe (1999), Brand et al. (2003), Zeebe and Wolf-Gladrow (2003) and Zeebe (2005). Boron isotopes have received much attention in chemical oceanography during the last few years, partly due to their use as a means of reconstructing paleo-pH Zeebe and Wolf-Gladrow (2003). Since different proxies are affected by different parameters, the application of multi-proxy data received more attention in the reconstruction of the paleo environmental conditions of $CaCO_3$ production (e.g Immenhauser et al. (2005)). Using calcium isotope ratios ($^{44}Ca/^{40}Ca$) in biogenic and inorganic calcite as a robust proxy for paleo-temperature or not is still under debate. According to Nägler et al. (2000) and Gussone et al. (2003), there is a clear inverse correlation between ($^{44}Ca/^{40}Ca$) fractionation and temperature in cultured foraminifera. In contrast, it was suggested by Sime et al. (2005) that temperature was not the controlling factor for Ca isotope fractionation of different foraminifera species from marine core top samples. Similar little is known about fractionation mechanisms of strontium isotopes ($^{88}Sr/^{86}Sr$) during mineral formation.

This study focus on the incorporation of Sr in $CaCO_3$ in combination with Ca and Sr isotope fractionation when inorganic calcite and aragonite are precipitated from the same solution. Calcium has six stable, naturally occurring isotopes: ^{40}Ca (96.941%), ^{42}Ca (0.647%), ^{43}Ca (0.135%),^{44}Ca (2.086%), ^{46}Ca (0.004%) and ^{48}Ca (0.187%) (Russell et al. (1978)). Strontium has four stable, naturally occurring isotopes: ^{84}Sr (0.56%), ^{86}Sr (9.86%), ^{87}Sr (7.0%) and ^{88}Sr (82.58%). It has a relative atomic mass of 87.62 (1). Only ^{87}Sr is radiogenic; it is produced by decay from the radioactive alkali metal ^{87}Rb, which has a half-life of 4.88×10^{10} years. Thus, there are two sources of ^{87}Sr in any material: primordial that formed during nucleosynthesis along with ^{84}Sr, ^{86}Sr and ^{88}Sr, as well as that formed by radioactive decay of ^{87}Rb (Koch (2007)).

The knowledge of Sr incorporation into inorganically precipitated $CaCO_3$ (calcite and aragonite), Mg incorporation into inorganic aragonite as function of both rate and temperature and Sr isotope fractionation during minerals formation are still very rare. Although there is information on the fractionation behaviour of Ca available still literature values are discrepant to a certain extent. For example in Lemarchand et al (2004) as R* increases $\Delta^{44/40}$Ca increases. Whereas opposite behaviour was obtained in Tang et al. (2008) as precipitation rate increases $\Delta^{44/40}$Ca decreases (Fig 1.1). In Lemarchand et al (2004) two main sets of solutions were prepared to produce calcite in an ammonium buffered solutions (NH_4/NH_3) at 21 (±1 °C). The first set was composed of 0.395 M NH_4Cl and 15 mM $CaCl_2$, while the second one was 0.395 M NH_4Cl and 150 mM $CaCl_2$. Calcite crystals were precipitated at different R* from these stirred and not stirred solutions in a sealed volume, when they were exposed to NH_3 and CO_2 gases which were produced by spontaneous decomposition of solid ammonium carbonate $(NH_4)_2CO_3$. In the Lemarchand et al (2004) study R* ($\mu mol/m^2 \cdot h$) was not empirically determined rather than estimated using an equation originally derived by Zuddas and Mucci (1994) for NaCl-$CaCl_2$ solutions at 25 °C.

In Tang et al. (2008a) calcite was precipitated at different temperatures and R* using aCO_2-diffusion technique originally used by Dietzel et al. (2004), in which a polyethylene (PE) bottle containing 0.5 L of 0.83 M $NaHCO_3$ solution was soaked in a vessel containing 5 L of the growth solution (10 Mm $CaCl_2$ + 0.1mM $SrCl_2$ + 5mM NH_4Cl, with certain pH adjusted by adding NaOH or HCl and was kept by pH-stat titration). The outer solution was stirred at 300 rpm. Usually pH of the inner solution was kept lower than that of the outer solution by adding A certain amount of HCl. The difference in CO_2 gradient between the two solutions induce CO_2 to diffuse from the inner to the outer solution. Flux of CO_2 through the membrane controlled R*. In this study R* was measures by measuring Ca^{2+} concentration as function of time and/or from the added volume of NaOH solution to the outer solution during precipitation process. As shown in Fig 1.1, for all temperatures as R* $\Delta^{44/40}$Ca become more negative.

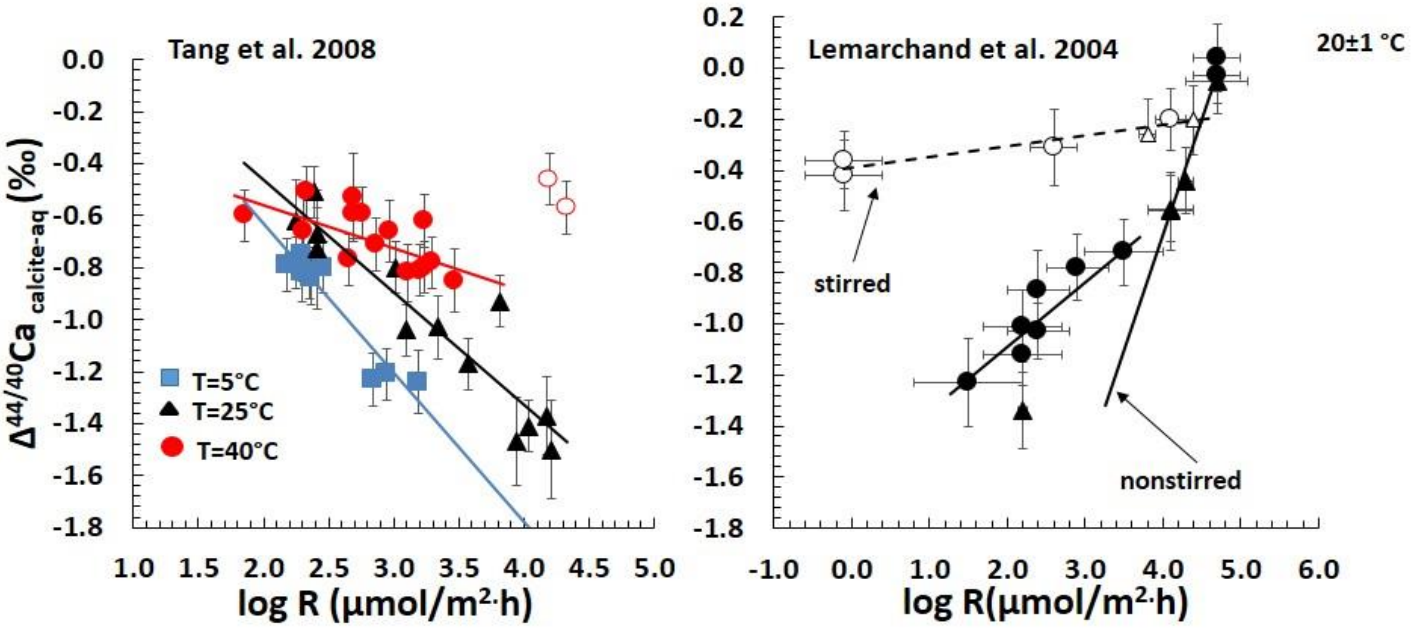

Fig. 1.1: Discrepant results of $\Delta^{44/40}Ca$ as function of precipitation rate (µmol/m^{2}·h).

The reconciliation of the discrepant observation between the Lemarchand et al (2004) and the Tang et al (2008b) study is the major impetus of this study. In the chapters 2 and 3 we partly repeated but also completed and extended the original approach of Lemarchand et al (2004) and compare their original results with our results here and discuss them in the light of the Tang et al (2008b) measurements. In a simple qualitative model we then provide explanations in order to reconcile the observations. In order to complete and extend the original approach by Lemarchand et al (2004) we extended the experiments to three different temperatures (12.5, 25.0 and 37.5±0.2 °C) and to different R* values. Furthermore, we extend the experimental approach in order to precipitate aragonite. The differences in trace element partitioning and isotope fractionation between calcite and aragonite are then extensively discussed in the light of a qualitative model emphasizing the role of complexation of ions in solution in general and the blocking effect of Mg^{2+} for the aragonite precipitation in particular.

Chapter 2

The chapter below has been submitted for publication to Geochimica Cosmochimica Acta. The current status is in revision after a first round of reviews.

Calcium and Strontium Isotope Fractionation during Precipitation from Aqueous Solutions as a Function of Temperature and Reaction Rate; I. Calcite

Abstract: In order to study both the Strontium (Sr) and Calcium (Ca) isotope fractionation simultaneously as a function of the specific precipitation rate (R*) and temperature (T) calcite was precipitated at 12.5, 25.0 and 37.5 °C by diffusing NH_3 and CO_2 gases into aqueous solutions closely following the experimental setup of Lemarchand et al (2004). R* for every sample was determined applying the initial rate method and from the specific surface area of almost all samples for each reaction. The order of reaction with respect to Ca^{2+} ions was determined to be one and independent of T. However, the order of reaction with respect to HCO_3^- changed from three to one as temperature increases from 12.5, 25 °C and 37.5 °C. Strontium incorporated into calcite (expressed as D_{Sr}= [Sr/Ca] $_{calcite}$/ [Sr/Ca] $_{solution}$) was found to be R* and T dependent. As a function of increasing R* the $\Delta^{88/86}$Sr-values become more negative and as temperature increases the $\Delta^{88/86}$Sr values also increase at constant R*. The D_{Sr} and $\Delta^{88/86}$Sr-values are correlated to a high degree and depend only on R* being independent of temperature, complexation and varying initial ratios. Latter observation may have important implications for the study of diagenesis, the paleo-sciences and the reconstruction of past environmental conditions. Calcium isotope fractionation ($\Delta^{44/40}$Ca) was also found to be R* and T dependent. For 12.5 and 25.0 °C we observe a general increase of the $\Delta^{44/40}$Ca values as a function of R* (Lemarchand et al type behavior, Lemarchand et al (2004)). Whereas at 37.5 °C a significant decreasing $\Delta^{44/40}$Ca is observed relative to increasing R* (Tang et al type behavior, Tang et al. (2008)). In order to reconcile the discrepant observations we suggest that the temperature triggered change from a Ca^{2+}-NH_3-aquacomplex covalent controlled bonding to a Ca^{2+}-H_2O-aquacomplex van-der-Waals controlled bonding caused the change in sign of the R* - $\Delta^{44/40}$Ca slope due to the switch of an equilibrium type of isotope fractionation related to the

covalent bonding during lower temperatures to a kinetic type of isotope fractionation at higher temperatures. This is supported by the observation that the $\Delta^{44/40}$Ca ratios are independent from the [Ca] : [DIC] ratio at 12.5 and 25°C but highly dependent at 37.5°C. Our observations imply the chemical fluid composition and temperature dependent complexation controls the amount and direction of Ca isotope fractionation in contrast to the Sr isotopes which do not show any change of its fractionation behaviour as a function of complexation in the liquid phase.

2.1. Introduction

Carbonate minerals contribute to a large extent to the global carbon budget (Morse and Mackenzie, 1990), play an important role in adsorption and desorption processes in the environmental systems (e.g., Langmuir 1997) and control long term climate change (Berner 2004). Calcium carbonate ($CaCO_3$) is usually produced by biogenic and inorganic precipitation processes from aqueous solutions and has three major polymorphs aragonite, calcite and vaterite of which calcite is the most abundant one. Inorganic precipitation of Ca carbonate is usually induced by increasing the concentration of one of the reactants until the aqueous solution becomes supersaturated with these ions (c.f. Niedemayer et al. 2013). Inorganic natural calcite formation is usually related to evaporates and carbonate cements in sediments. In contrast biogenic calcite is produced along different ways of biomineralisation by uni- and multi-cellular calcifying organisms like coccoliths, foraminifera, calcareous sponges, brachiopods (c.f. Niedemayer et al. 2013) and others. The calcite mineral is not pure (Garrels and Christ, 1965) rather contains a variety of trace elements mostly other divalent positively charged alkaline-earth elements like magnesium (Mg), Strontium (Sr), Barium (Ba), but also other elements like Lithium (Li), Boron (B), Cadmium (Cd), Uranium (U), Thorium (Th) and others. The enrichment of these trace elements relative to Ca reflects their specific environmental conditions in the adjacent bulk solution at the time of formation (Morse and Bender 1990) and may eventually be used as a chemical indicator of past environmental conditions (proxy). These conditions include the composition of solutions, concentration of dissolved trace elements, temperature, pH, salinity and the degree of saturation of these minerals. In calcite beside Mg the most important trace element is Sr. For example foraminifera which are responsible for about 20% of the total calcite sediments and 5 to 10% of the total sediments in the marine environments form the main sink of Sr (Böhm et al. 2012, Vollstaedt et al. 2014). In addition, the

Sr/Ca ratio measured in aragonite has been widely used in paleo-oceanographic studies to estimate past sea surface temperatures (SST) (e.g., Smith et al., 1979; Rosenthal et al., 1997; Gagan et al., 1998). This elemental ratio is also used to understand the composition of past seawater, to study the diagenetic reactions that involve carbonate sediments (e.g., Lorens, 1981; Baker et al., 1982, Mucci and Morse, 1983; Richter and Liang, 1993; Banner, 1995; Humphrey and Howell, 1999; Malone and Baker, 1999). The Sr/Ca ratio in biogenic calcite was also correlated to both nutrient level and growth rate (e.g., Weinbauer and Velimirov, 1995; Stoll and Schrag, 2000; Stoll et al., 2002a, b).

In addition numerous experimental studies have been carried out to evaluate effects of different environmental conditions (temperature, R*, pH and salinity changes) on Sr incorporation into calcite. Earlier culturing experiments using foraminifera and coccoliths (e.g., Lea et al., 1999; Stoll and Schrag, 2000; Stoll et al., 2002a, b) suggested that Sr/Ca ratios increase (corresponding to an increasing Sr partitioning coefficient (D_{Sr}) = $[Sr/Ca]_{calcite}/[Sr/Ca]_{solution}$) with increasing calcite R* and/or increasing temperature. Similar results were shown by experiments to examine inorganic calcite precipitation of (Lorens, 1981; Tesoriero and Pankow, 1996; Huang and Fairchild, 2001; Nehrke et al., 2007; Tang et al., 2008a; Tang et al., 2012; Gabitov et al., 2014). Although the slope and general behavior is similar in all previous experiments the gradients and values mostly differ depending on the experimental conditions of each single experiment. In particular only Tang et al., 2008a studied the combined effect of temperature and R*. They found at constant rate of precipitation as temperature increase D_{Sr} values decrease. Furthermore, Tang et al., 2012 studied the effect of salinity parallel to the effect of rate of precipitation and found that it has insignificant effect on the D_{Sr} values. Also for biogenic calcite and experimental transformation of aragonite to calcite a positive or insignificant temperature dependence was observed (Katz et al., 1972; Jacobson and Usdowski 1976; Baker et al. 1982; Stoessell et al., 1987; Lea et al., 1999; Humphrey and Howell, 1999; Malone and Baker, 1999; Stoll et al., 2002a, b).

According to our knowledge there is only one study in the literature dealing with Sr isotope fractionation (expressed as $\Delta^{88/86}Sr$) between experimentally precipitated calcite and aqueous solution presented earlier by our group (Böhm et al. 2012). The authors found at 25 °C that Sr isotope fractionation in calcite is strongly dependent on R*, as rate increase more lighter Sr isotopes are incorporated into calcite corresponding to increasingly lower $\Delta^{88/86}Sr_{calcite\text{-}aq}$ values.

They also compared these results with Sr isotope fractionation in biogenic foraminiferal calcite samples and interpreted the strong Sr isotope fractionation of these samples to be due to calcification at high R*.

Nevertheless the literature values available concerning Ca isotopic fractionation between calcite and aqueous solution are discrepant to a certain extent. Tang et al, 2008b found that Ca isotope fractionation is both rate and temperature dependent, as rate increases more lighter Ca isotopes are incorporated into calcite corresponding to increasingly lower $\Delta^{44/40}Ca_{calcite\text{-}aq}$ values. Concerning temperature $\Delta^{44/40}Ca_{calcite\text{-}aq}$ increases as a function of temperature at constant rate of precipitation. In contrast earlier experiments by Lemarchand et al, 2004 found that as rate of precipitation increase more heavier Ca isotopes are incorporated into calcite corresponding to increasingly higher $\Delta^{44/40}Ca_{calcite\text{-}aq}$ values**.** The latter discrepant observation of lower and higher $\Delta^{44/40}Ca_{calcite\text{-}aq}$ values as a function of increasing R* was the impetus for this study to repeat the original experiment of Lemarchand et al 2004. In this study we closely followed the original experimental setup of Lemarchand and precipitated calcite from aqueous ammonium buffered solution through spontaneous decomposition of solid ammonium carbonate into aqueous solutions containing Ca^{2+} ions. This experimental setup allows us to precipitate calcite with different R* at three selected temperatures (~12.5, ~ 25.0 and ~37.5°C). The goal of this experimental approach is to do a whole kinetic study in order to evaluate how R*, temperature and Sr/Ca ratios in the precipitating solutions will affect the D_{Sr} values, Sr isotopic fractionation $\Delta^{88/86}Sr_{calcite\text{-}aq}$ and Ca isotopic fractionation $\Delta^{44/40}Ca_{calcite\text{-}aq}$**.** Finally, we intend to provide a qualitative model in order to reconcile the discrepant results concerning earlier observations on Ca isotopic fractionation.

2.2. Material and Methods

2.2.1 Materials and Experimental Setup

The original experimental setup of this method to precipitate Ca carbonates ($CaCO_3$) was described initially by (Gruzensky, 1967), later used by (Paquette and Reeder, 1990; Paquette and Reeder 1995; Hemming et al. 1995; Lemarchand et al. 2004) and finely by (Gabitov, 2013) to precipitate calcite, high-Mg calcite and aragonite. In this work we modified the sealed chamber with a copper tubing coil to control the temperature inside as it is shown in Fig. 2.1.

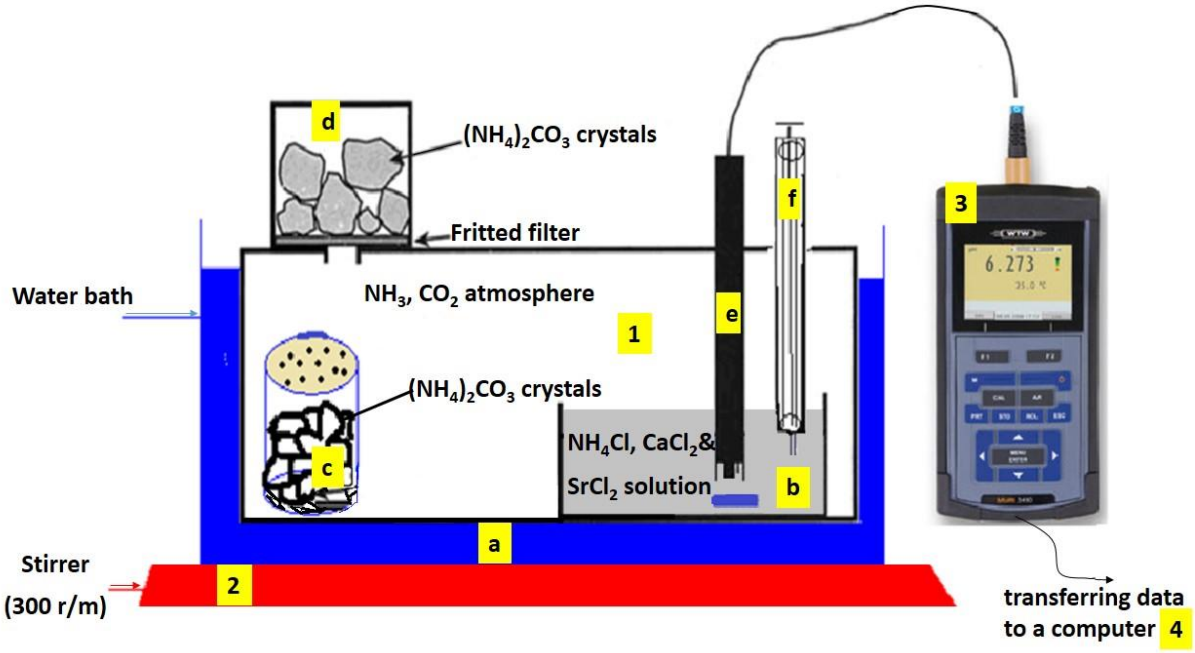

Figure 2.1: schematic design of the experimental setup: (**1**) the reaction chamber which is a sealed plastic container consisting of a copper tubing (**a**) where water is circulating to keep a constant temperature, (**b**) beaker that contains the reacting solution, (**c**) a beaker that contains some ammonium carbonate granules that decompose spontaneously to provide ammonia and carbon dioxide gases, (**d**) fritted filter funnel that also contains some ammonium carbonate granules, (**e**) pH and temperature sensors, (**f**) syringe to withdraw samples from the reacting solution, (**2**) magnetic stirrer, (**3**) pH meter and (**4**) computer recording the measured data in an excel sheet.

Two main sets of solutions were prepared to produce calcite in an ammonium buffered solutions (NH_4/NH_3) at three different temperatures 12.5, 25.0 and 37.5 (±0.2 °C). The first set is composed of 0.395 M NH_4Cl, 10.0 mM $CaCl_2$ and 0.10 mM $SrCl_2$. The second solution shows the same composition except for a $SrCl_2$ to be 0.050 mM $SrCl_2$. In order to verify differences in chemical composition three solutions were prepared differently following the original experiment by Lemarchand et al (2004) which either contained either 15 or 150 mM [Ca], respectively: No. 4 is composed of 0.395 M NH_4Cl, 19.84 mM $CaCl_2$ and 0.11 mM $SrCl_2$, reaction No. 7 is composed of 0.395 M NH_4Cl, 149.00 mM $CaCl_2$ and 0.00 mM $SrCl_2$ and reaction No. 8 is composed of 0.395 M NH_4Cl, 148.42 mM $CaCl_2$ and 1.5 mM $SrCl_2$. NH_4Cl is used here to buffer the solution and to adjust the ionic strength of the solutions. All the chemicals are ACS grade of Merck and all aqueous solutions were prepared using deionized water (18.2 MΩ).

In this technique 400 to 550 ml of NH_4Cl-$CaCl_2$-$SrCl_2$- solution and the solid $(NH_4)_2CO_3$ (ammonium carbonate) are contained within the sealed reacting chamber. In all experiments the reacting solution is stirred with a magnetic stirrer at 300 rounds per minute. Ammonium carbonate decomposes spontaneously and produces an ammonia/carbon dioxide atmosphere within the chamber by the reaction:

(1) $(NH_4)_2CO_{3\,(S)} \leftrightarrow 2NH_{3\,(g)} + CO_{2\,(g)} + H_2O_{\,(g)}$

Ammonia and carbon dioxide gases diffuse and dissolve in the experimental solution increasing pH and alkalinity by the following reactions

(2) $NH_{3(g)} + H_2O \rightleftharpoons NH_4^{+}{}_{(aq)} + OH^{-}{}_{(aq)}$

(3) $CO_{2(g)} + H_2O \rightleftharpoons CO_{2(aq)}$

(4) $CO_{2(aq)} + H_2O \rightleftharpoons H_2CO_3$

(5) $H_2CO_3 \rightleftharpoons HCO_3^{-}{}_{(aq)} + H^{+}{}_{(aq)}$

(6) $HCO_3^{-}{}_{(aq)} \rightleftharpoons CO_3^{-}{}_{(aq)} + H^{+}{}_{(aq)}$

The overall spontaneous reaction of the steps (1) to (6) is:

$(NH_4)_2CO_3\,(s) \rightarrow 2NH_4^{+}\,(aq) + CO_3^{2-}\,(aq)$

The result of these reactions is the supersaturation of the reacting solution with respect to calcite. The dynamic of the reaction was monitored by a WTW 3100 pH meter which was standardized against buffer solutions of pH 4, 7 and 10 before each single experiment. This pH meter connected to a computer monitors the pH values and the temperature of the solution online (see Fig. 1) continuously and stores the measured data in an excel sheet. We controlled the rate of reaction as well as the time needed to reach the precipitation point by the quantity, the surface area of the granules of ammonium carbonate and by the surface area through which the gases diffuse. For example for slow reaction rates we use 5 to10 g of ammonium carbonate with a radius of about one centimeter. In this case we found the rate of reaction ranging between 1.2 to 3.0 mmol/m^2·h and the time needed for precipitation to start range between 3 to 12 days depending on individual reaction temperature. To accelerate the reactions we put additional beaker containing solid ammonium carbonate (different quantities and different particle size) inside the reacting chamber. This beaker was covered with parafilm and perforated with a distinct number of holes. In certain cases the beaker was not covered at all, then the rate of

reaction increased ranging from 4.4 to 33.2 mmol/m^{2}·h and the time needed to start precipitation ranging between 24.7 and 3.2 hour depending on the temperature of individual reaction.

During the experiment the chemical evolution of the reacting solution was monitored by sampling 2 to 5 ml at distinct time intervals ranging between 5 to 30 minutes depending on the reaction time to be analyzed later. We allowed each reaction to run for a certain period of time depending on its rate then stopped it by removing the reacting solution from the sealed chamber and filter the solution as fast as possible by vacuum filtration through a regenerated cellulose filter paper with a pore size of 0.2 µm. Then the solid was washed with deionized water (18.2 MΩ) and mixed with a small volume of pure ammonium hydroxide solution to make it slightly alkaline. Furthermore, the filter was finally washed with pure ethanol in order to remove any adsorbed $CaCl_2$ or/and $SrCl_2$ aqueous solutions on the surface of the crystals.

2.2.2 Analysis

2.2.2.1 Dissolved Inorganic Carbon (DIC)

In order to calculate DIC, the total alkalinity (TA) of each experiment through the whole period of reaction has to be calculated. We did this by titrating 0.2 ml of the reaction mixture at different intervals of time during the precipitation reaction against 0.02 N HCl (dilution of MERCK-Titrisol-solution^{TM}). This HCl solution is initially standardized against IAPSO seawater (Certified alkalinity of 2.325 mM) using a micro titration apparatus Metrohm 665 Dosimat equipped with a titration vessel of 7 cm. During the titration the sample is degassed with nitrogen continuously to remove any CO_2. The indicator used in this titration is prepared from two solutions. Solution 1: about 1 to 32 mg Methyl Red (or 37 mg of sodium salt of Methyl Red) mixed with 1.19 ml of 0.1 M NaOH and dissolved in 80 ml 96% ethanol. Solution 2: about 2 to 10 mg Methylene Blue dissolved in 10 ml 96% ethanol. Taking 4.8 ml of solution 2 and mixing it with 80 ml of solution 1 to obtain a greenish-brown solution, at the end point of the titration solution becomes pink. In each titration the volume of indicator used was 20 µl added to 4.8 ml of water and 0.2 ml sample. Each sample was titrated three times and the average volume was used to calculate the total alkalinity.

Furthermore the concentration of ammonia (NH_3 aq) in our samples has to be determined and the apparent acid dissociation constant of ammonium chloride in our experimental condition has to be calculated ($K_a = [NH_3]\,[H^+]/[NH_4^+]$; K_a = apparent dissociation constant). The value for Ka

had to be determined because only one value for 20°C was known before! Following this 6 ml aliquot of the mother solution was titrated potentiometrically against 1M NaOH aq using the micro titration apparatuses. The average volume of the three titration trials was 2.40 ml NaOH. Then the pH of half neutralized mother solution was measured in a thermostat at different temperatures. At each temperature the half neutralized solution was kept at least 30 minutes in the thermostat in order to reach thermal equilibrium before measuring its pH. The salinity of the reaction mixtures was measured by WTW cond. 3110 set 1.

2.2.2.2 Elemental analysis

We analyzed the concentrations of Ca and Sr ions in the bulk solutions at different intervals of time during the course of each reaction. Furthermore, after dissolution of the solid carbonate samples the elemental ratio was measured by inductively coupled plasma mass spectrometry (ICP-MS-QP Agilent 7500cx) together with Indium (In) as an internal standard. All samples were diluted in 2% HNO_3 to reach 25.0±2.5 ppm Ca in order to avoid matrix effects. Coral standard JCP-1 was used as a reference material and measured as every fifth sample and in a total of ten times during the course of this study (N=10).The JCP-1 Sr/Ca ratio was calculated to be 8.82±0.02 mmol/mol which matches within the error the reported value of 8.84±0.08 mmol/mol of Hathorne et al. (2013). In addition we also measured standard JCT-1 to be 1.693±0.004 mmol/mol which is also in agreement with the value of Hathorne et al (2013) to be 1.680±0.055 mmol/mol. The average uncertainty for our Sr/Ca mmol/mol ratios are less than 1% and correspond to the 95% confidence level.

2.2.2.3 Crystalline structure and specific surface area of calcite products

The crystalline structure of the solid products was analyzed by X-ray diffraction and by scanning electron microscope (SEM) CamScan-CS-44, equipped with a secondary electron detector, backscattered electron detector, thermal evaporator Edwards Auto 306 and sputtering-coater EMITECH K550, Au/Pd (80/20). Measurements were performed with an X-Ray-diffractometer "D8 Discover" (Bruker AXS). The samples were analyzed in a 2Θ-range from 4° to 90° with a step size of 0.007° and counting time 1.5 s/step using a Cu X-ray radiation source. Software was evaluated by High Score Plus Version 3.0d (3.0.4) by PANalytical. All measurements were carried out at the Geology Department of Kiel University.

2.2.2.4 Strontium and calcium isotope analysis

Measurements were carried out at the GEOMAR mass spectrometer facilities in Kiel, Germany, with a ThermoFisher Triton T1 Thermal-Ionization-Mass-Spectrometer (TIMS). Strontium ($\delta^{88/86}$Sr) and Ca ($\delta^{44/40}$Ca) isotope composition were measured for all solid products as well as for the mother solution of these reactions closely following the procedure as described earlier by (Krabbenhöft et al. 2009). At least two isotope measurements have to be performed. One unspiked run (ic-run, isotope composition) and one run with a ^{87}Sr/^{84}Sr-double spike added to the sample solution (id-run, isotope dilution). Sample size was selected to be in the order of 1500 ng of Sr. Spike correction and normalization of the results was carried out as described by (Krabbenhöft et al. 2009). During the course of this project two ic-run and id-run for each sample in each session were measured. For quality control the following standard materials were applied: SRM987 $SrCO_3$ standard from the National institute of standards and technology (NIST), JCp-1 coral standard and IAPSO seawater standard. We report the statistical uncertainties of our measurements as twice the standard deviation of the mean ($2\sigma_{mean} = 2\sigma/n^{0.5}$); where n is the number of measurements. The measured ^{88}Sr/^{86}Sr ratios are reported in the common δ-notation relative to NIST SRM987: $\delta^{88/86}$Sr (‰) = $[(^{88}Sr/^{86}Sr)_{sample}/(^{88}Sr/^{86}Sr)_{SRM987}-1]*1000$. The blank values of our chromatographic column separations were <0.10 ng Sr as a whole procedure blank in all batches we prepared. The $\delta^{88/86}$Sr-values of column separated SRM987 chemistry was measured in three different batches and has these values (0.00±0.02, 0.018±0.014 and 0.003±0.005 ‰, n = 4 for each) showing insignificant deviations from the reference values due to the column separation of the standard. The $\delta^{88/86}$Sr-values of separated IAPSO of our three batches resulted into (0.372±0.006, 0.399±0.001 and 0.392±0.005 ‰, n = 4 for each) which compares well with the long term IAPSO average of the instrument measurements 0.391±0.004 ‰, n = 63. The $\delta^{88/86}$Sr-values of separated JCP-1 of our three batches respectively (0.188±0.006, 0.200±0.010 and 0.196±0.004 ‰, n = 4 for each), while the mean value of measurements carried out by this instrument is (0.195±0.003 ‰, n = 87). The method adopted for Ca isotope measurement follows Heuser et al. 2002 and Böhm et al. 2006, respectively. For each sample to be analyzed 3000 ng of Ca were spiked with 120 µl ^{43}Ca/^{48}Ca double spike to correct for isotope fractionation in the mass spectrometer during the course of the Ca isotope analysis. The mixture was evaporated to dryness and then redissolved in 100 µl 0.9 N HCl, this solution was loaded onto ion exchange column (BIO RAD of 800µl bed volume; cation

exchange resin MCI Gel, CK08P, 75~ 150 µ, Mitsubishi chemical composition) in order to extract the Ca-fraction. After washing the column with water (18.2 MΩ) and then with 1.5 N HCl, sample then was loaded to the column, washed with 3.5 ml 1.5 N HCl. The Ca-fraction was then eluted after rinsing the column with 9 ml 1.5 N HCl. Then the solution was evaporated to dryness and redissolved in 20 µl 2.5N HCl. This quantity is enough to load ten filaments to be measured into ten separate runs. Details of the measurement procedure can be found in (Heuser et al. 2002 and Böhm et al. 2006). In each run session NIST SRM915a was measured four times, CaF_2 was measured twice (which used as a control standard) and each sample was measured at least five times. The isotopic ratio of each sample as well as CaF_2 was normalized to the mean of the four $^{44}Ca/^{40}Ca$ NIST SRM915a analysis and reported in the common delta notation $\delta^{44/40}Ca$ (‰) = $[(^{44}Ca/^{40}Ca)_{sample}/ (^{44}Ca/^{40}Ca)_{standard} -1]*1000$. The blank values of our chromatographic column separations were <15 ng of Ca as a whole procedure blank in all batches we prepared. The average of $\delta^{44/40}Ca$ of separated NIST SRM915a by column chemistry was measured 12 times in three different batches was 0.02±0.02‰, it shows insignificant deviation due to the column separation of the standard. The average of $\delta^{44/40}Ca$ of CaF_2 measured in 20 different runs was 1.4±0.2 ‰ (n = 40) which is in absolute agreement with earlier measurements (c.f. Heuser et al. 2005).

We are reporting Sr and Ca fractionation in the big delta notations $\Delta^{88/86}Sr = \delta^{88/86}Sr_{calcite} - \delta^{88/86}Sr_{initial\ solution}$ and $\Delta^{44/40}Ca = \delta^{44/40}Ca_{calcium\ carbonate} - \delta^{44/40}Ca_{initial\ solution}$ respectively. All Δ-values are corrected for Rayleigh distillation effect (Zeebe and Wolf-Gladrow, 2003) in order to account for the reservoir effect as shown in the following equation (information about the derivative of eq. 7 are presented in the appendix):

(7) $$\alpha_{corrected} = \left(ln\left[\frac{\Delta f}{1000} + f - \left(\frac{\Delta}{1000}\right)\right]\right)/lnf$$

Where f is the fraction of metal ions remaining in the aqueous solution and α is the isotope fractionation factor defined as $(^{44}Ca/^{40}Ca_{calcium\ carbonate}/^{44}Ca/^{40}Ca_{initial\ solution})$

(8) $$\Delta_{corrected} \approx (\alpha_{corrected} - 1) \cdot 1000$$

In table 2.5 the original data together with the corrected data for Rayleigh fractionation are presented.

2.3. Results

The concentrations of NH_3 and NH_4 in our experimental setup are relatively high when compared f.e. with the concentrations used in Tang et al. (2008). Latter fact inhibits the calculations of activity coefficients applying geochemical modeling and the PHREEQC software. Consequently, all calculations are based on concentrations only.

2.3.1. pH, total alkalinity and Saturation indexes (SI) with respect to calcite, amorphous calcium carbonate (ACC) and strontianite ($SrCO_3$).

The experiment shows that the pH of the solution gradually increase (Fig. 2.2) as soon as the absorption of the evolved gases (CO_2 and NH_3) into aqueous solution starts until it reaches a maximum value (marked with a red point in Fig. 2.2) and then decrease slightly after the real precipitation point. The Ca^{2+} -ions react with HCO_3^- but then it is redistributed to CO_3^{2-} which results in a pH drop according to Eq (9). The start of the precipitation is also characterized by a simultaneous drop of dissolved [Ca] and [Sr] in the solution exactly at this pH.

(9) $HCO_3^- + Ca^{2+} \rightleftharpoons CaCO_{3(S)} + H^+$

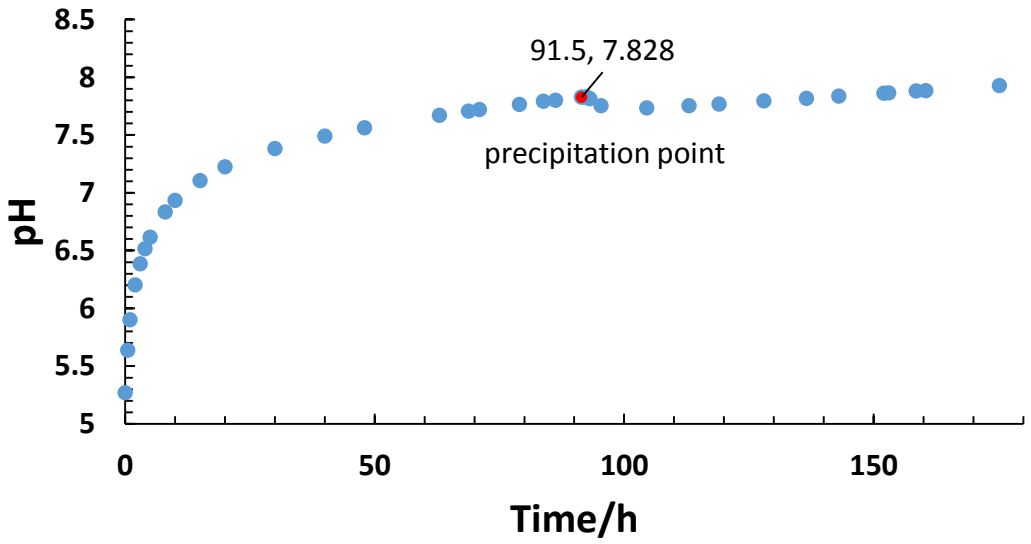

Figure 2.2: The pH variations of the solution versus time of sample reaction 2 at 25 °C. The time needed to reach the saturation point is 91.5 hour.

Throughout the reaction the pH of the reacting solution (when precipitation starts) remains relatively constant (±0.02 units) as well as the temperature of all reactions (±0.2 °C). In the appendix we show details of calculating acid dissociation constant of ammonium ions (K_a) as function of temperature and molar concentrations of different alkaline species in reacting solutions (NH_3, HCO_3^- and CO_3^{2-}). The results of this part are summarized in table 2.1. SI values with respect to calcite, ACC and SrCO3 are calculated as described in appendix and presented in table 2.5.

2.3.2 Kinetics of calcite formation reactions

2.3.2.1 Initial rate of reaction (R) and order of reaction with respect to calcium ions

During the course of the experiment we determined TA by online measurement and verified that TA of the precipitation solutions are kept almost constant throughout time. Therefore, we can assume that DIC is constant and that the majority of the DIC (Dissolved Inorganic carbon) is bicarbonate (see table 2.1). As a consequence we can simplify the rate law of reactions:

(10) $R = K^* [Ca]^x$

where R is the initial rate of reaction in mM/h, K* equals the rate constant (see equation (11)), [Ca] is the molar concentration of Ca ions in mM and x is the order of reaction with respect to Ca ions.

(11) $K^* = K [HCO_3^-]^y$

$[HCO_3^-]$ is the concentration of bicarbonate ions in mM and y is the order of reaction with respect to bicarbonate ions. The rate law in the previous literature, as in Zuddas and Mucci (1994), is written in the form:

(12) $R = k [aCa]^x \cdot [aHCO_3]^y$

where k is the rate constants for the forward (precipitation) reaction; a, x and y are respectively the activity and the partial reaction order of the species involved in the reaction. For simplicity we use molar concentration instead of activity.

Here we can apply the initial rate method to solve the rate law of calcite precipitation reaction following Atkins and De Paulla (2006). As an example for all reactions we plotted [Ca] versus time of randomly selected sample 38C and fitted the curve to a polynomial equation (Fig. 2.3a).

The instantaneous rate of precipitation R is corresponding to the first derivative of the polynomial function (equation 13) in Fig. 2.3a of data set 38C (table 2.2):

(13) $d[Ca]/dt = 0.64t - 2.59$

Table 2.1: Temperature (T), total alkalinity (TA), pH, salinity, concentration of ammonia, dissolved inorganic carbon (DIC), carbonate and bicarbonate ions concentrations, mole fraction of bicarbonate in DIC, initial and final concentrations of both Ca and Sr and their remaining fraction at the end of each experiment, Sr: Ca ratio in the mother solution ($[Sr]_0/[Ca]_0$), ratio of initial $[Ca]_0$ to the concentration of the dissolved inorganic carbon (Ca_0 : DIC), time needed for each reaction to start precipitation and the period of precipitation, volume of aqueous solution, moles of $CaCO_3$ produced and its surface area.

Sample label	T/ °C ± 0.2	TA / mM	pH	Salinity	$[NH_3]$ / mM	DIC / mM	$[CO_3]$/ mM	$[HCO_3]$ / mM	Mole fraction Of $[HCO_3^-]$in [DIC]	$[Ca]_0$ / mM	$[Ca]_f$ / mM	Fraction of Ca remain	$[Sr]_0$ / mM	$[Sr]_f$ / mM	Fraction of Sr remain	$[Ca]_0$:[DCI]	$[Sr]_0/[Ca]_0$	Time needed to start precipitation/h	Time of precipitation/h	Volume of solution /ml	Moles of $CaCO_3$	Area of $CaCO_3$ / m^2
1	2	3	4	5	6	7	8	9	10	11	12	13	14	15	16	17	18	19	20	21	22	23
20A	37.5	15.63	8.008	33.3	9.82	5.81	0.79	4.24	0.84	9.85	5.71	0.58	0.104	0.099	0.95	1.70	0.011	93.67	21.70	500	0.00207	0.122
20B	37.5	16.90	8.048	33.7	10.77	6.13	0.89	4.36	0.83	9.61	4.54	0.47	0.053	0.049	0.92	1.57	0.005	95.00	21.67	500	0.00254	0.150
21A	37.5	31.65	8.313	32.7	20.10	11.55	2.47	6.61	0.73	9.89	2.09	0.21	0.103	0.081	0.79	0.86	0.010	8.65	5.95	525	0.00410	0.242
21B	37.5	26.57	8.264	32.3	17.83	8.74	1.75	5.24	0.75	9.65	2.64	0.27	0.052	0.043	0.83	1.10	0.005	8.00	5.63	525	0.00368	0.217
22A	37.5	21.10	8.162	32.1	14.04	7.06	1.22	4.62	0.79	9.30	3.87	0.42	0.100	0.091	0.91	1.32	0.011	18.50	5.27	550	0.00298	0.176
22 B	37.5	17.10	8.112	32.2	12.44	4.66	0.75	3.17	0.81	9.30	4.25	0.46	0.050	0.046	0.92	2.00	0.005	18.50	4.10	550	0.00278	0.164
23C	37.5	30.58	8.313	32.5	20.05	10.53	2.25	6.02	0.73	9.31	1.82	0.20	0.100	0.075	0.75	0.88	0.011	5.00	3.75	550	0.00412	0.243
23D	37.5	29.11	8.310	32.3	19.85	9.27	1.98	5.31	0.73	9.31	1.62	0.17	0.050	0.037	0.74	1.00	0.005	6.00	3.75	550	0.00423	0.249
47A	37.5	17.58	8.025	31.5	10.25	7.34	1.02	5.29	0.84	9.82	3.61	0.37	0.094	0.078	0.83	1.34	0.010	6.35	1.43	400	0.00249	0.147
47B	37.5	16.12	8.019	32.3	10.07	6.04	0.83	4.38	0.84	10.12	4.80	0.47	0.049	0.043	0.88	1.68	0.005	6.73	1.25	400	0.00213	0.126
48C	37.5	67.41	8.755	30.7	55.64	11.77	3.97	3.83	0.49	9.61	4.93	0.51	0.092	0.085	0.92	0.82	0.010	3.17	0.97	400	0.00187	0.110
48D	37.5	63.20	8.716	31.6	50.92	12.28	4.02	4.24	0.51	10.12	5.69	0.56	0.049	0.045	0.92	0.82	0.005	2.85	0.97	400	0.00177	0.105
6	37.5	24.61	8.315	32.6	9.47	15.14	0.82	14.32	0.95	9.97	0.25	0.03	0.119	0.077	0.65	0.66	0.012	7.80	16.63	400	0.00389	0.229
43C	25.0	28.33	8.330	31.7	20.70	7.63	1.24	5.16	0.81	10.03	5.36	0.53	0.101	0.088	0.87	1.31	0.010	7.25	0.88	400	0.00187	0.110
43D	25.0	37.51	8.458	31.8	27.93	9.59	1.88	5.83	0.76	10.04	2.82	0.28	0.052	0.040	0.77	1.05	0.005	5.00	2.32	400	0.00289	0.171
44A	25.0	26.77	8.343	31.5	21.22	5.55	0.92	3.72	0.80	10.45	6.95	0.67	0.051	0.047	0.92	1.88	0.005	5.50	0.90	400	0.00140	0.083
44B	25.0	33.70	8.443	31.8	26.80	6.90	1.32	4.26	0.76	10.37	5.59	0.54	0.051	0.046	0.90	1.50	0.005	4.60	2.02	400	0.00191	0.113
45C	25.0	15.63	8.058	31.0	10.98	4.65	0.47	3.70	0.89	9.94	5.80	0.58	0.096	0.086	0.90	2.14	0.010	16.00	1.18	400	0.00166	0.098

Sample label	T/ °C ± 0.2	TA / mM	pH	Salinity	[NH_3] / mM	DIC / mM	[CO_3]/ mM	[HCO_3] / mM	Mole fraction Of [HCO_3^-]in [DIC]	[$Ca]_0$ / mM	[$Ca]_f$ / mM	Fraction of Ca remain	[$Sr]_0$ / mM	[$Sr]_f$ / mM	Fraction of Sr remain	[$Ca]_0$:[DCI]	[$Sr]_0$/[$Ca]_0$	Time needed to start precipitation/h	Time of precipitation/h	Volume of solution /ml	Moles of $CaCO_3$	Area of $CaCO_3$ / m^2
45D	25.0	14.85	7.973	31.5	9.06	5.79	0.50	4.79	0.91	10.57	6.79	0.64	0.052	0.048	0.92	1.83	0.005	18.50	1.83	400	0.00151	0.089
46E	25.0	12.80	7.847	31.2	6.78	6.02	0.41	5.20	0.93	10.21	5.08	0.50	0.098	0.083	0.85	1.70	0.010	12.80	1.33	400	0.00205	0.121
46F	25.0	11.23	7.786	31.6	5.88	5.35	0.32	4.71	0.94	10.50	6.51	0.62	0.051	0.046	0.90	1.96	0.005	12.80	1.83	400	0.00160	0.094
2	25.0	12.81	7.828	31.0	8.23	4.58	0.28	4.03	0.94	9.74	2.48	0.25	0.107	0.094	0.88	2.13	0.011	91.50	83.70	400	0.00290	0.171
3	25.0	20.91	8.092	31.9	15.16	5.75	0.64	4.48	0.88	9.28	0.14	0.02	0.107	0.068	0.64	1.61	0.012	7.13	50.80	400	0.00366	0.216
4	25.0	8.58	7.654	33.0	5.50	3.08	0.15	2.79	0.95	19.84	7.96	0.40	0.108	0.095	0.88	6.44	0.005	9.05	14.25	400	0.00475	0.280
7	25.0	4.64	7.753	48.0	3.64	1.00	0.04	0.92	0.96	149.00	143.80	0.97	0.000	n.d.	n.d	49.00	n.d.	3.40	3.00	400	0.00208	0.122
8	25.0	2.46	7.383	48.0	1.34	1.10	0.02	1.06	0.98	148.42	139.73	0.94	1.510	1.480	0.98	34.93	0.010	3.40	3.10	400	0.00348	0.205
37A	12.5	18.46	8.020	32.0	10.15	8.31	0.52	7.27	0.93	10.05	2.39	0.24	0.101	0.076	0.75	1.21	0.010	10.25	3.55	400	0.00306	0.181
37B	12.5	16.70	7.993	31.8	9.52	7.19	0.42	6.34	0.94	9.93	3.32	0.33	0.051	0.040	0.78	1.38	0.005	11.70	2.12	400	0.00264	0.156
38C	12.5	11.53	7.839	31.7	6.64	4.89	0.21	4.47	0.96	10.05	4.65	0.46	0.101	0.089	0.88	2.06	0.010	14.00	4.38	400	0.00216	0.127
38D	12.5	18.46	8.084	31.9	11.72	6.74	0.48	5.79	0.92	10.00	3.06	0.31	0.051	0.041	0.80	1.48	0.005	12.50	5.17	400	0.00278	0.164
39A	12.5	14.16	8.019	31.8	10.03	4.14	0.26	3.62	0.93	9.97	7.84	0.79	0.101	0.099	0.98	2.41	0.010	84.00	4.07	400	0.00085	0.050
39B	12.5	14.07	8.008	31.8	9.78	4.29	0.26	3.77	0.94	9.96	7.30	0.73	0.052	0.050	0.96	2.32	0.005	76.00	5.00	400	0.00106	0.063
40C	12.5	11.43	7.767	31.8	5.64	5.79	0.21	5.37	0.96	9.91	5.28	0.53	0.101	0.090	0.89	1.71	0.010	19.00	3.25	400	0.00185	0.109
41E	12.5	16.12	8.048	31.7	10.75	5.37	0.35	4.66	0.93	9.94	5.46	0.55	0.102	0.089	0.87	1.85	0.010	15.37	2.50	400	0.00179	0.106
41F	12.5	15.14	7.986	31.8	9.33	5.81	0.34	5.13	0.94	10.06	4.85	0.48	0.052	0.046	0.88	1.73	0.005	21.75	3.38	400	0.00208	0.123
42A	12.5	20.42	8.181	31.5	14.62	5.80	0.50	4.80	0.91	9.84	5.29	0.54	0.103	0.089	0.86	1.70	0.010	15.00	2.95	400	0.00182	0.108
42B	12.5	17.88	8.099	31.7	12.10	5.77	0.42	4.93	0.92	9.88	6.19	0.63	0.052	0.046	0.88	1.71	0.005	24.75	2.38	400	0.00148	0.087

Notes: n.d.= not detected. TA was measured from titrating the final solution with HCl, pH and salinity were measured at the end of each reaction. [NH_3], [CO_3^{2-}], [DIC] and [HCO_3^-] were calculated from equations a2, a4 and a1 as seen in the appendix, respectively. Mole fraction of HCO_3^- (**column10**) = column **9** /(column **9** + column **8**). Initial and final concentration of Ca and Sr (columns **11, 12, 14** and **15**) are measured by ICP-MS. **Column13** = column **12** /column **11**. **Column16** = column **15** /column **14**. **Column17** = column **11/** column **7**. **Column18** = column **14**/ column **11**. **Column 22** = [(column **11** - column **12**)*column **21**]*10^{-6}. **Column 23 =** column **22** x 59 m^2/mol.

The first six points of sample 38C can be approximate with a linear function (Fig. 2.3a) according to the "initial rate method" as f.e. described by Atkins and De Paulla (2006).

(13a) $[Ca] = -2.31t + 10.03$

Table 2.2: Data of reaction 38C to produce calcite at 12.5 °C.

Sample:	[Ca]/ppm	± 2 SD of the mean	Time/h ± 0.008	[Ca]/ mM	± 2 SD of the mean	Instantaneous rate mM/h	log [Ca]	log Rate
C0	404	3	0	10.08	0.08	2.59	1.004	0.41
C1	379	2	0.25	9.45	0.05	2.43	0.975	0.39
C2	353	0	0.57	8.80	0.01	2.23	0.944	0.35
C3	320	1	0.82	8.00	0.04	2.07	0.903	0.32
C4	294	3	1.07	7.33	0.07	1.91	0.865	0.28
C5	264	2	1.57	6.59	0.04	1.59	0.819	0.20
C6	236	1	2.13	5.90	0.03			
C7	224	1	2.63	5.59	0.03			
C8	213	1	3.13	5.30	0.02			
Cf	187	2	4.38	4.65	0.04			

Note: Instantaneous rate is calculated by substituting time in equation 13**.**

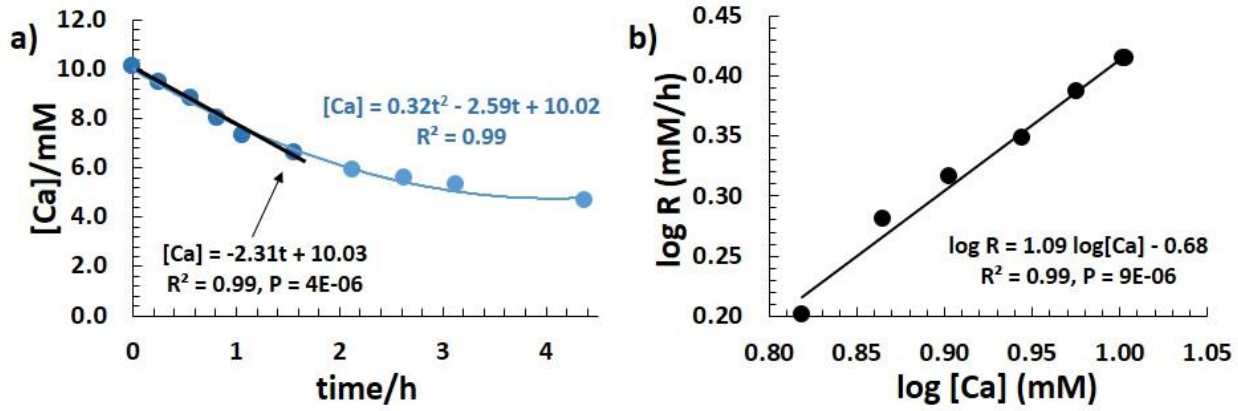

Figure 2.3: Example for the kinetics of calcite formation reaction. **(a)** Changes of Ca^{2+}-ion concentration as function of time for arbitrarily selected sample reaction 38C to produce calcite at 12.5 °C. Latter values fit a quadratic polynomial function. The instantaneous rate of reaction corresponds to the first derivative of the polynomial equation. The linear approximation of the first samples of the curve equals the initial rate of reaction. **(b)** Plotting log instantaneous rate as a function of log [Ca]. The slope of this linear relationship equals to the order of reaction with respect to Ca ions.

For further discussion we choose the initial rate method instead of the "integration rate method" because of the closed system character of the experiment. See an extensive discussion of the use

of the initial rate method in section 2.3.2.4! In brief, the problem determining the "rate" is that depending on the experimental conditions we do not know when chemical equilibrium is finally reached. Based on the fact that the reaction is fast and linear in the beginning the initial rate method is a good approximation and measure of the average rate of reaction (see Fig. 2.3). In this regard for the first data points falling along the linear part of the curve equation (13a) is a good approximation for the more general curve (13). Repeating this for all experiments we make all values much more comparable and exclude the problem of reaching the chemical equilibrium. For more details see section 2.3.2.4.

In order to calculate the order of reaction (x) we took the log of both sides of (Eq. 10), we get:

(14) $\log R = \log K^* + x \log [Ca]$

Plotting log R versus log [Ca] we get a linear relationship where the slope is the order of reaction (x) with respect to Ca ions as shown in (Fig. 2.3b). We can see that the order of reaction for the formation of $CaCO_3$ with respect to Ca ions for sample 38C is about 1.09 for sample 38C and hence approximately first order. We repeated these calculations for all reactions (table 2.5) at all temperatures. These calculations show that all measurements range from 0.77 to 1.26 for the order or reaction (x) with an average value of 1.02±0.17 (1 SD). Hence, we report the order of reaction with respect to [Ca] is one. However, applying the average value of one to one specific experiment will reproduce inconsistent results when not taking the standard deviation of the order of reaction into account. Note that our results are in general accord with in the literature as f.e. in Kazmierczak et al. (1982).

2.3.2.2 Order of reaction with respect to bicarbonate ions

For simplicity we assume that DIC ~ $[HCO_3^-]$ because the majority of DIC are bicarbonate ions (see table 2.1 column 10). In this case we can write:

(15) $R = k [Ca]^{1} \cdot [HCO_3^-]^y$

At time zero for most of reactions (eq. 15) can be written as:

(16) $R = 10\ k [HCO_3^-]^y$

taking logarithm of both sides of (eq.16) we get:

(17) $\log R = \log 10\ k + y \log [HCO_3^-]$.

There is a relatively large individual variation in the k value from one experiment to the other. Taking the k value from one single experiment only is not sufficient because it is burdened with large uncertainties. For example for all 12.5 °C experiments the k value varies from 0.00043 to 0.00142 with an average value of 0.0008±0.0003 corresponding to an uncertainty of about 40%. Latter value can also be calculated from Eq. 10 and from the graphic extrapolation of equation 17 as seen from (Fig. 2.4).

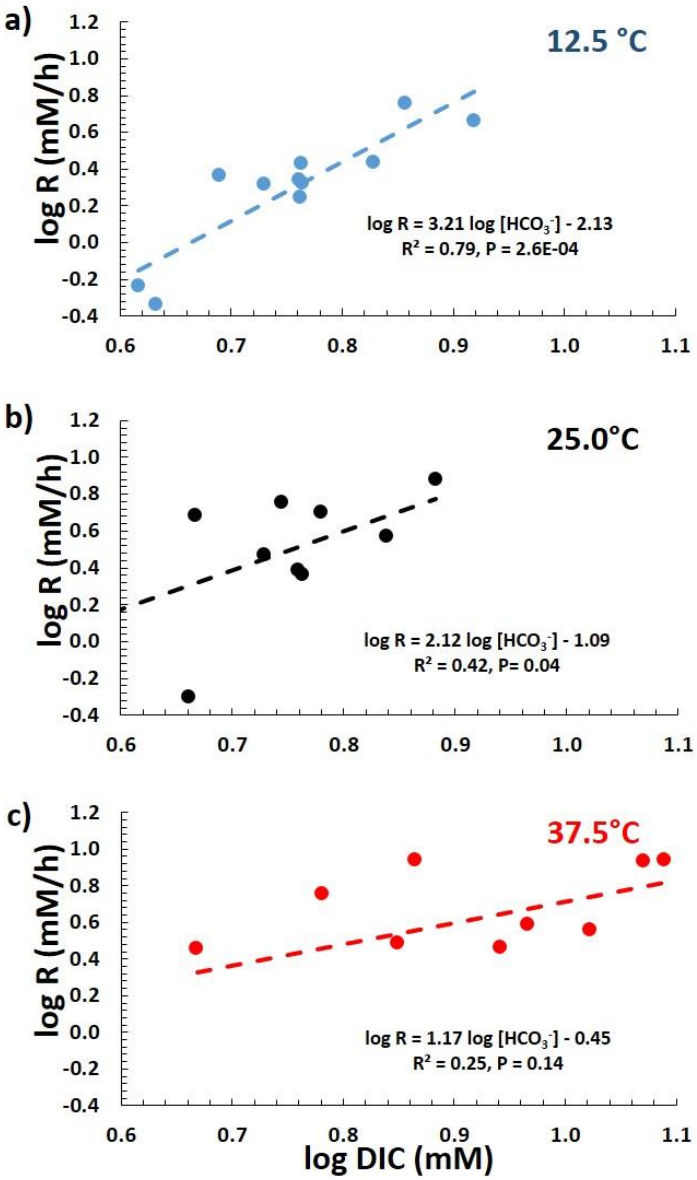

Figure 2.4**:** Log initial rate versus log DIC at **(a)** 12.5, **(b)** 25.0 and **(c)** 37.5 °C. The slopes of these curves equal the orders of reaction with respect to bicarbonate ions and y-intercept equals log (10 * rate constant).

From a fit of our three calculated rate constants (for 12.5°C, 25 °C, 37.5°C) we fit the Arrhenius equation and from the slope calculated to be ~-13756 and we can estimate the activation energy (Ea) for the calcite formation to be ~114 kJ/mol. Latter value is in general agreement with literature data as reported by (Kazmierczak et al. (1982), Nancollas and Reddy (1971) and Wiechers et al (1975)) who estimated Ea of calcite growth in the range of 40 to 50 kJ/mol, while Koutsoukos and Kontoyannis (1984) estimated Ea in the absence of seed crystals to be 155 kJ/mol. The slight discrepancy between data is attributed to different experimental setups. However, the general agreement of our calculated data with those from earlier experiments supports our experimental approach.

If we plot log R versus log [DIC] then the slope of this relationship is y, the order of reaction with respect to bicarbonate ions and its y-intercept equals to log 10k, as shown in (Fig. 2.4) and summarized in table 2.3. The order of reaction with respect to [HCO_3^-] is changing with temperature from around one (37.5°C), to around two (25°C) and three (12.5°C). this means that the mechanism of calcite formation dependent on the experimental conditions as reported earlier in Burton and Walter (1987), Zuddas and Mucci (1998), Lopez et al., (2009) and Zuddas and Mucci (1994). Literature values of the order of reaction "y" with respect to carbonate ions are summarized in table 2.4. There it can be seen by raising temperature from 12.5 to 25 °C results in an about 11 fold increase in the rate constant value. While raising it from 25 to 37.5 °C resulting in about 4.4 fold increasing in the rate constant value as reported for most of noncomplex mechanism chemical reactions as in Atkins and De Paulla (2006).

Table 2.3: Order of reactions with respect to HCO_3^- ions and the rate constant at three different temperatures.

Temperature /°C	**Order of reaction with respect to HCO_3^-**	**Rate constant $mM^{-x} \cdot h^{-1}$**
1	**2**	**3**
12.5	3	7.38×10^{-4}
25.0	2	80.6×10^{-4}
37.5	1	352×10^{-4}

Note: Values of this table are obtained from Fig.4. **Column 2:** rounded to the closest integer. **Column 3**: obtained from the y-intercept of equation 17. x = values in Column 2.

Table 2.4**:** Literature values concerning the order of reaction of carbonate ions in calcite precipitation as function of experimental conditions.

Literature value	**Order of reaction with respect to CO_3^{2-} ions**	**Order of reaction with respect to HCO_3^- ions**	**Experimental condition**
Burton and Walter (1987)	0.6 – 2.3		Temperature changes from 5 – 37 °C
Zuddas and Mucci (1998)	1 - 3		Ionic strength changes from 0.10 - 0.93 molal
Lopez et al. (2009)	2 - 5		Temperature changes from 5 – 70 °C
Zuddas and Mucci (1994)		2	At 25 °C

2.3.2.3 Crystalline Structure and rate of reactions normalized to the average specific surface area (R*)

The X-ray diffraction spectra show that more than 95% of the signal intensity refers to calcite. The residual of less than 5% of the signal is a contribution of unspecified background noise. In this regard, the abundance of strontianite ($SrCO_3$) in significant quantities in any of the solid samples cannot be confirmed.

The SEM images as seen in (Fig. 2.5) indicate that all calcite crystals of our experiments show the typical rhombohedra micro-morphology. We utilized secondary electron (SE) images from SEM to estimate the average specific surface area of calcite obtained from different experiments since the quantity of calcite products were insufficient for BET-determination (BET = Brunauer-Emmett-Teller) of the surface area. In order to calculate the specific rate of precipitation (R*) we determined the surface area and the volume of 50 randomly selected calcite crystals from 10 samples which differ in precipitation rate and temperature (Fig. 2.5a). For the randomly selected crystals the dimension of the length, width and height are measured individually from which than the surface area as well as the volume has been calculated. Then the average value of all individual surface areas and volumes are taken. From this the specific surface area was calculated according to:

$$S = \frac{\text{total area } (\mu m^2)}{[\text{total volume } (\mu m^3) \text{ x density of calcite } (2.71.10^{-12} g \mu m^{-3})]} \quad (18)$$

The results corresponds to an average value for S of 0.59 m^2/g. In order to verify the S values for temperature dependency ten different calcite samples which were precipitated at different rate

and temperature are measured and calculated in the same way (Fig. 2.5a). It can be seen from Fig. 2.5a that the S values are independent of temperature and the initial rate of reaction. As a consequence we can assume that S is constant for all calcite precipitates and that an average values of 0.59 m^2/g or equivalent to 59.0 m^2/mol can be adopted. Values of normalized rate of precipitation R* (μmol/m^2·h) are summarized in table .2.5 and are calculated by:

$$(19) \qquad R^* = \frac{\text{initial rate (mM/h) x volume of reacting solution (ml)}}{\text{Area of } CaCO_3 \ (m^2)}$$

where the value of the numerator equals the initial rate (μmol/h), the total area of $CaCO_3$ in each sample reaction equals the moles of $CaCO_3$ produced at the end of each experiment multiplied by S.

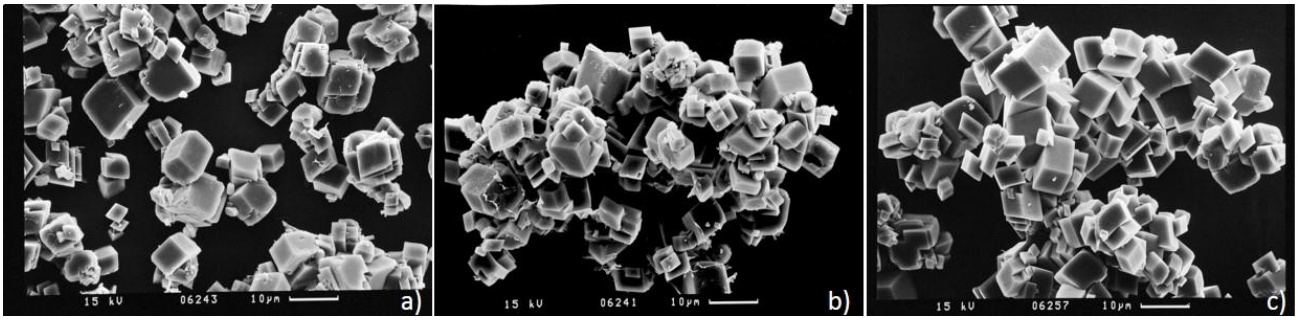

Figure 2.5: SEM images of some calcite crystals, **(a)** T= 12.5 ºC of sample reaction 37B; **(b)** T= 25.0 ºC, of sample reaction 43C and (**c**) T= 37.5 ºC of sample reaction 48D.

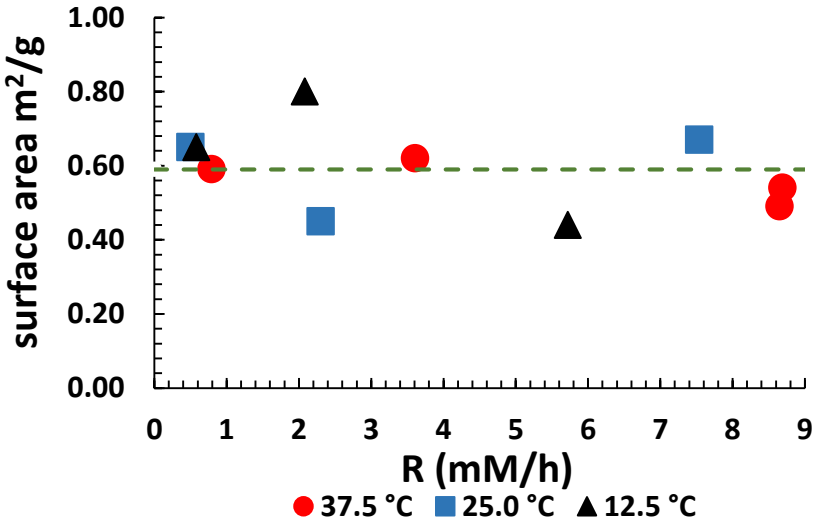

Figure 2.5a: Specific surface area of randomly selected 10 samples of calcite at different rate and temperature, calculated as described in the text. The dashed line represents the average surface area.

2.3.2.4 Calculation of rate and the Order of Reaction with Respect to the "Initial Rate Method" versus Lemarchand et al. (2004) estimation of rate.

One of the most important parameters in chemical precipitation experiments is the rate law and the specific precipitation rate (R*). There are several methods known in the literature to determine R* depending on the individual experimental setup like the initial rate method (this study), the integration rate method (Atkins and De Paulla (2006)) and the average rate method (c.f. Tang et al (2008)).

Depending on the experimental conditions when [Ca] decreases fast, the linear relationship at the beginning of the experiment very quickly deviates from linearity. Hence, the problem then is to estimate an average R* for the whole experiment. From the three methods mentioned above we choose the "initial rate method" for our closed system approach. Although laborious it is straight forward, neither assumption have to be made and nor constants have to be known in advance. Furthermore, this method also allows a precise correction of the measured trace element and isotope ratios for later corrections of the reservoir effect applying the Rayleigh distillation equations (c.f. Zeebe and Wolf-Gladrow (2003)). The "initial rate method" actually provides an excellent approximation of the average rate law within a certain time interval from the beginning of the precipitation experiment (t_0) to a certain time (t_1) at which the drop of [Ca] is linear. For example in Fig. 3 it can be seen that the values of randomly selected sample 38C can be approximated by a linear curve for about one third of the total experimental time and about 35% of the initial [Ca].

In contrast, Lemarchand et al (2004) used equation (20) in their experimental system to estimate R*(μmol/m^2·h), where the values for "n_2" and "k_f" are calculated for seawater and seawater like systems Zuddas and Mucci (1994). For NaCl-$CaCl_2$ solutions at 25 °C corresponding to ionic strength, I = 0.55 and I = 0.93 (n_2 = 3.34, log k_f = 6.24 and n_2 = 2.73, log k_f = 6.07, respectively) and [CO_3^{2-}] is in mM.

(20) Log R* = log k_f + n_2 log ([CO_3^{2-}]), where "k_f" is the rate constant "n_2" refers to the order of reaction

In contrast to Lemarchand et al (2004) we did not estimate R* rather measured it for every precipitate. In Fig. B and table C of the appendix we compare our measured R* values with those calculated using the Lemarchand et al (2004) approach. As it can be seen there is no relationship between the measured and estimated R* values which are except for two values tend to be

significantly lower than the measured ones. Hence, for further discussions we consider our approach and the measured R* value to be the best approach for the precipitation rate.

2.3.3. Strontium incorporation into calcite

In a closed system Sr incorporation into calcite can be described by Usdowski (1975) as:

(21) $([Sr]/[Ca])_{\text{bulk calcite}} = ([Sr]/[Ca])_{aq,0} \times \{\{1-([Ca]/[Ca]_0)^{DSr_{aq}}\}/\{1-([Ca]/[Ca]_0)_{aq}\}$.

Where $([Sr]/[Ca])_{\text{bulk calcite}}$ is the molar ratio of the bulk calcite, $([Sr]/[Ca])_{aq,0}$ is the molar ratio of these ions in the mother solution, $([Ca]/[Ca]_0)$ is the fraction of calcium that remains in aqueous solution at any time and D_{Sr} is the distribution constant of strontium between aqueous solution and the solid phase ($(([Sr]/[Ca])_{\text{bulk calcite}}/([Sr]/[Ca])_{aq}$). We validate this equation to our system of precipitation reactions as in Tang et al. (2008a) by plotting $\log\{([Sr]/[Ca]_{aq}/([Sr]/[Ca])_{aq,0}\}$ versus $\log([Ca]_{aq}/[Ca])_{aq,0})$. The slope of this relationship equals D_{Sr} -1 (see Fig C in the appendix and table 2.5 for more details).

From Fig. 2.6 we see for all temperatures as precipitation rate increase more strontium will be incorporated into calcite (D_{Sr} increases).There is one critical observation in the 25 °C data set for the lowest R* values where it seems that D_{Sr} depend on $(Sr/Ca)_0$ values. Whereas for the other data sets no such behavior can be recognized but can also not be excluded for R* values not covered by our study. Except for the 12.5°C data set it can be seen that at 25 and 37.5°C the values apparently reach kind of plateaus for low and high values of R*. For low R* this plateau may reflect the chemical equilibrium corresponding to a zero net growth. Whereas at higher R* the D_{Sr} may approach a distinct D_{Sr} value below about one. Beside the dependency on R* there is also a dependency on temperature visible in particular for lower growth rates below about 3.5 µmol/m^2·h. Although not well defined there is the tendency that at D_{Sr} is decreasing as temperature increases. This is actually an interesting observation indicating that influence of the precipitation rate R* and temperature affect D_{Sr} differently.

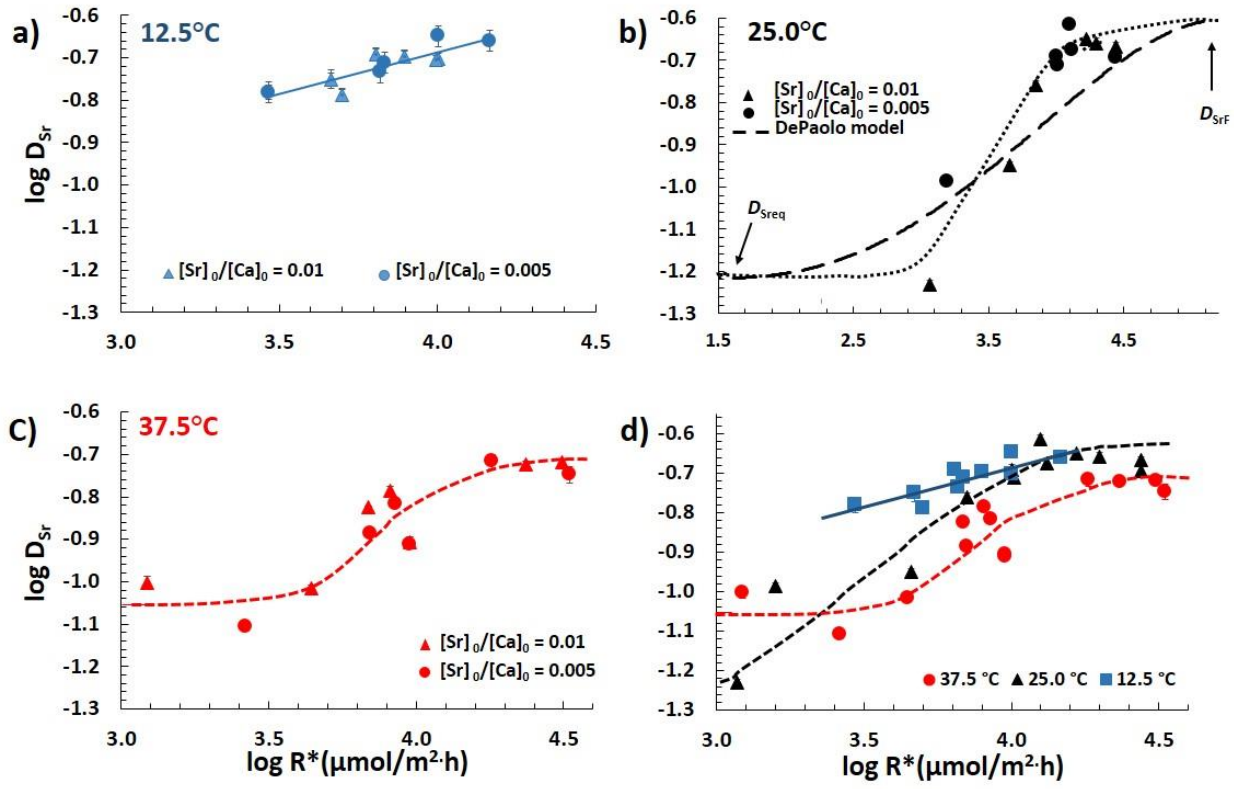

Figure 2.6: log D_{Sr} versus log R* (µmol/m^2·h) of calcite precipitated at **(a)** 12.5 °C, **(b)** at 25.0 °C of our results compared with DePaolo data model which is presented as dashed line curve, **(c)** 37.5 °C. Note, for all temperatures two different solutions have been measured (Sr/Ca ratios of 0.01 and 0.005 in order to verify the influence of different chemical compositions on the results. **d)** summarizes the results of the three experiments showing that there is a separate effect of temperature and precipitation rate. Temperature sets the initial value and rate is modifying the initial ratio following distinct rate dependent functions**.**

2.3.4. Isotope analysis

2.3.4.1 Results of Sr isotope fractionation measurements.

The $\delta^{88/86}$Sr value of the mother liquid solution was measured to be 0.175±0.002 ‰ (n = 4). For all temperatures (table 2.5, Fig. 2.7) as rate of precipitation increase more lighter Sr isotopes will be incorporated into calcite corresponding to decreasing $\Delta^{88/86}Sr_{calcite-aq}$ values. In contrast, as temperature increases the isotope difference to the mother solution decreases and isotope fractionation $\delta^{88/86}$Sr values increases at the same precipitation rate.

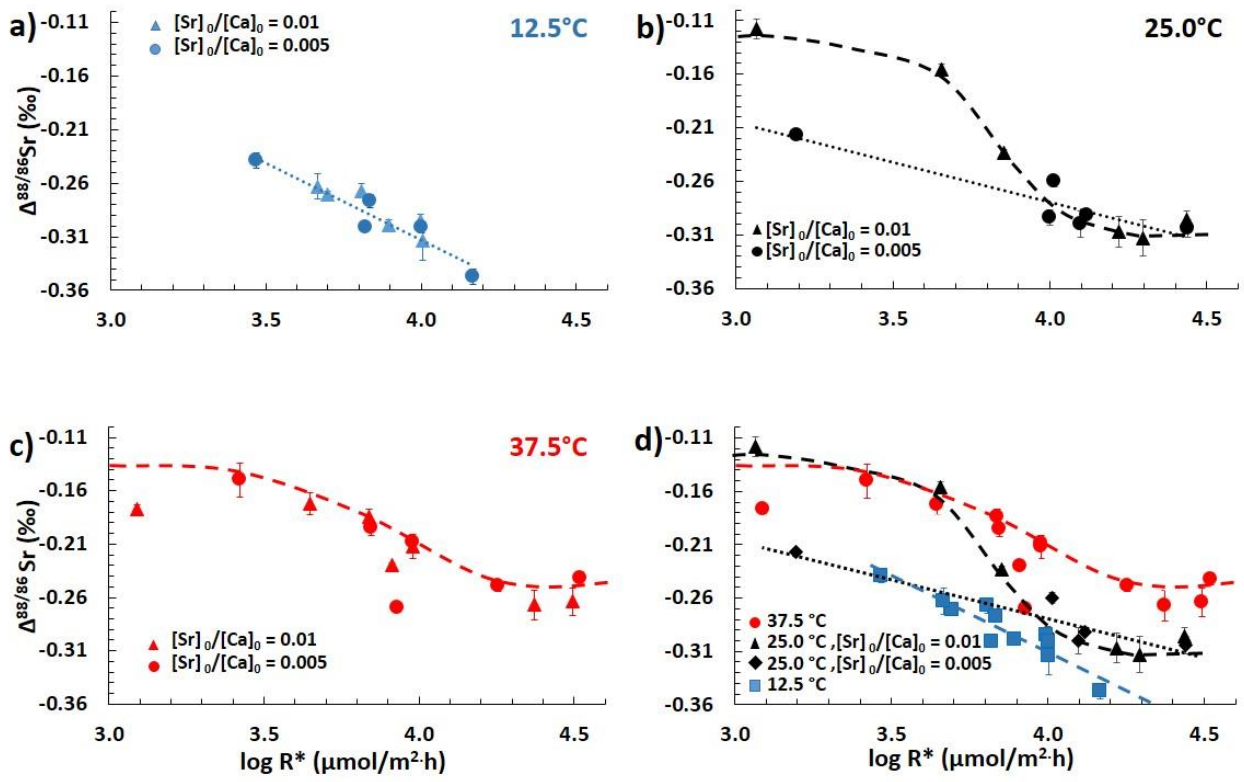

Figure 2.7: This diagram shows all $\Delta^{88/86}Sr_{calcite\text{-}aq}$ values as a function of their corresponding log R*(µmol/m^2·h) data. For all temperatures, as rate of reaction increases $\Delta^{88/86}Sr$ become more negative. Data approach equilibrium states at low and high rates of reaction at 25 and 37.5 °C (**b** and **c)** respectively). At 25 °C (b) above ~3.6 µmol/m^2·h the effect of the Sr/Ca ratio in the mother solution is insignificant. However, below ~3.6 µmol/m^2·h the 0.005 ratio solution tend to approach a lower equilibrium. Fig. **(d)** summarizes the data emphasizing the role of temperature showing that at constant precipitation rate initial $\Delta^{88/86}Sr_{calcite\text{-}aq}$ increase as a function of increasing temperature.

It is interesting to note that the Sr trace element partitioning and isotope fractionation in calcite resemble each other indicating that there is an inverse linear correlation between D_{Sr} and $\Delta^{88/86}$ Sr (Fig. 2.8). Relationships for the different temperatures are:

(22) **12.5 °C**: $\Delta^{88/86}Sr = -1.14\pm0.74\ D_{Sr} - 0.07\pm0.14$, $R^2 = 0.61$, $P = 0.008$

(23) **25.0 °C and [Sr]/[Ca]$_0$ = 0.01**

$$\Delta^{88/86}Sr = -1.22\pm0.24\ D_{Sr} - 0.033\pm0.044,\ R^2 = 0.98,\ P = 0.0002$$

(24) **25.0 °C and [Sr]/[Ca]$_0$ = 0.005**

$$\Delta^{88/86}Sr = -0.65\pm0.41\ D_{Sr} - 0.152\pm0.081,\ R^2 = 0.83,\ P = 0.01$$

(25) **37.5 °C**: $\Delta^{88/86}Sr = -0.91\pm0.32\ D_{Sr} - 0.086\pm0.048,\ R^2 = 0.78,\ P = 0.00006$

The confidence intervals in the above expressions were calculated at a 95% confidence level. Fig. 8 shows our results are in good agreement with results of inorganic precipitated calcite of Böhm et al (2012), since at 25°C the linear correlation was

(26) **25.0 °C and $[Sr]/[Ca]_o = 0.01$**

$$\Delta^{88/86}Sr = - 1.5\pm0.7\ D_{Sr} - 0.03\pm0.09, \qquad R^2 = 0.89,\ P = 0.002$$

Fig. 2.8 shows that this linear correlation between D_{Sr} and $\Delta^{88/86}$ Sr depends only on the precipitation rate but is completely independent of precipitation conditions (temperature and origin either biogenic or inorganic calcite), since all curves are overlapping with each other. The linear correlation between D_{Sr} and $\Delta^{88/86}$ Sr for all data points in Fig. 2.8 is presented by the solid line in the figure, it has the following general equation:

(27) $\Delta^{88/86}Sr = - 1.21\pm0.12\ D_{Sr} - 0.047\pm0.019, \quad R^2 = 0.89,\ P = 1.65E\text{-}25$

It is noteworthy to emphasize that the D_{Sr} -$\Delta^{88/86}$ $Sr_{\ calcite-aq}$ relationship depend only on the precipitation rate and hence mainly on [Ca] and [HCO_3^-], respectively. However, in contrast to [Ca] which rate of reaction is one the order of reaction for [HCO_3^-] varies from 1 to 3 as a function of temperature from 12.5 to 37.5°C, respectively. Hence, in particular for relatively cooler temperatures of 12.5 and 25 °C the influence of [HCO_3^-] is larger relative to [Ca] than for higher temperatures. As an example the inspection of sample 4 and 2 the Ca concentration is relatively high (see table 2.1, column 11, 4: [Ca] =19.84, 2: [Ca] = 9.74 mM at 25.0 °C), nevertheless R* is relatively low (see table 2.5, column 4, 4: log R* = 3.20, 2: log R* = 3.07). Concerning the [DIC] the situation is different and the two samples show the lowest concentrations of 2: 3.08 mM and 4.58 mM, respectively (see table 2.1, column 7). The order of reaction for HCO_3^- at 25°C is two in contrast to one for Ca which means that the effect of [DIC] on precipitation rate is much larger than the one of [Ca]. Hence, one can expect these samples to have lower R* values related to relatively high D_{Sr} but relatively low $\Delta^{88/86}$ $Sr_{\ calcite-aq}$ values as seen from table 2.5. Furthermore, looking at sample 3 it shows a relatively low [DIC] value of 5.75 mM and the lowest [Ca] at 25°C = 9.28 mM. However, due to the fact that at 25 °C the order of reaction is 2 R* shows a moderate value of (log R*=3.66) among the data points in table 2.5.

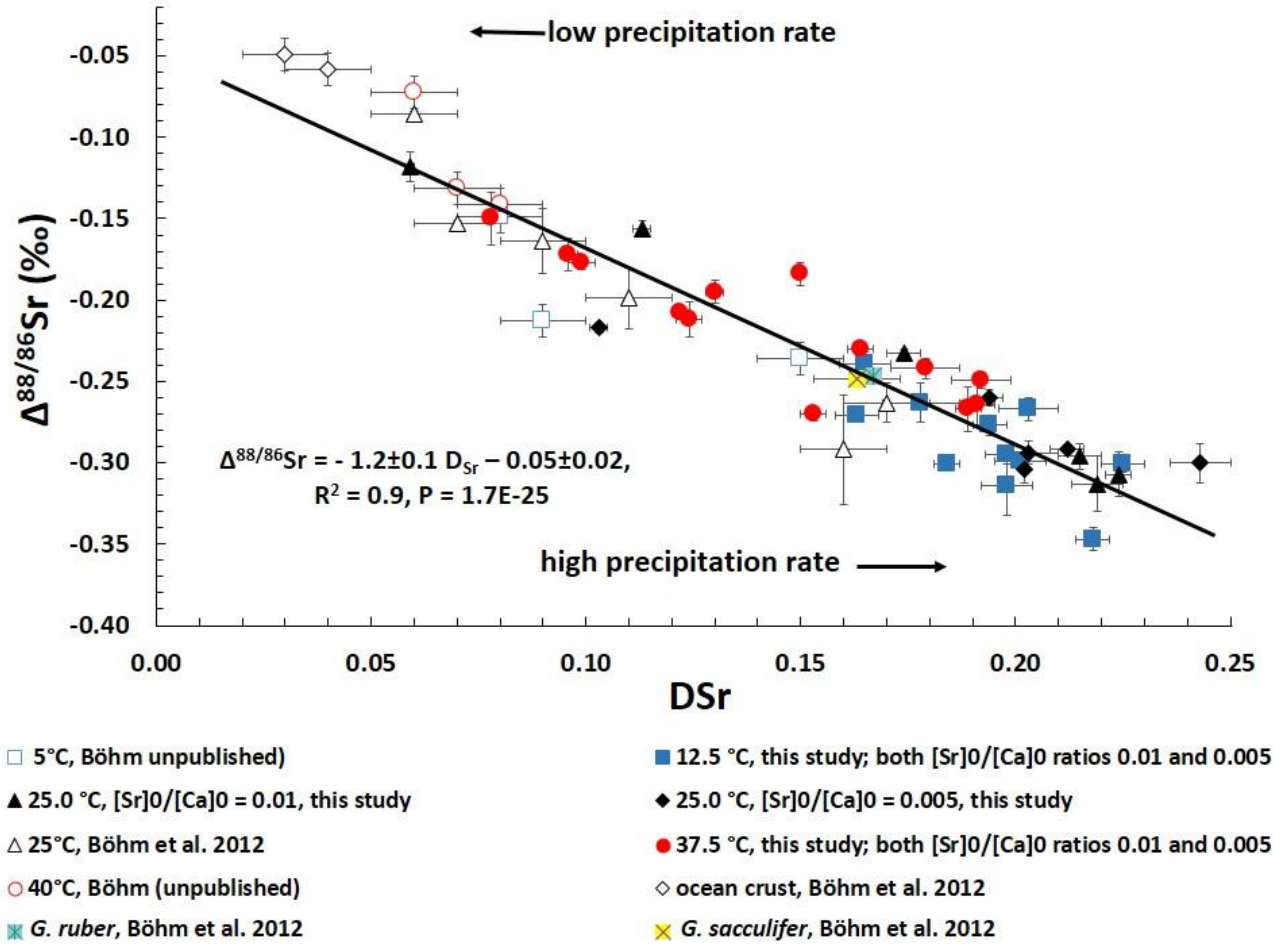

Figure 2.8: Linear correlation between $\Delta^{88/86}Sr_{calcite\text{-}aq}$ and D_{Sr} for all temperatures in this study, compared with some unpublished data (courtesy of Dr. Florian Böhm, GEOMAR) of inorganic precipitated calcite at 5 and 40°C and values of Böhm et al (2012) which includes results of inorganic precipitated calcite at 25 °C, calcites from ocean crust basalts and two species of planktic foraminifera (*Globigerinoides ruber* and *Globigerinoides sacculifer*). This Fig. shows that our result is in good agreement with literature values. Note: The solid line represents the average value of all data points in the figure.

2.3.4.2 Calcium isotope analysis

The results of the calcium isotope analysis are presented in Fig. 2.9 and in table 2.5, respectively. At 12.5 and 25.0 °C as rate of precipitation increase more heavier calcium isotopes will become incorporated into calcite which means that $\Delta^{44/40}Ca_{calcite\text{-}aq}$ values increase as a function of rate (Fig. 2.9 a, b). However at 37.5 °C as rate of precipitation increase the $\Delta^{44/40}Ca_{calcite\text{-}aq}$ decrease. Observations at 12.5 and 25.0 °C are in general accord with the earlier observations of

Lemarchand et al. (2004) at 20±1 °C. Whereas the record at 37.5°C resembles the earlier measurements of Tang et al. (2008b). However, there is one critical point marked by an arrow in Fig. 2.9b. This point is not falling along with the other points. Even more, extrapolating this single point to the rest of the data an inverse relationship between precipitation rate and calcium fractionation could be assumed liked at 37.5 °C. At higher rates above ~3.6 µmol/m^{2}·h the influence of temperature on the $\Delta^{44/40}Ca_{calcite\text{-}aq}$ values are minor whereas at lower rates below about ~3.6 µmol/m^{2}·h calcium isotopic fractionation largely depend on temperature with much more negative values for low temperature and higher values for higher temperatures (Fig. 2.9d).

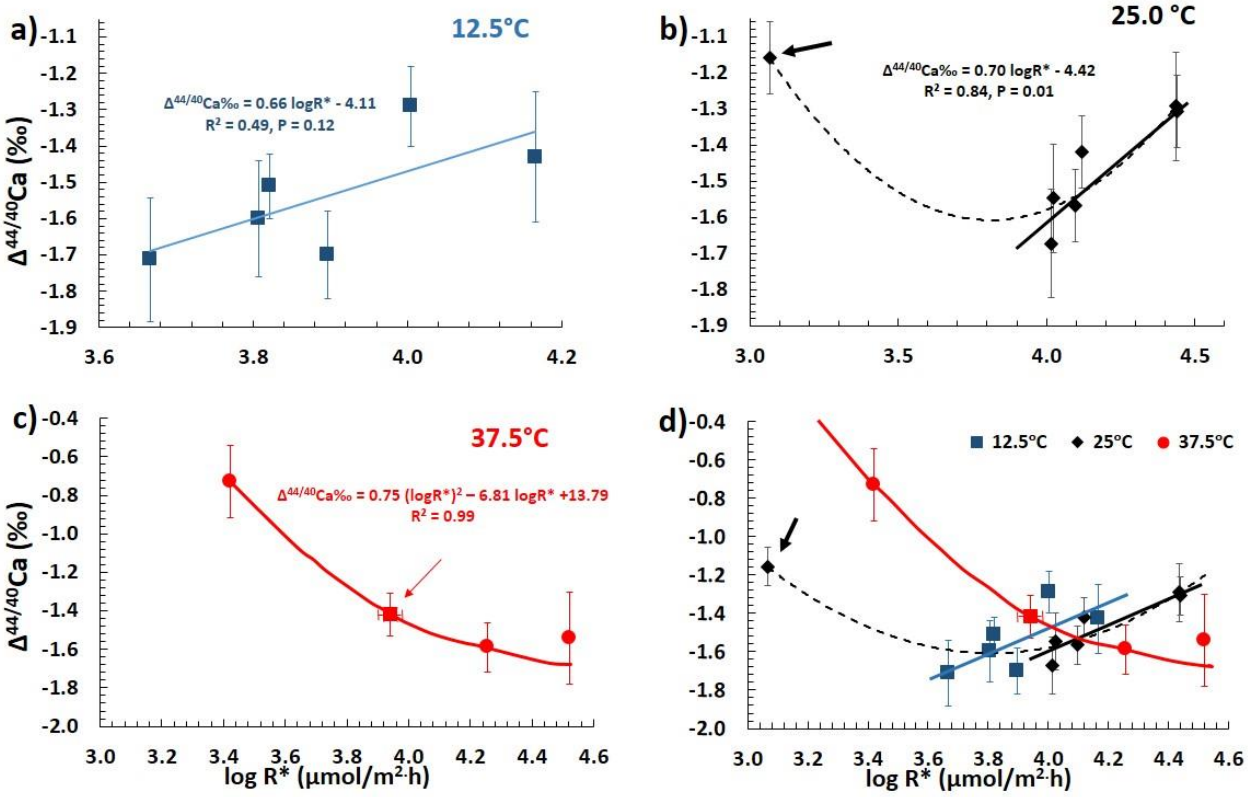

Figure 2.9: $\Delta^{44/40}Ca_{calcite\text{-}aq}$ as function of log R*(µmol/m^{2}·h) at 12.5 and 25.0 °C, respectively. As rate increase $\Delta^{44/40}Ca_{calcite\text{-}aq}$ become more positive ($\|\Delta^{44/40}Ca_{calcite\text{-}aq}\|$ decrease). It should be noted that the point marked with an arrow at 3.067 µmol/m^{2}·h can't be excluded because repeated measurement confirmed its reproducibility. In contrast, at 37.5 °C, as rate increase $\Delta^{44/40}Ca_{calcite\text{-}aq}$ values become more negative ($\|\Delta^{44/40}Ca_{calcite\text{-}aq}\|$ increase), the square point marked with an arrow in (c) is the average value of points 22B, 23C and 23D presented in table 2.5. Fig **(d)** summarizes the measurement emphasizing the role of temperature. Above a threshold value of ~3.6 µmol/m^{2}·h a temperature effect is negligible. However, below the threshold value temperature effect is significant the lower the temperature the lower are the $\Delta^{44/40}Ca_{calcite\text{-}aq}$ values the higher the amount of fractionation $\|\Delta^{44/40}Ca_{calcite\text{-}aq}\|$.

Table 2.5: Initial rate, rate normalized to surface area (R*), log R*, saturation index with respect to [amorphous CaCO3 (ACC), calcite and SrCO3], strontium distribution constant (DSr), log DSr, Δ88/86 Sr (‰) uncorrected and corrected values, Δ44/40Ca (‰) uncorrected and corrected values

Sample label	Initial rate/ mM/h	Normalized rate (R*)/ μmol/ m^{-2}h	log R*	SI. ACC	SI. calcite	SI. $SrCO_3$	D_{Sr}	±(2SEM)	Log D_{Sr}	±(2SEM)	$\Delta^{88/86}Sr$ (‰) uncorrected	$\Delta^{88/86}Sr$ (‰) corrected	±(2SEM)	$\Delta^{44/40}Ca$ (‰) uncorrected	$\Delta^{44/40}Ca$ (‰) corrected	±(2SEM)
1	2	3	4	5	6	7	8	9	10	11	12	13	14	15	16	17
20A	0.30	1230	3.09	1.10	1.32	2.22	0.099	0.003	-1.003	0.014	-0.173	-0.177	0.004			
20B	0.79	2640	3.42	1.14	1.36	1.98	0.078	0.002	-1.107	0.011	-0.145	-0.150	0.016	-0.49	-0.73	0.19
21A	3.17	6890	3.84	1.60	1.82	2.71	0.150	0.001	-0.824	0.003	-0.163	-0.184	0.007			
21B	2.90	7010	3.85	1.44	1.66	2.26	0.130	0.002	-0.886	0.005	-0.177	-0.195	0.007			
22A	3.06	9560	3.98	1.26	1.48	2.39	0.124	0.003	-0.906	0.012	-0.202	-0.212	0.011			
22B	2.84	9530	3.98	1.05	1.27	1.88	0.122	0.002	-0.912	0.006	-0.198	-0.208	0.004	-0.82	-1.24	0.09
23C	3.61	8170	3.91	1.53	1.75	2.65	0.164	0.003	-0.785	0.009	-0.199	-0.230	0.002	-0.41	-1.04	0.15
23D	3.85	8490	3.93	1.48	1.70	2.30	0.153	0.003	-0.816	0.010	-0.231	-0.270	0.004	-0.73	-1.97	0.10
47A	8.65	23580	4.37	1.21	1.43	2.28	0.189	0.003	-0.723	0.008	-0.242	-0.267	0.014			
47B	5.66	18030	4.26	1.13	1.35	1.91	0.192	0.007	-0.717	0.016	-0.233	-0.249	0.005	-1.07	-1.59	0.13
48C	8.62	31220	4.49	1.79	2.01	2.87	0.191	0.004	-0.719	0.009	-0.253	-0.264	0.013			
48D	8.69	33210	4.52	1.82	2.04	2.60	0.179	0.008	-0.748	0.020	-0.232	-0.242	0.006	-1.14	-1.54	0.24
6	2.54	4430	3.65	1.12	1.34	2.29	0.096	0.002	-1.016	0.009	-0.137	-0.172	0.010			
43C	7.54	27360	4.44	1.14	1.52	2.37	0.215	0.005	-0.668	0.009	-0.275	-0.296	0.008	-0.93	-1.29	0.15
43D	4.26	9990	4.00	1.32	1.70	2.26	0.203	0.007	-0.692	0.015	-0.257	-0.294	0.007			
44A	5.68	27510	4.44	1.02	1.41	1.94	0.202	0.001	-0.695	0.000	-0.292	-0.304	0.008	-1.06	-1.31	0.10
44B	3.70	13120	4.12	1.18	1.56	2.10	0.212	0.004	-0.674	0.009	-0.276	-0.292	0.001	-1.03	-1.42	0.10
45C	4.82	19720	4.30	0.71	1.10	1.93	0.219	0.006	-0.659	0.012	-0.297	-0.313	0.017			
45D	2.30	10320	4.01	0.76	1.15	1.69	0.194	0.003	-0.712	0.007	-0.250	-0.260	0.005	-1.33	-1.67	0.15
46E	5.01	16550	4.22	0.66	1.05	1.87	0.224	0.003	-0.65	0.006	-0.283	-0.307	0.014			

Sample label	Initial rate/ mM/h	Normalized rate (R*)/ µmol/ m^2h	log R*	SI. ACC	SI. calcite	SI. $SrCO_3$	D_{Sr}	±(2SEM)	Log D_{Sr}	±(2SEM)	$\Delta^{88/86}Sr$ (‰) uncorrected	$\Delta^{88/86}Sr$ (‰) corrected	±(2SEM)	$\Delta^{44/40}Ca$ (‰) uncorrected	$\Delta^{44/40}Ca$ (‰) corrected	±(2SEM)
46F	2.94	12490	4.10	0.57	0.95	1.48	0.243	0.007	-0.615	0.012	-0.282	-0.300	0.012	-1.22	-1.57	0.10
2	0.50	1170	3.07	0.48	0.86	1.75	0.059	0.001	-1.231	0.010	-0.111	-0.118	0.009	-0.54	-1.16	0.10
3	2.44	4520	3.66	0.82	1.20	2.11	0.113	0.002	-0.949	0.007	-0.123	-0.156	0.005			
4	1.10	1570	3.20	0.52	0.88	1.48	0.103	0.002	-0.987	0.008	-0.203	-0.217	0.003			
7	3.19	10471	4.02	0.82	1.20									-1.52	-1.55	0.15
8	3.65	7120	3.85	0.51	1.15	1.75	0.174	0.004	-0.76	0.010	-0.231	-0.233	0.003			
37A	4.56	10090	4.00	0.58	1.13	2.00	0.198	0.006	-0.703	0.012	-0.272	-0.314	0.018	-0.58	-1.29	0.11
37B	5.72	14660	4.17	0.48	1.03	1.61	0.218	0.004	-0.661	0.009	-0.305	-0.347	0.007	-0.79	-1.43	0.18
38C	2.31	7250	3.70	0.18	0.74	1.61	0.163	0.005	-0.789	0.013	-0.254	-0.271	0.004			
38D	2.71	6620	3.82	0.54	1.10	1.67	0.184	0.003	-0.735	0.007	-0.267	-0.301	0.003	-0.79	-1.51	0.09
39A	0.58	4630	3.67	0.27	0.83	1.70	0.178	0.009	-0.751	0.021	-0.260	-0.263	0.012	-1.52	-1.71	0.17
39B	0.46	2940	3.47	0.27	0.83	1.41	0.165	0.006	-0.782	0.017	-0.234	-0.239	0.007			
40C	1.75	6410	3.81	0.18	0.73	1.61	0.203	0.007	-0.693	0.014	-0.252	-0.267	0.007	-1.15	-1.60	0.16
41E	2.08	7870	3.90	0.40	0.95	1.83	0.201	0.006	-0.698	0.012	-0.278	-0.299	0.005	-1.24	-1.70	0.12
41F	2.1	6840	3.84	0.39	0.95	1.53	0.194	0.004	-0.712	0.010	-0.260	-0.277	0.006			
42A	2.67	9930	4.00	0.55	1.11	1.99	0.198	0.005	-0.704	0.010	-0.275	-0.295	0.006			
42B	2.19	10050	4.00	0.48	1.03	1.62	0.225	0.005	-0.648	0.009	-0.285	-0.301	0.005			

Notes: For all reactions the initial rate (mM/h) was calculated according to the initial rate law (see text). R* is calculated according to equation 19 in the text. SI of different minerals (columns 5, 6 and 7) are calculated as in appendix 3. DSr is calculated from equation 21. Columns 12 and 15: these columns show the measured isotope values of Sr and Ca respectively, uncorrected for the reservoir effect. Columns 13 and 16: are the corrected values of columns 12 and 15 respectively using equations 7 and 8 in the text.

2.4. Discussion

2.4.1. Strontium incorporation in calcite

Although not seen for the 12.5°C data set for the higher temperatures at 25.0 and 37.5 °C we observe a non-linear behavior where the D_{Sr} values approach plateaus for relatively high and low R* (Fig.2. 6). In the surface entrapment model of Watson (2004) it is assumed that the trace element and isotope ratios reflect the fluxes of ions and isotopes from the liquid towards the solid and from the solid towards the liquid. It is suggested that the growing crystal will have the composition of its surface unless diffusion of trace metal ions from its interior toward the fluid-solid transition competes with the uptake of Sr from the fluid during growth. Away from chemical equilibrium conditions (R*≈0) and for all temperatures (see Fig. 2.6) as R* increase more Sr will become incorporated. However, at very slow rates almost approaching equilibrium the diffusion rate toward the fluid-solid transition is high enough to maintain a chemical equilibrium with the input flux characterized by a distinct value (D_{Sreq}). We estimate the equilibrium D_{Sreq} at 25.0 °C ≈ 0.06 (log D_{Sreq} ≈ -1.22) and at 37.5 °C ≈ 0.09 (log D_{Sreq} ≈ -1.05), respectively. Latter values are slightly larger than those estimated earlier by Tesoriero and Pankow (1996) who estimated D_{Sreq} to be 0.021±0.003 at 25 °C, in Lorens (1981) and to be 0.027±0.011 and 0.034 as well as 0.039 at 40 and 98 °C in Katz et al (1972) respectively. However, our D_{Sreq} value for the 25°C experiment of 0.06 fits quite well into the predicted range of values (0.020 - 0.07) estimated earlier by DePaolo (2011) depending on the conditions of the precipitating solution. Note, below a R* of ~3.6 μmol/m^2·h there is an increasing superimposing effect of T on R* causing the log D_{Sr} values to deviate from each other to a larger extend.

At relatively high R* D_{Sr} remains constant (D_{SrF}) which equals K_f in the DePaolo (2011) publication. At this steady state for 25.0 °C we estimate D_{SrF} (K_f) to be ≈ 0.24 (log D_{SrF} ≈ -0.62) as can be seen from Fig. 2.6b. Latter value is in agreement with the estimation for K_f of DePaolo (2011) to be 0.24 at 25.0 °C. In Fig .2.6c we calculated D_{SrF} ≈ 0.19 (log D_{SrF} ≈ -0.72) for the 37.5 °C experiment.

We compared our results of log D_{Sr} versus log R* (μmol/m^2·h) at 25.0 °C with the model data of DePaolo (2011) which is the dashed line in Fig. 2.6b. The parameters of the DePaolo model are: (R_b) = 2160 (μmol/m^2·h) which is held constant in the DePaolo model and considered the dissolution rate of calcite in pure water at 25.0 °C. The net R* (R_p) in the DePaolo model (R* in our study) correspond to a range of values from 32 to 100.000 μmol/m^2·h as it can be seen from

Fig. 2.6b. For calculation we took D_{Sreq} (K_{eq}) = 0.06 (log (-1.2) in Fig 2.6b) which we extrapolated from our experimental results and D_{SrF} (K_f) = 0.24 (log (0.24) ≈ -0.62 in Fig. 2.6b). It can be seen from Fig. 2.6b that our results are in general accord with DePaolo model.

2.4.2. Calcium and strontium isotopic fractionation in calcite

The Ca isotope aspect of the current study is based on the discrepant observations of Lemarchand et al. (2004) and Tang et al. (2008). Arguments have been put forth by DePaolo 2011, Nielsen et al. (2012) and Watkins et al. (2013) that the Lemarchand et al and the Gussone et al (2004, 2005) datasets were performed at saturations that exceeded the solubility of amorphous Ca carbonate (ACC). Thus they are not expected to be consistent with the Tang et al. (2008) data. Our data are not in favor of this model because, at 37.5 °C the saturation index values ($SI_{ACC;}$ table 2.5, column 5) for ACC are higher than at any other temperature used so far and hence the probability of forming ACC is expected to be high nevertheless this data show a Tang et al. (2008) like behaviour.

Furthermore, the transition from spiral growth to 2D nucleation may have a significant influence on the fractionation of $\delta^{44/40}Ca$ (Nielsen et al. 2012). However, our data show that spiral (dislocation driven) growth mechanism is totally excluded since $SI_{calcite}$ >0.34 (table 2.5, column 6) for all sample reactions. However 2D nucleation mechanism is still theoretically possible since $\Omega_{calcite}$ > 0.43 Teng et al. (2000).

The contradiction of our data to this earlier explanation implies that there must be alternative models. In order to provide a model to reconcile the discrepant observations we assume that at lower temperatures up to about 25 °C NH_3 complexes with Ca^{2+} to form a Ca^{2+}-NH_3-aquacomplex by a coordinate covalent bonding (Fig. 2.10). The formation constant of this reaction ($K_{formation}$= ($[CaNH_3]^{2+}$/$[NH_3][Ca^{2+}]$) is about one (Bjerrum 1941 and Seward 1954). We calculated the average fraction of Ca^{2+}-ions bonded to NH_3 is 0.60±0.07 NH_3-ligands per Ca^{2+} in our experimental conditions based on the experimental results of Seward (1954). In order to reach a minimum oscillation potential between Ca^{2+} and NH_3 the covalent bonding of the Ca^{2+}-NH_3-aquacomplex prefers the isotopically heavy Ca-isotopes where the bonding energy (c.f. Criss (1999)) is inversely related to the isotope mass ($\Delta E \approx 1/m$). In this case relatively more light Ca isotopes are statistically available to leave the coordinated complex to become incorporation into the $CaCO_3$ lattice. Whereas relatively more heavy Ca^{2+}-isotopes remain complexed and dissolved in solution. At a certain relatively low temperature and R* the $\Delta^{44/40}Ca_{calcite\text{-}aq}$ value is

low because more light Ca isotopes are available for incorporation into the calcite lattice. However, increasing the HCO_3^- concentration and hence R*, respectively, will shorten the mean free path travel time (Rohlf (1994)) between ions. This increases the internal energy of the system allowing relatively more heavy Ca isotopes to overcome the binding energy of the Ca^{2+}-NH_3-aquacomplex to eventually become incorporated into the calcite lattice. Hence, $\Delta^{44/40}Ca_{calcite\text{-}aq}$ correlates positively to the calcite R*. This type of fractionation was observed in Lemarchand et al. (2004) already at about 20°C and is in general accord with our observations at 12.5 and 25°C, respectively.

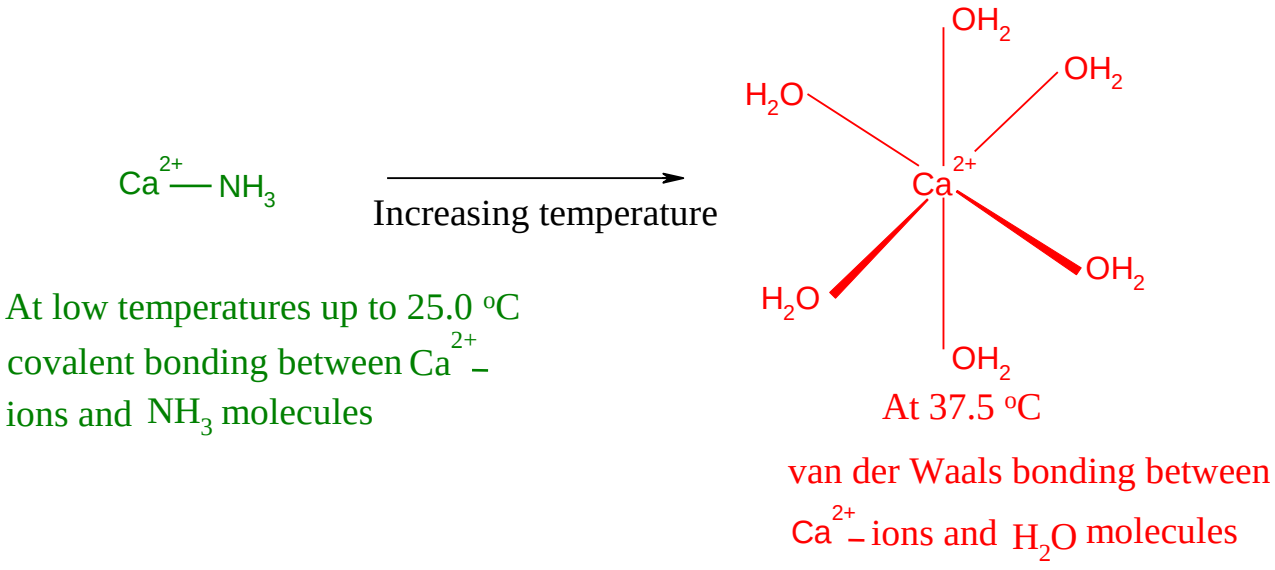

Figure 2.10: Schematic illustration of our qualitative model. At and below ~25 °C the Ca^{2+}-ions form a Ca^{2+}-NH_3-aquacomplex with a relative strong covalent bonding between Ca^{2+} and NH_3. This type of bonding is following isotope equilibrium type fractionation were the heavier isotope is preferred for bonding guaranteeing a low potential energy. Hence, the lighter isotopes are statistically more available for precipitation in $CaCO_3$.
However, with increasing rate and increasing internal energy more heavy isotopes are statistically available then leading to a positive rate-$\Delta^{44/40}Ca_{calcite\text{-}aq}$ relationship. In contrast above a temperature of ~25 °C (e.g. at 37.5 °C) the Ca^{2+}-NH_3-aquacomplex is changing towards a Ca^{2+}-H_2O-aquacomplex which is formed by a relatively weak van-der-Waals bonding. In latter case only the reaction velocity matters preferring the isotopically lighter Ca^{2+}-ions (kinetic isotope fractionation). As a function of higher internal energy and precipitation rates more and more lighter isotopes are statistically incorporated forming an inverse rate-$\Delta^{44/40}Ca_{calcite\text{-}aq}$ relationship.

However, increasing the temperature to about 37.5 °C eventually water molecules will replace NH_3 and solvate the Ca^{2+}-ions. Hence at a certain temperature above ~25°C there is a transition from a Ca^{2+}-NH_3-aquacomplex to a Ca^{2+}-H_2O-aquacomplex (Irving and Williams (1953)). In this

regard, we may speculate that the temperature range around 25 °C marks the transition from Ca^{2+}-NH_3 to Ca^{2+}-H_2O complexation. Probably, at low R* the transition from the Ca^{2+}-NH_3 to Ca^{2+}-H_2O already occurs at 25°C as indicated by one data point in Fig 2.9b but not at the higher R*. Definitely this is still speculation considered to be preliminary until final verification.

In contrast to the Ca^{2+}-NH_3-aquacomplex we infer that the bonding between the Ca^{2+}-ion and the H_2O-molecules is a weak electrostatic (van der Waals) bonding different from the covalent bonding. In particular this means that the equilibrium between the strong distracting electrostatic forces of the protons and the attracting nuclear forces do not play any distinct role anymore. In the absence of these forces causing covalent bonding the only process able to fractionate ions is the kinetic velocity of the ions and the chemical reaction itself. This means the higher the internal energy and R* the higher is the discrimination between light and heavy isotopes. Having the same amount of energy the lighter isotope is simply traveling faster than the heavier one ($v \approx \sqrt{(2 \cdot \Delta E/m)}$). This results in an enrichment of lighter isotopes in the product as a function of increasing rate (the $\Delta^{44/40}Ca_{calcite\text{-}aq}$-value decreases but the amount $\|\Delta^{44/40}Ca_{calcite\text{-}aq}\|$ increases). The temperature effect on $\Delta^{44/40}Ca_{calcite\text{-}aq}$ is almost insignificant in the range between 12.5 to 25.0 °C and at R* above ~3.6 µmol/m^2·h. The influence of temperature may become more obvious at lower rates of reaction (< 3.6 µmol/m^2·h) when the temperature is raised to 37.5 °C (Fig. 2.9d).

Our explanation offered here to explain the change of slope as a function of temperatures for the discrepancy between Lemarchand et al. (2004) and Tang et al. (2008) is based on a difference in the preferred complexation of Ca in solution as a function of temperature. Tang et al (2008) reported the opposite trend to the Lemarchand et al (2004) data at all temperatures of 5, 25 and 40°C. In particular, the 40°C dataset did not show the trend described here for the weak electrostatic explanation although also NH_3 has been in the solution. Latter discrepancy is most likely simply based on [NH_4Cl] which was set to 5 mM in the Tang et al. (2008) experiment in contrast to our solution set to 395 mM (similar to Lemarchand et al (2004)) and about a factor of 80 higher than in the Tang et al. (2008) approach. Hence, in our solution the [Ca] : [NH_3] ratio is about one and the effect can be expected to be seen.

Multiple recent studies (c.f. Nielsen et al. 2012) have demonstrated that the [Ca[:[HCO_3^-] ratio in solution influence the carbonate R*. Hence some influence of this potential effect on both R* and either Ca and Sr isotope fractionation should be recognized. In our study the [Ca] : [HCO_3^-] ratio in the solution range between 0.66 to 2.41, with an average ratio of ~1.54. As seen from Fig

2.11 we do not recognize any relationship between [Ca] : [HCO_3^-] and R*. The same observations accounts for the [Ca] : [HCO_3^-] to $\Delta^{44/40}Ca_{calcite\text{-}aq}$ relationship at least for the 12.5 and 25°C data. However, in the 37.5°C data set there is a significant positive [Ca] : [HCO_3^-] to $\Delta^{44/40}Ca_{calcite\text{-}aq}$ relationship in the order of about 0.5 ‰. Latter spread of data may account for about one third of the spread of the $\Delta^{44/40}Ca_{calcite\text{-}aq}$ from about -0.6 to about -1.8 ‰. We speculate that the sudden dependency of the [Ca]:[HCO_3^-] ratio of the 37.5 °C data set to the $\Delta^{44/40}Ca_{calcite\text{-}aq}$ values in contrast to the 12.5 and 25 °C data may reflect the switch from a Ca^{2+}-NH_3 to a Ca^{2+}-H_2O dominated complex system. Note, according to (Andersson et al (2016)) carbonate (CO_3^{2-}) and bicarbonate (HCO_3^-) ions can be regarded as single species because the reaction free energy for both is similar. During HCO_3^- surface adsorption, i.e. terraces as well as step sites, it deprotonate spontaneously at any pH for which $CaCO_3$ is stable. In order to also account for this recent finding we do plot [Ca] : [DIC] rather than [Ca] : [HCO_3^-] in Fig. 2.11.

A similar effect of changing slopes at different temperatures is not observed for the Sr isotopes. Probably because of its lower ionic potential based on the larger ionic radius (Sr^{2+}~132 pm; Ca^{2+} ~114 pm) solvation of Sr with water molecules is more dominant than the formation of covalent bondings with NH_3 during solvation. Furthermore, it is also well known that Sr is not complexing with most ligands due its lower ionization potential when compared to Ca (Irving and Williams (1953)). In this case only kinetic fractionation is observed like for Ca at 37.5 °C.

In this regard as rate increase more lighter Sr isotopes will incorporated into calcite and $\Delta^{88/86}Sr_{calcite\text{-}aq}$ decreases ($\|\Delta^{88/86}Sr_{calcite\text{-}aq}\|$ increase). The presence of $\Delta^{88/86}Sr_{calcite\text{-}aq}$ plateaus at lower and higher R* values do not necessarily imply equilibrium type fractionation but can also be reached by kinetic fraction as modelled by DePaolo (2011). Following the DePaolo (2011) model the lower plateau is reached because the backward reaction is dominated whereas the higher plateau is reached because the forward reaction is dominated.

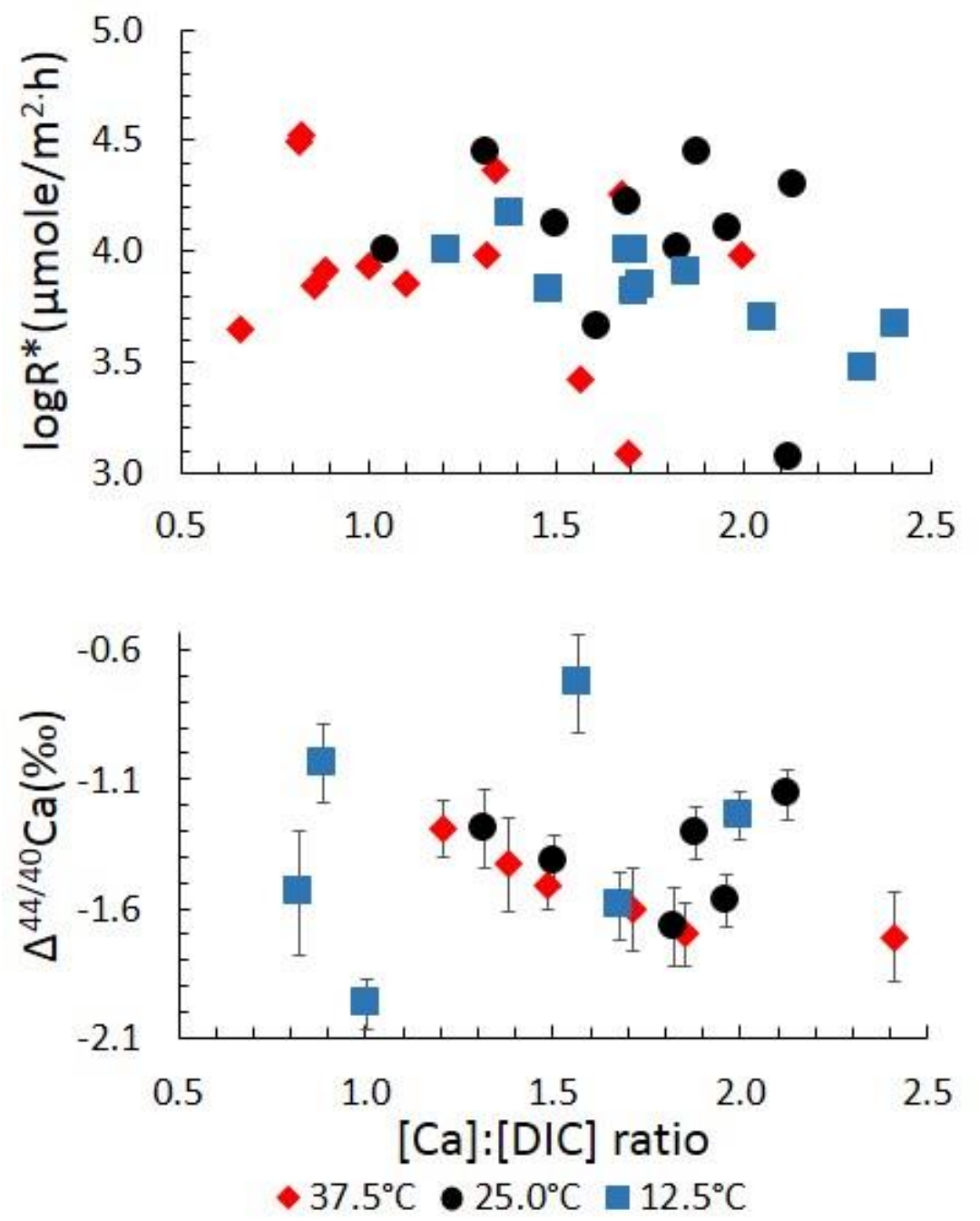

Figure 2.11: Effect of [Ca]: [DIC] ratio on both precipitation rate and $\Delta^{44/40}Ca_{calcite\text{-}aq}$

2.5. Implications

One major implication of the results of this study is that the chemical composition of the bulk solution has a major influence on the Ca isotope composition. Latter observation may be used to study the kinetics of solute complexation in more detail.

The finding that there is a strong inverse D_{Sr}-$\Delta^{88/86}Sr_{calcite-aq}$ relationship just depending on R*has major implications for the marine paleo-sciences. In addition, latter observation may also be applied as a self-consisting criterial for chemical dagenesis and alteration. This is because any original D_{Sr}-$\Delta^{88/86}Sr_{calcite-aq}$ pair of data must fall along the line as seen from Fig. 2.8.

Temperature dependency for both Ca- and Sr-isotopes only matters for low R* whereas for higher rates the influence diminishes. This implies that the $\Delta^{88/86}Sr_{calcite-aq}$ values in carbonate are less suited for paleo-temperature reconstructions.

The finding that the order of reaction for [HCO_3^-] changes as a function of increasing temperature from three to one, respectively, implies that at lower temperatures [HCO_3^-] has a much stronger influence on R* than [Ca].

2.6. Summary

- The mechanism of calcite precipitation is T and R* dependent, the order of reaction with respect to Ca^{2+} ions is first order while the order with respect to HCO_3^- changes from 1 via 2 to 3 as temperature decrease from 37.5 via 25.0 to 12.5 °C, respectively.
- Strontium incorporation in calcite increase with increasing R* but decrease with increasing temperature. However, the sensitivity of the temperature-D_{Sr} relationship strongly depend on R* and is largest for lower rates.
- Strontium isotope fractionation during the precipitation of calcite is controlled by kinetic processes only. There is no influence of chemical complexation visible as for the Ca isotopes. This is probably because of Sr´s lower ionic potential solvation dominanted by H_2O molecules only.
- Ca isotope fractionation depend on the complexation with either NH_3 or H_2O switching between equilibrium type like isotope fractionation as seen earlier from Lemarchand et al (2004) and a kinetic type like fractionation as seen by Tang et al (2008b).

- At constant rate for both Sr and Ca isotopes their fractionation factors $\Delta^{88/86}Sr_{calcite\text{-}aq}$ and $\Delta^{44/40}Ca_{calcite\text{-}aq}$ become more positive but $\|\Delta^{88/86}Sr_{calcite\text{-}aq}\|$ as well as $\|\Delta^{44/40}Ca_{calcite\text{-}aq}\|$ decrease as temperatures increase.
- An important conceptual observation is that the effect of temperature and rate are decoupled. While the temperature sets the initial conditions of Sr and Ca elemental discrimination and isotope fractionation R* modifies this initial value accordingly.temperature- D_{Sr} relationship is most sensitive for lower R* (<3.5 µmol/m^{2}·h).
- Our inferences concerning Ca and Sr elemental and isotope fractionation are based on a limited range of R* (~3 to 4.5 µmol/m^{2}·h), whereas the Lemarchand et al (2004) and the Tang et al (2008) experiments include calcite R* down to ~2 µmol/m^{2}·h. In addition, we observed that the chemical composition e.g. changes of the initial Sr/Ca ratio $Sr/Ca]_0$ may influence chemical participation and isotope fractionation. Therefore we are fully aware that we are possibly not capturing the full range of Sr and Ca behaviour during calcite precipitation, and that significant discrepancy's to those observed in this study may be expected under higher or lower R*.

Chapter 3

In its present form the chapter below has been submitted for publication to Geochimica Cosmochimica Acta.

Calcium and Strontium Isotope Fractionation during Precipitation from Aqueous Solutions as a Function of Temperature and Reaction Rate; II. Aragonite

Abstract: In order to study Magnesium (Mg) and Strontium (Sr) partitioning and isotope fractionation in aragonite we performed precipitation experiments decoupling temperature and precipitation rate (R*). Only aragonite is the pure solid phase precipitated from a stirred solutions (0.395 M NH_4Cl, 10.0 mM $CaCl_2$, 30 mM $MgCl_2$, 0.10 and 0.05 mM $SrCl_2$) exposed to an atmosphere of NH_3 and CO_2 gases throughout the spontaneous decomposition of $(NH_4)_2CO_3$. The order of reaction with respect to Ca ions is one and independent of temperature. However, the order of reaction with respect to the dissolved inorganic carbon (DIC) is temperature dependent and decreases from three and two to one as temperature increases from 12.5 and 25.0 to 37.0 °C respectively. Strontium distribution coefficient (D_{Sr}) increases with decreasing temperature. However, concerning R* it responds differently depending on the initial Sr/Ca concentration and temperature: at 37.5°C D_{Sr} increase as a function of increasing R* but decrease for 12.5 and 25 °C. At 25°C D_{Sr} is also sensitive to the initial Sr/Ca ratio in contrast to the temperatures above and below. Magnesium distribution coefficient between aragonite and aqueous solution (D_{Mg}) decreases with temperature but increases with R* in the range of 2.4 to 3.8 μmol/m^2·h. Strontium isotope fractionation ($\Delta^{88/86}Sr_{aragonite\text{-}aq}$) follows the kinetic type of fractionation and become increasingly negative reflecting the isotopic difference between aragonite and bulk solution to increase as a function of R*. In contrast Ca isotope fractionation ($\Delta^{44/40}Ca_{aragonite\text{-}aq}$) shows a different behavior than the Sr isotopes. At low temperatures (12.5 and 25°C) Ca isotope fractionation ($\Delta^{44/40}Ca_{aragonite\text{-}aq}$) becomes slightly positive as a function of R*. However, at 37.5°C and as a function of increasing R* the $\Delta^{44/40}Ca_{aragonite\text{-}aq}$ show a Sr type like behavior and become increasingly negative. Concerning both the discrepant behavior of D_{Sr} as a function of temperature as well as for the Ca isotopes as a function of temperature we infer that

the solubility increasing effect of increasing Mg^{2+} -concentrations controls the material flux back (R^*_{detach}) from the crystal to the solution to a large extend. As a consequence R* values for aragonite tend to be lower than for calcite. Except for the rate the Ca isotope fractionation behavior is the same for calcite and for aragonite. This is particular true for the switch of direction in Ca isotope fractionation above about 25°C. We consider this switch either to be due to the Mg^{2+} blocking effect or due to the switch of complexation from NH_3 at and below 25 °C to H_2O at 37.5 °C. The D_{Sr} - $\Delta^{88/86}Sr_{aragonite\text{-}aq}$ correlation for calcite is independent of temperature in contrast to aragonite. Latter correlation may have important implications as a self-consistent criteria for the verification of carbonate alteration.

3.1. Introduction

From the three main calcium carbonate ($CaCO_3$) polymorphs, aragonite, calcite and vaterite, aragonite is the second most abundant in the marine environment (c.f. Morse and Mackenzie 1990 and Morse et al. 2007) where it is produced either by uni- and multicellular calcifying organisms or by inorganic precipitation processes. Aragonite preferentially incorporates alkaline-earth metals like Sr^{2+}, Mg^{2+}, and Ba^{2+} as trace elements of which their concentrations and ratios reflect the chemical conditions in the adjacent water during mineral precipitation. Being of particular interest in paleoceanography for the reconstruction of seawater temperatures Sr/Ca ratios usually expressed as the distribution coefficient D_{Sr} ($[Sr/Ca]_{CC}/[Sr/Ca]_{SW}$) shows an inverse relationship with temperature during calcification (c.f. Weber 1973, Smith et al. 1979, De Villiers et al. 1994). Along inorganic pathways D_{Sr} approaches the thermodynamic expected equilibrium. However, in biologically mediated $CaCO_3$ the D_{Sr} values tend to be off the expected thermodynamically value, an effect generally known as the "vital effect". The latter effect reflects the physiological control of the calcifying organisms and the species dependent biomineralization pathways for $CaCO_3$ precipitation. In the recent past various studies (Beck et al. 1992, Gagan et al. 1998, Gaetani et al. 2011,). Beck et al. (1992) showed that Sr/Ca ratios in coral skeletons are not only dependent on temperature but also on the Sr/Ca ratio in seawater itself which can also be used to reconstruct the composition of paleo-water as well as the diagenetic reactions that involve carbonate sediments (Scherer and Seitz 1980, Enmar et al., 2000). Ever since many experimental studies have been carried out to study the kinetics of precipitating aragonite, isotopic fractionation and trace element discrimination between aqueous

solution and inorganic precipitated aragonite (e.g. c.f. Kinsman and Holland 1969, Burton and Walter 1987, Dietzel et al. 2004, Gaetani and Cohen 2006, Niedermayr et al. 2013, Gabitov et al. 2008, Gabitov 2013 and Kim et al. 2014). Most studies focused on the effect of temperature on the Sr/Ca ratio in aragonite in terms of D_{Sr} showing that these values decrease with increasing temperature. However, only a few data are available about the kinetics of inorganic precipitation of aragonite and how R* affects simultaneously $D_{Sr,}$ D_{Mg} and the isotope fractionation of both Ca- and Sr isotopes during inorganic precipitation of aragonite.

Although it has been discussed that Ca ($\delta^{44/40}$Ca) and Sr ($\delta^{88/86}$Sr) isotopes measured in aragonite may be used as proxies to reconstruct environmental conditions from the adjacent seawater (Fantle and Higgins 2014). Up to now there are only few studies available about Ca isotope fractionation during inorganic aragonite precipitation (c.f. Gussone et al. 2003). Even more, no study is yet available about Sr isotope fractionation during inorganic aragonite precipitation.

This lag of data and information is the impetus for this study, in which we precipitated aragonite at three different temperatures (12.5, 25.0 and 37.5±0.2 °C) from buffered aqueous ammonium by controlled diffusion of CO_2 (g) and NH_3 (g) with a wide range of R*. Note, this study extends and completes a similar study we have performed concerning calcite. Experimental setup, chemical solutions (except for the Mg concentration) and equations are identical with the calcite study (chapter 2).

3.2. Material and Methods

3.2.1 Materials and Experimental Setup

The experiments performed to precipitate aragonite is based on the earlier set up as described in chapter 2 to precipitate calcite (Fig. 2.1). All solutions to precipitate aragonite are the same as in chpter 2 except for the molar [Mg/Ca] ratio which we set for this study to be 3:1.

3.2.2 Analysis

3.2.2.1 Dissolved in organic carbon (DIC)

The details to determine [DIC] in our system has been described earlier in chapter 2.

3.2.2.2 Elemental analysis

Elemental analysis have been performed in the same way as described in chapter 2. In brief, the JCP-1 Sr/Ca and Mg/Ca ratios were calculated to be 8.80±0.06 and 4.18 ±0.03 mmol/mol respectively, which matches within statistical error the reported values of 8.84±0.09 Sr/Ca and 4.2 ±0.1 Mg/Ca mmol/mol of Hathorne et al. (2013). The average uncertainty for our Sr/Ca mmol/mol ratios is 0.04 and for Mg/Ca mmol/mol is 0.02 corresponding to the 95% confidence level.

3.2.2.3 Crystalline structure and specific surface area of aragonite products

The crystalline structure of the solid products were determined the same way as in chapter 2.

Specific surface area of the final aragonite products were analyzed applying the Brunauer-Emmett-Teller (BET) gas adsorption method (De Kanel and Morse 1979). Of the total number of 35 aragonite samples we analyzed 23 having enough material (60 mg) to become analyzed by the BET method. Measurements were carried out at the Ruhr Bochum University, Germany, Institute of Geology, Mineralogy and Geophysics.

For the late comparison of rates during calcite (Alkhatib and Eisenhauer (under review)) and aragonite (this study) we note that R* values for calcite have been determined via SEM measurements in contrast to the applied BET method in this study. Although both methods deliver reasonable values as expected we have yet no information about the compatibility of the two methods. Hence we consider the comparisons based on R* for calcite and aragonite pending until further confirmation.

3.2.2.4 Strontium and calcium isotope analysis

Isotope measurements for Ca and Sr isotope were carried out at the GEOMAR mass spectrometer facilities in Kiel, Germany, with a ThermoFisher Triton T1 Thermal-Ionization-Mass-Spectrometer (TIMS) as it is described in chapter 2.

3.3 Results

As discussed in chapter 2 the concentrations of NH_3 and NH_4 in our experimental setup are about one order of magnitude higher when compared f.e. with the concentrations used in Tang et al. (2008). Latter fact inhibits the calculations of activity coefficients applying geochemical

modeling and the PHREEQC software. Consequently, all calculations are based on concentrations only.

3.3.1 pH, TA, NH_3, DIC, metal ions concentrations and saturation indexes with respect to different forms of $CaCO_3$ and with respect to $SrCO_3$.

In chapter 2 we show the details of calculating acid dissociation constant of ammonium ions (K_a) as function of temperature and molar concentrations of different alkaline species in reacting solutions (NH_3, HCO_3^- and CO_3^{2-}). Throughout the reaction the pH of the reacting solution (when precipitation starts) remains relatively constant (±0.02 units) as well as the temperature of all reactions (±0.2 °C). During the course of the experiment we determined the total alkalinity (TA) by online measurement and verified that TA of the precipitation solutions is kept constant within ±10% throughout time. Concentrations of [NH_3], [HCO_3^-] and [CO_3^{2-}] were calculated as in chapter 2. Details on carbonate speciation, [DIC] as well as the metal ion concentrations in the initial and final solutions are summarized in table 3.1. Saturation state (Ω) is calculated from Millero (1995):

(1) $\Omega = [Me^{2+}][CO_3^{2-}]/k_{sp}$, saturation index (SI) = log Ω,

where Me is Sr or Ca and k_{sp} is the solubility product constant of the solid product. Values of k_{sp} of aragonite, amorphous $CaCO_3$ (ACC) and $SrCO_3$ are shown in table 3.2. It can be seen from table 3.4 that all sample reactions are over saturated with respect to aragonite, ACC and $SrCO_3$.

Table 3.1: Temperature, total alkalinity (TA), pH, salinity, concentration of ammonia [NH_3], dissolved inorganic carbon (DIC), carbonate and bicarbonate ions concentrations, mole fraction of bicarbonate in DIC, initial and final concentrations of both Ca and Sr and their remaining fraction at the end of each experiment, mmol Sr/mole Ca and mmol Mg/mole Ca in aragonite, ratio of initial $[Ca]_0$ to the concentration of the dissolved inorganic carbon (Ca_0: DIC), Sr: Ca ratio in the mother solution ($[Sr]_0/[Ca]_0$), volume of aqueous solution, moles of $CaCO_3$ produced and its surface area.

Sample label	T/ °C± 0.2	TA/ mM	pH	Salinity	$[NH_3]$ / mM	DIC / mM	$[CO_3]$/ mM	$[HCO_3]$ / mM	Mole fraction Of $[HCO_3^-]$in [DIC]	$[Ca]_0$ / mM	$[Ca]_f$ / mM	Fraction of Ca remain	$[Sr]_0$ / mM	$[Sr]_f$ / mM	Fraction of Sr remain	mmoSr/molCa in aragonite	mmolMg/molCa in aragonite	$[Ca]_0$:[DCI]	$[Sr]_0/[Ca]_0$	Volume of solution /ml	Moles of $CaCO_3$	Area of $CaCO_3$ / m^2
1	2	3	4	5	6	7	8	9	10	11	12	13	14	15	16	17	18	19	20	21	22	23
50C	37.5	57.93	8.629	34.7	42.05	15.88	4.97	5.94	0.54	10.22	3.03	0.30	0.100	0.029	0.29	9.94	4.14	0.64	0.010	400	0.00288	0.768
50D	37.5	74.83	8.722	35.0	52.86	21.97	7.41	7.15	0.49	10.11	2.13	0.21	0.049	0.010	0.20	5.06	5.30	0.46	0.005	400	0.00319	0.852
51E	37.5	27.35	8.230	35.2	16.57	10.78	2.16	6.47	0.75	10.33	4.86	0.47	0.101	0.046	0.46	10.06	2.67	0.96	0.010	400	0.00219	0.584
51F	37.5	30.67	8.293	35.5	19.19	11.49	2.50	6.48	0.72	10.16	4.30	0.42	0.049	0.020	0.41	4.96	2.83	0.88	0.005	400	0.00234	0.626
52G	37.5	32.63	8.344	35.1	21.56	11.07	2.57	5.93	0.70	10.61	5.81	0.55	0.051	0.027	0.53	4.91	2.58	0.96	0.005	400	0.00192	0.513
52H	37.5	31.36	8.327	35.1	20.71	10.65	2.42	5.80	0.71	10.13	6.59	0.65	0.099	0.064	0.65	10.02	2.37	0.95	0.010	400	0.00142	0.378
24A	37.5	21.98	8.130	38.2	13.10	8.88	1.54	5.80	0.79	11.16	5.30	0.47	0.110	0.052	0.47	9.92	2.16	1.26	0.010	550	0.00322	0.861
24 B	37.5	19.05	8.080	38.8	11.63	7.42	1.19	5.04	0.81	11.19	5.79	0.52	0.056	0.029	0.52	4.80	2.15	1.51	0.005	550	0.00297	0.793
25D	37.5	45.23	8.452	35.6	28.06	17.17	4.52	8.12	0.64	10.50	2.42	0.23	0.052	0.012	0.23	4.98	5.08	0.61	0.005	550	0.00445	1.187
26E	37.5	32.53	8.300	35.4	19.57	12.96	2.85	7.26	0.72	10.42	2.59	0.25	0.103	0.025	0.24	9.74	2.76	0.80	0.010	550	0.00431	1.151
26F	37.5	28.13	8.235	35.8	16.78	11.35	2.29	6.77	0.75	10.39	3.65	0.35	0.052	0.018	0.35	4.89	3.55	0.92	0.005	550	0.00371	0.990
27H	37.5	29.01	8.242	35.7	17.08	11.93	2.43	7.07	0.74	10.32	3.52	0.34	0.103	0.034	0.33	9.84	3.27	0.87	0.010	550	0.00374	0.998
28A	25.0	21.49	8.156	36.3	13.80	7.69	1.00	5.70	0.85	10.73	7.58	0.71	0.109	0.071	0.65	10.51	1.91	1.40	0.010	550	0.00174	0.464
28B	25.0	21.59	8.160	36.4	13.93	7.66	1.00	5.66	0.85	10.39	6.88	0.66	0.053	0.033	0.62	5.62	1.65	1.36	0.005	550	0.00193	0.515
29C	25.0	27.26	8.223	35.0	16.24	11.02	1.60	7.82	0.83	10.31	4.25	0.41	0.105	0.038	0.37	10.32	3.49	0.94	0.010	550	0.00333	0.890
29D	25.0	21.69	8.116	35.2	12.63	9.06	1.10	6.86	0.86	10.11	4.85	0.48	0.051	0.022	0.43	5.33	2.63	1.12	0.005	550	0.0029	0.773
30E	25.0	19.15	7.944	35.3	8.53	10.61	0.94	8.74	0.90	10.12	4.53	0.45	0.103	0.040	0.39	10.44	3.14	0.95	0.010	550	0.00307	0.820

Sample label	T/ °C± 0.2	TA/ mM	pH	Salinity	[NH_3] / mM	DIC / mM	[CO_3]/ mM	[HCO_3] / mM	Mole fraction Of [HCO_3^-]in [DIC]	[Ca]$_0$ / mM	[Ca]$_f$ / mM	Fraction of Ca remain	[Sr]$_0$ / mM	[Sr]$_f$ / mM	Fraction of Sr remain	mmoSr/molCa in aragonite	mmolMg/molCa in aragonite	[Ca]$_0$:[DCI]	[Sr]$_0$/[Ca]$_0$	Volume of solution /ml	Moles of $CaCO_3$	Area of $CaCO_3$ / m^2
30F	25.0	20.32	8.029	35.2	10.36	9.96	1.03	7.90	0.88	10.34	4.23	0.41	0.051	0.019	0.37	5.40	3.17	1.04	0.005	550	0.00336	0.897
31A	25.0	45.62	8.370	35.3	23.41	22.21	4.05	14.12	0.78	10.05	1.49	0.15	0.103	0.012	0.11	10.54	5.90	0.45	0.010	550	0.00471	1.256
31B	25.0	40.15	8.348	35.2	22.03	18.12	3.19	11.73	0.79	10.09	1.63	0.16	0.052	0.006	0.12	5.35	4.35	0.56	0.005	550	0.00465	1.241
49A	25.0	35.27	8.386	34.6	23.67	11.60	2.16	7.27	0.77	10.11	4.33	0.43	0.049	0.020	0.40	5.28	4.83	0.87	0.005	400	0.00231	0.617
49B	25.0	39.86	8.438	34.5	26.78	13.08	2.62	7.83	0.75	10.17	4.18	0.41	0.049	0.019	0.38	5.18	5.79	0.78	0.005	400	0.0024	0.640
9	25.0	15.20	7.820	79.0	7.90	7.30	0.55	6.20	0.92	142.77	132.39	0.93	1.550	1.411	0.91	12.41	3.88	19.56	0.011	400	0.00415	1.109
10	25.0	22.30	8.069	40.0	12.10	10.20	1.05	8.10	0.89	18.54	9.77	0.53	0.236	0.111	0.47	12.50	6.20	1.82	0.013	400	0.00351	0.936
11	25.0	21.67	8.113	35.0	13.37	8.30	0.87	6.57	0.88	8.96	2.82	0.31	0.120	0.032	0.26	12.60	3.34	1.08	0.013	400	0.00246	0.656
32A	12.5	12.89	7.791	36.2	5.95	6.95	0.29	6.37	0.96	10.49	5.44	0.52	0.104	0.048	0.46	12.22	1.44	1.51	0.010	550	0.00278	0.741
32B	12.5	15.63	7.850	36.4	6.84	8.79	0.41	7.96	0.95	10.40	7.16	0.69	0.052	0.034	0.65	6.11	2.28	1.18	0.005	550	0.00178	0.475
33C	12.5	17.68	8.028	35.1	10.27	7.41	0.50	6.40	0.93	10.39	7.33	0.71	0.104	0.072	0.69	12.14	2.23	1.40	0.010	550	0.00168	0.449
33D	12.5	16.61	8.004	35.0	9.71	6.90	0.45	6.01	0.93	10.18	6.86	0.67	0.051	0.032	0.63	6.11	2.36	1.48	0.005	550	0.00183	0.488
34E	12.5	20.71	8.029	35.0	10.37	10.34	0.70	8.93	0.93	10.31	4.39	0.43	0.102	0.038	0.37	11.42	3.83	1.00	0.010	550	0.00326	0.870
34F	12.5	22.18	8.000	35.3	9.75	12.42	0.80	10.83	0.93	10.26	3.53	0.34	0.050	0.014	0.28	5.73	3.86	0.83	0.005	550	0.00371	0.989
35A	12.5	16.51	7.962	35.0	8.83	7.68	0.46	6.77	0.94	9.89	6.58	0.67	0.101	0.062	0.61	11.61	4.31	1.29	0.010	550	0.00182	0.486
35B	12.5	18.27	8.002	35.3	9.70	8.56	0.55	7.46	0.93	9.75	5.06	0.52	0.050	0.022	0.44	5.84	3.91	1.14	0.005	550	0.00258	0.688
36C	12.5	21.10	8.071	35.2	11.41	9.70	0.72	8.26	0.92	9.76	5.42	0.56	0.100	0.050	0.50	11.41	5.96	1.01	0.010	400	0.00174	0.464
36D	12.5	26.47	8.167	35.3	14.31	12.16	1.08	10.00	0.90	9.77	3.82	0.39	0.050	0.016	0.32	5.58	6.88	0.80	0.005	400	0.00238	0.636

Notes: TA was measured from titrating the final solution with HCl, pH and salinity were measured at the end of each reaction. [NH3], [CO32-], [DIC] and [HCO3-] were calculated as in Lemarchand et al. (2004) and (Alkhatib and Eisenhauer, submitted). Mole fraction of HCO_3^- (column10) = column 9 / (column 9 + column 8). Initial and final concentration of Ca and Sr (columns 11- 18) are measured by ICP-MS. Column13 = column 12 /column 11. Column16 = column 15 /column 14. Column19 = column 11/ column 7. Column 20 = column 14/ column 11. Column 22 = [(column 11 - column 12)*column 21]*10^{-6}. Column 23 = column 22 x 267 m^2/mole.

Table 3.2: Ksp of aragonite, ACC and strontianite.

T/°C	$K_{sp\text{-}aragonite} * 10^7$	$K_{sp\text{-}ACC} * 10^7$	$K_{sp\text{-}SrCO3} * 10^{10}$
37.5	6.13	6.17	4.98
25.0	6.60	9.09	5.36
12.5	6.87	13.85	5.24

Notes: K_{sp}-aragonite calculated as in Millero (1995) at salinity (S) = 35.5 except for samples 9 and 10 K_{sp} = $35.60*10^{-7}$ and $7.71*10^{-7}$ respectively, K_{sp}-ACC as in Clarkson et al. (1992) and K_{sp}-SrCO3 as in Busenberg et al. (1984).

3.3.2 Kinetics of aragonite formation reactions

3.3.2.1 Initial rate of reaction (R) and the order of reaction with respect to Ca and bicarbonate ions

In order to determine R we applied the "initial rate method". This method and its advantages relative to other methods to determine R* has been extensively discussed in chapter 2 and will not be repeated here. Similar the equations applied to describe the kinetics of the aragonite chemistry is the same than the one for calcite. All values directly pertinent to this study are summarized in tables 3.3 and 3.4.

Table 3.3: Order of reactions with respect to HCO_3^- ions and the rate constant at three different temperatures.

T/ °C	Order of reaction with respect to DIC	Rate constant $mM^{-x}\cdot h^{-1}$
1	**2**	**3**
12.5	3	1.01×10^{-4}
25.0	2	17.32×10^{-4}
37.5	1	154.67×10^{-4}

Note: Values of this table are obtained by treating data as described in chapter 2 part 2.3.2.2.

From a fit of our three calculated rate constants (table 3.3) at 12.5, 25 and 37.5°C we fit the Arrhenius equation:

(2) $\ln k = -\frac{E_a}{RT} + \ln A$, k is the rate constant ($mM^{-x}\cdot h^{-1}$),

where x is the order of reaction with respect to bicarbonate ions E_a = activation energy, R = gas constant (8.314 J/°K·mole)) and T(°K) is the temperature, A ("frequency factor") is a constant which corresponds to the intercept of the line at $1/T = 0$ (at infinite temperature).

From the slope calculated to be ~ -17881 we can estimate E_a for the aragonite formation to be ~149 kJ/mole about ~ 45 kJ/mole higher than the one for calcite (chapter 2). Latter value for aragonite is in general agreement with the expectation to have Ea for aragonite to be higher than the one for calcite. The comparison with literature data as reported by Romanek et al (2011) who estimated E_a of inorganic precipitated aragonite using a seeded-growth technique, in absence of both ammonia and ammonium to be 71.2 kJ/mole. Probably, latter slight discrepancy between the data is attributed to different experimental setups and the use of seed crystals.

When E_a is higher than 50 kJ/mole, precipitation mechanism is surface or chemical-controlled and not diffusion-controlled (Petrou and Terzidaki (2014), Gutjahr et al. (1996a)). Which means that transport of material to the mineral surface from the bulk solution through a distinct boundary layer is not the rate determining step. Rather processes at the solid surface might be the rate determining step, which includes adsorption of reactive solutes to the surface itself, surface diffusion, bond formation or cleavage, ionic exchange with the solid and loss of solvent water (Morse et al. (2007)).

3.3.2.2 Crystalline Structure and Precipitation Rate Normalized to the Surface Area.

X-ray diffraction showed that 100% of all solid products are pure aragonite without detecting any amount of $SrCO_3$ in any of the solid samples even though all samples are oversaturated with respect to strontianite ($SrCO_3$) (table 3.4). SEM images showed that aragonites precipitated similar under different experimental conditions having needle like crystalline structures as shown in Fig. 3.1. From Fig. 3.2 it can be seen that the specific surface areas (S) of aragonite products are independent of temperature and R. Hence it can be assume that S of all aragonite products are equal to the average value 2.67±0.2 m^2/g or equivalent to 267±20 m^2/mole (± is 1σ). From this value the normalized rate of reaction **R*** (μmol/m^2·h) is calculated from equation 19 as in chapter 2 and summarized in table 3.4. Note that the specific surface area of aragonite is a factor of 4.5 higher than the one of calcite estimated to be 59 m^2/mole (chapter 2).

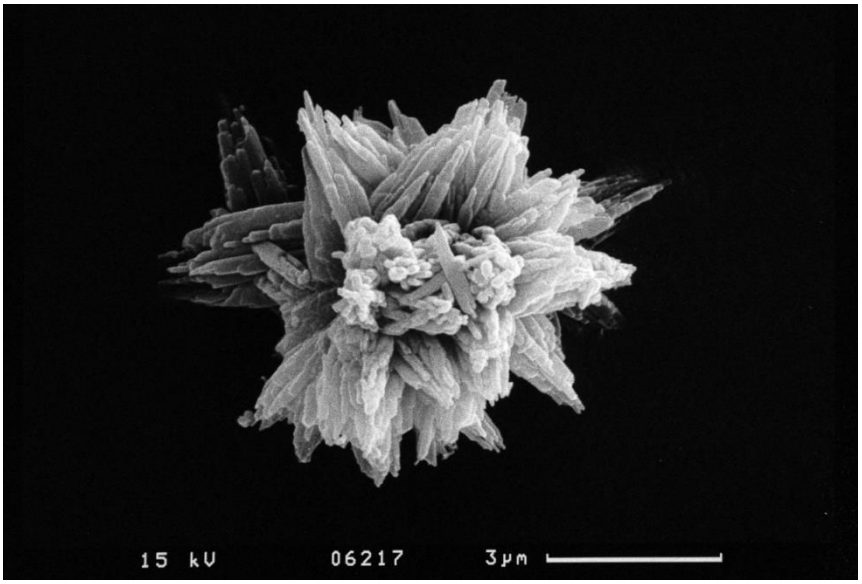

Figure 3.1: SEM images of a typical aragonite aggregate (from experiment 35B).

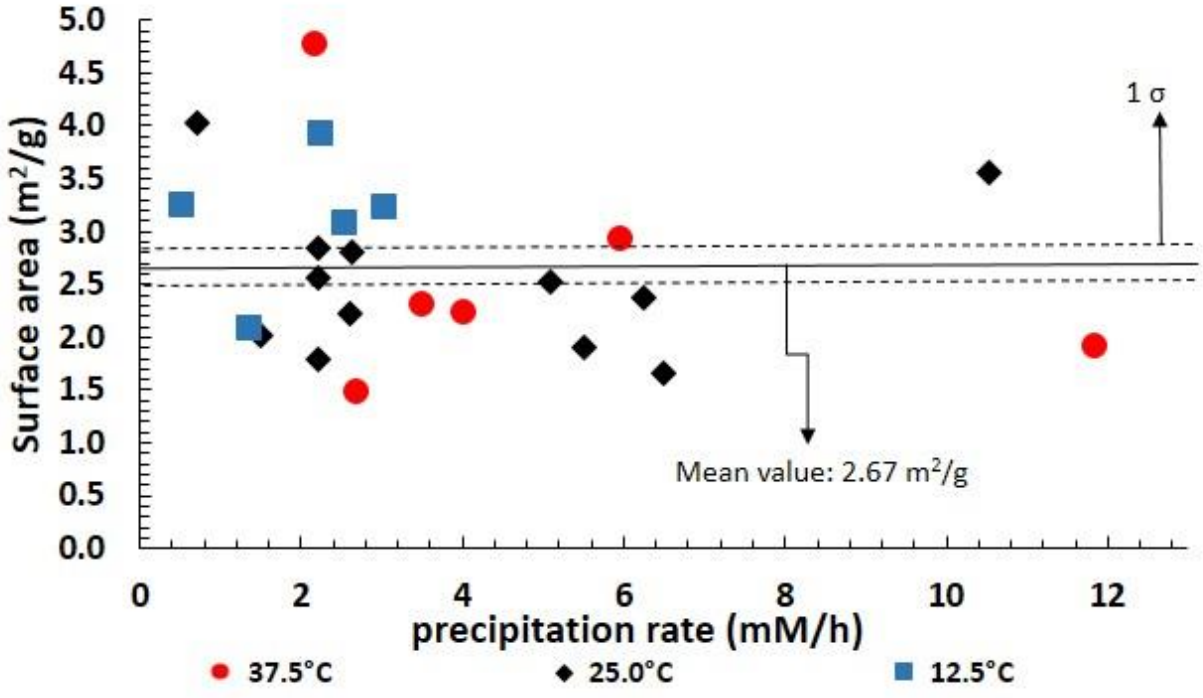

Figure 3.2**:** Specific surface area (S) determined by the BET method (BET= Brunauer-Emmett-Teller gas adsorption method) of some aragonite products versus precipitation rate (mM/h) at different temperatures. The value of S is independent of both temperature and precipitation rate. The average value of S corresponds to 2.67±0.2 m^2/g. Note: solid line represents the mean value and the area within dashed lines 1-sigma error of the mean.

3.3.3 Strontium and magnesium incorporation into aragonite

Incorporation of Sr and Mg can be calculated among other approaches described by the equation of Holland et al. (1963) and Usdowski (1975) where D_{Sr} and D_{Mg} are the distribution coefficients as defined in chapter 2. Although both equations deliver results which agree within 2% we arbitrarily use the equation of Usdowski (1975) which was also used by Tang et al (2008) for compatibility.

From Fig. 3.3 it can be seen that at 12.5°C as R* increases D_{Sr} values decrease without any dependency on the initial $([Sr]/[Ca]_{0,aq})$-ratio in the reacting solution. However at 25.0°C a discrepant behavior of D_{Sr} values can be observed. At a $([Sr]/[Ca]_{0,aq})$ initial ratio of 0.01 D_{Sr} values tend to increase as a function of rate. In contrast when the initial $([Sr]/[Ca]_{0,aq})$ ratio is 0.005 mmol/mol D_{Sr} values tend to decrease. At 37.5°C as R* increases D_{Sr} values increase without any significant effect of the initial $([Sr]/[Ca]_{0,aq})$ ratio. Moreover, it can be seen that temperature effect on the D_{Sr} values is more significant than the rate effect itself. The R*- D_{Sr} relationships are:

(3) **37.5 °C**: $\log D_{Sr} = 0.03\pm0.01 \log R^* - 0.10\pm0.04$, $R^2 = 0.80$, P = 9.40E-05

(4) **25.0 °C and $[Sr]/[Ca]_0 = 0.01$**

$\log D_{Sr} = 0.04\pm0.04 \log R^* - 0.08\pm0.14$, $R^2 = 0.53$, P = 0.065

(5) **25.0 °C and $[Sr]/[Ca]_0 = 0.005$**

$\log D_{Sr} = -0.02\pm0.02 \log R^* + 0.11\pm0.08$, $R^2 = 0.53$, P = 0.1

(6) **12.5 °C**: $\log D_{Sr} = -0.03\pm0.02 \log R^* + 0.17\pm0.05$, $R^2 = 0.69$, P = 0.0028

From Fig. 3.4 it can be seen that D_{Mg} values increase with increasing R* but decreases as temperature increase. The dependency on R* can be determined as follows:

(7) **37.5 °C**: $\log D_{Mg} = 0.16\pm0.22 \log R^* - 3.73\pm0.76$, $R^2 = 0.22$, P = 0.127

(8) **25.0 °C**: $\log D_{Mg} = 0.38\pm0.16 \log R^* - 4.34\pm0.51$, $R^2 = 0.77$, P = 3.82E-04

(9) **12.5 °C**: $\log D_{Mg} = 0.66\pm0.18 \log R^* - 5.04\pm0.53$, $R^2 = 0.90$, P = 2.58E-05

D_{Mg} values may also depend on [Mg]. The D_{Mg} values of samples 9 (430 mM) and 10 (60 mM) precipitated at 25 °C (marked by arrows in Fig. 4) are much higher when compared to the other samples precipitated at the same temperature but with [Mg] values of only 30 mM.

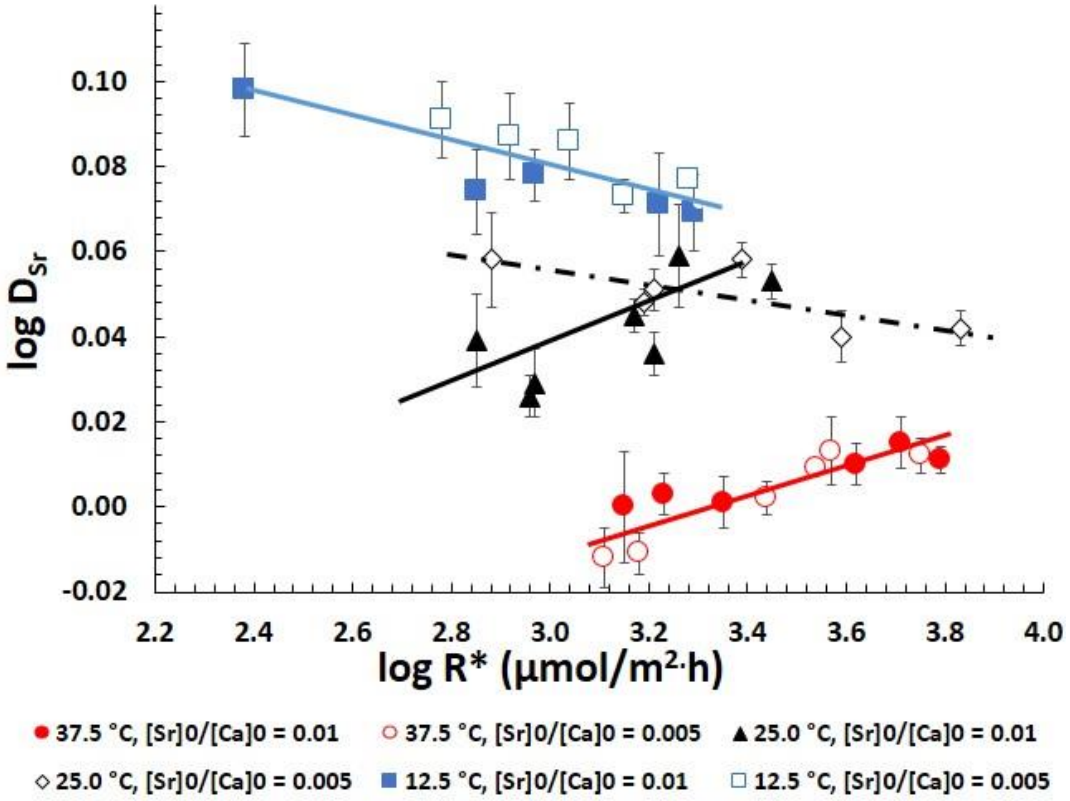

Figure 3.3: Log D_{Sr} versus log R* (µmol/m^2·h) of aragonite precipitated at different temperatures. Two different solutions have been measured (Sr/Ca ratios of 0.01 and 0.005) in order to verify the influence of different chemical compositions on the results. It can be seen that the relation of log R* is different for certain temperatures and rates. In particular, this figure shows a separate effect of temperature and precipitation rate.

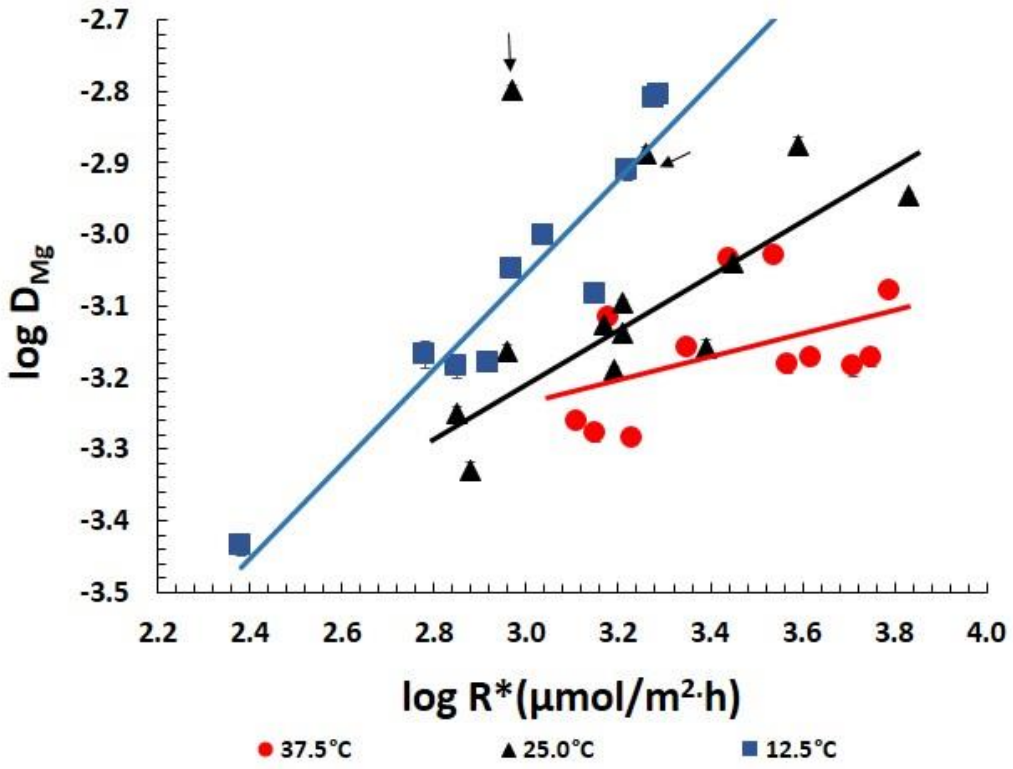

Figure 3.4: This figure shows log D_{Mg} at different temperatures versus log R* (µmol/m^2·h). The log D_{Mg} values increase with increasing R* and with decreasing temperature, clearly indicating that there is a separate effect of temperature and R*. Note: black triangles represent reactions 9 and 10 (marked by arrows) at 25.0 °C which have a higher Mg^{2+} concentration (430 and 60 mM respectively).

3.3.4 Strontium and calcium isotopes

The $\delta^{88/86}Sr$ value of the bulk solution was measured to be 0.173±0.002 ‰ (n = 4), and $\delta^{44/40}Ca$ = 0.98±0.09 ‰ (n = 20). In order to avoid reservoir effects we are reporting Sr and Ca isotopic fractionation in the Δ-notation: $\Delta^{88/86}Sr_{aragonite\text{-}aq} = \delta^{88/86}Sr_{aragonite} - \delta^{88/86}Sr_{initial\ solution}$ and $\Delta^{44/40}Ca_{aragonite\text{-}aq} = \delta^{44/40}Ca_{aragonite} - \delta^{44/40}Ca_{initial\ solution}$, respectively. All Δ-values are corrected for Rayleigh distillation effect according to equation (7) in chapter 2. Uncorrected and corrected values of $\Delta^{88/86}Sr_{aragonite\text{-}aq}$ and $\Delta^{44/40}Ca_{aragonite\text{-}aq}$ are summarized in table 3.4.

As it can be seen for the Sr isotopes for all temperatures in Fig. 3.5 and table 3.4 as R* increases $\Delta^{88/86}Sr_{aragonite\text{-}aq}$-values become more negative. This implies that more light Sr isotopes will become incorporated into aragonite with increasing R*. In addition there is no effect of the initial ratio $[Sr]/[Ca]_{0,aq}$ on Sr isotopic fractionation. However, at 25 °C the two values (of samples 10 and 11) show unexpectedly low $\Delta^{88/86}Sr$ without any particular reason. Therefore a lab error

cannot be excluded and will be neglected for further discussions. All Sr isotope data are summarized in Fig 3.5d emphasizing the role of the temperature. It can be seen that the $\Delta^{88/86}Sr_{aragonite\text{-}aq}$ values become higher as a function of increasing temperature.

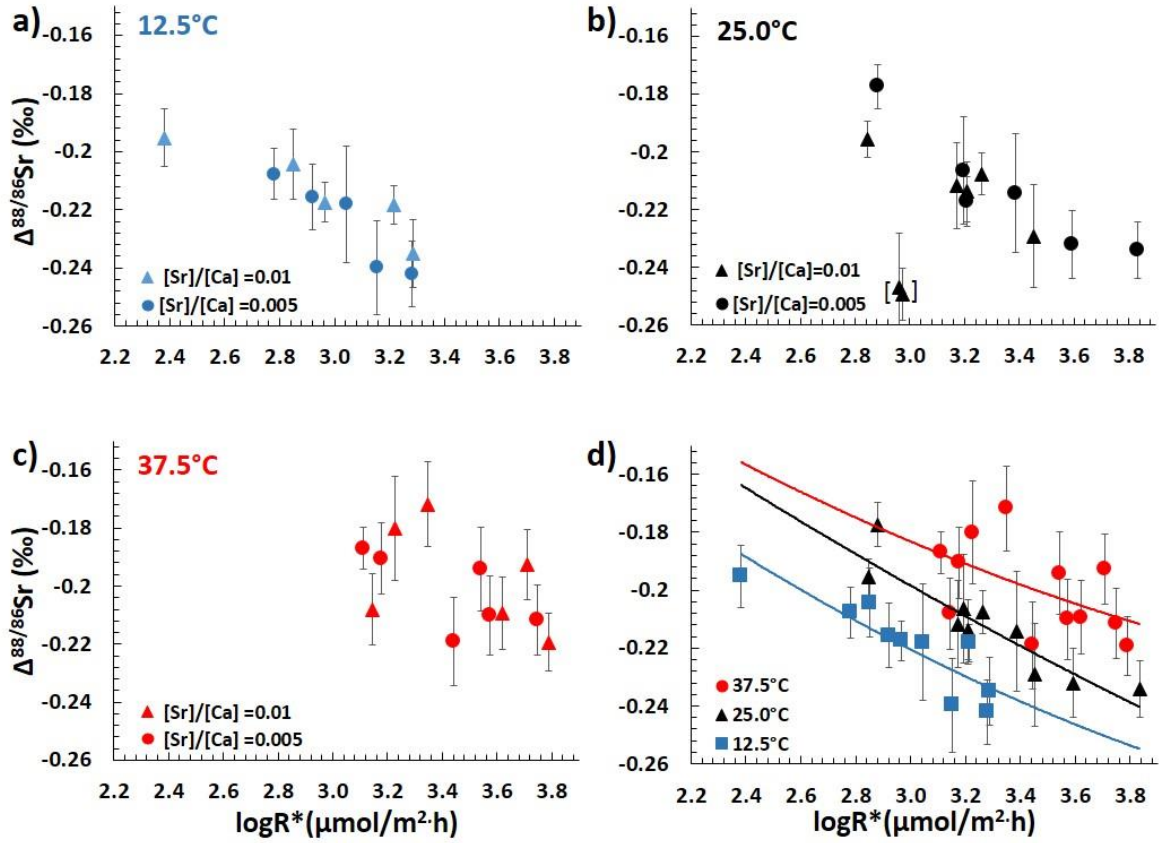

Figure 3.5: This diagram shows all $\Delta^{88/86}Sr_{aragonite\text{-}aq}$ values as a function of R*. For all temperatures, as R* increases $\Delta^{88/86}Sr$ become more negative. **(d)** This diagram summarizes the data emphasizing the role of temperature and showing that at constant R* the initial $\Delta^{88/86}Sr_{aragonite\text{-}aq}$ increases as a function of increasing temperature. Note: results of samples 10 and 11 being part of the 25°C experiment and marked in brackets are unexpectedly low without any particular reason. Therefore a lab error cannot be excluded and will be neglected for further discussions.

Table 3.4: Initial rate (R), normalized rate to surface area (R*), saturation index with respect to different carbonates (SI), strontium distribution coefficient (D_{Sr}), magnesium distribution coefficient (D_{Mg}), uncorrected and corrected values of $\Delta^{88/86}Sr$ and $\Delta^{44/49}Ca$.

Sample label	Initial rate (R) /mM/h	Normalized rate (R*)/ µmole/ m^2h	log R*	SI. ACC	SI. aragonite	SI. $SrCO_3$	D_{Sr}	±(2SEM)	Log D_{Sr}	±(2SEM)	10^3 * D_{Mg}	± (2SEM)	log D_{Mg}	± (2SEM)	$\Delta^{88/86}Sr$ (‰) uncorrected	$\Delta^{88/86}Sr$ (‰) corrected	±(2SEM)	$\Delta^{44/40}Ca$ (‰) uncorrected	$\Delta^{44/40}Ca$ (‰) corrected	±(2SEM)
1	2	3	4	5	6	7	8	9	10	11	12	13	14	15	16	17	18	19	20	21
50C	11.86	6178	3.79	1.92	1.92	3.00	1.031	0.007	0.013	0.003	0.834	0.013	-3.079	0.007	-0.110	-0.219	0.010	-1.00	-1.96	0.09
50D	7.43	3488	3.54	2.08	2.09	2.86	1.026	0.002	0.011	0.001	0.934	0.018	-3.030	0.008	-0.080	-0.194	0.014			
51E	7.49	5130	3.71	1.56	1.56	2.64	1.040	0.014	0.017	0.006	0.652	0.021	-3.185	0.014	-0.127	-0.193	0.012	-1.15	-1.72	0.17
51F	5.86	3745	3.57	1.61	1.62	2.39	1.034	0.019	0.015	0.008	0.659	0.020	-3.181	0.013	-0.131	-0.210	0.014	-0.67	-1.07	0.17
52G	7.21	5616	3.75	1.65	1.65	2.42	1.033	0.01	0.014	0.004	0.673	0.019	-3.172	0.013	-0.153	-0.212	0.012	-1.06	-1.45	0.13
52H	3.95	4176	3.62	1.60	1.60	2.68	1.028	0.011	0.012	0.005	0.670	0.013	-3.174	0.008	-0.167	-0.209	0.013	-1.11	-1.39	0.18
24A	2.19	1398	3.15	1.44	1.45	2.53	1.004	0.029	0.002	0.013	0.528	0.015	-3.278	0.013	-0.140	-0.208	0.012	-0.60	-0.90	0.10
24 B	1.87	1294	3.11	1.33	1.34	2.13	0.978	0.016	-0.01	0.007	0.547	0.007	-3.262	0.005	-0.131	-0.187	0.007			
25D	5.98	2771	3.44	1.89	1.89	2.67	1.009	0.01	0.004	0.004	0.925	0.012	-3.034	0.006	-0.096	-0.219	0.015			
26E	3.52	1680	3.23	1.68	1.69	2.77	1.011	0.012	0.005	0.005	0.518	0.007	-3.286	0.006	-0.081	-0.180	0.018			
26F	2.70	1500	3.18	1.59	1.59	2.38	0.981	0.012	-0.009	0.005	0.764	0.007	-3.117	0.004	-0.109	-0.191	0.012			
27H	4.04	2227	3.35	1.61	1.61	2.70	1.007	0.014	0.003	0.006	0.695	0.012	-3.158	0.007	-0.094	-0.172	0.015			
28A	0.59	700	2.85	1.07	1.21	2.31	1.099	0.027	0.041	0.011	0.562	0.012	-3.251	0.009	-0.157	-0.196	0.006			
28B	0.71	760	2.88	1.06	1.20	2.00	1.148	0.029	0.06	0.011	0.468	0.012	-3.329	0.011	-0.138	-0.177	0.008	-1.34	-1.66	0.10
29C	2.61	1613	3.21	1.26	1.40	2.50	1.092	0.011	0.038	0.005	0.804	0.008	-3.094	0.004	-0.124	-0.214	0.010			
29D	2.20	1565	3.19	1.09	1.23	2.02	1.122	0.009	0.05	0.003	0.646	0.008	-3.190	0.006	-0.132	-0.206	0.019			
30E	2.22	1490	3.17	1.02	1.16	2.26	1.114	0.01	0.047	0.004	0.750	0.009	-3.125	0.005	-0.128	-0.212	0.015	-1.07	-1.64	0.18
30F	2.64	1621	3.21	1.07	1.21	1.99	1.129	0.013	0.053	0.005	0.727	0.008	-3.138	0.005	-0.127	-0.217	0.009	-0.97	-1.57	0.15

Sample label	Initial rate (R) /mM/h	Normalized rate (R*)/ µmole/ m^2h	log R*	SI. ACC	SI. aragonite	SI. $SrCO_3$	D_{Sr}	±(2SEM)	Log D_{Sr}	±(2SEM)	10^3 * D_{Mg}	± (2SEM)	log D_{Mg}	± (2SEM)	$\Delta^{88/86}Sr$ (‰) uncorrected	$\Delta^{88/86}Sr$ (‰) corrected	±(2SEM)	$\Delta^{44/40}Ca$ (‰) uncorrected	$\Delta^{44/40}Ca$ (‰) corrected	±(2SEM)
31A	6.50	2845	3.45	1.65	1.79	2.89	1.134	0.009	0.055	0.004	0.915	0.017	-3.039	0.008	-0.064	-0.229	0.018			
31B	5.52	2446	3.39	1.55	1.69	2.49	1.149	0.011	0.06	0.004	0.695	0.017	-3.158	0.010	-0.063	-0.214	0.021			
49A	10.52	6827	3.83	1.38	1.52	2.30	1.107	0.01	0.044	0.004	1.131	0.014	-2.947	0.006	-0.143	-0.234	0.010	-0.96	-1.51	0.10
49B	6.25	3905	3.59	1.47	1.61	2.38	1.101	0.016	0.042	0.006	1.334	0.035	-2.875	0.011	-0.137	-0.232	0.012			
9	5.09	1837	3.26	1.94	1.34	3.20	1.150	0.05	0.061	0.012	1.298	0.028	-2.887	0.009	-0.198	-0.208	0.007	-1.49	-1.55	0.20
10	2.20	940	2.97	1.33	1.40	2.66	1.075	0.03	0.031	0.008	1.590	0.027	-2.798	0.007	-0.167	-0.249	0.009	-1.16	-1.62	0.20
11	1.50	915	2.96	0.93	1.07	2.29	1.067	0.014	0.028	0.005	0.688	0.012	-3.162	0.008	-0.118	-0.247	0.019			
32A	0.33	241	2.38	0.34	0.65	1.76	1.260	0.031	0.1	0.011	0.367	0.011	-3.436	0.013	-0.129	-0.195	0.011			
32B	0.72	832	2.92	0.49	0.79	1.61	1.228	0.028	0.089	0.01	0.660	0.016	-3.181	0.011	-0.173	-0.216	0.011	-1.24	-1.50	0.19
33C	0.58	710	2.85	0.57	0.88	2.00	1.192	0.04	0.076	0.01	0.654	0.025	-3.184	0.017	-0.169	-0.204	0.012	-1.41	-1.69	0.15
33D	0.53	601	2.78	0.52	0.82	1.64	1.239	0.055	0.093	0.009	0.679	0.029	-3.168	0.018	-0.164	-0.208	0.009			
34E	1.46	923	2.97	0.72	1.02	2.13	1.202	0.017	0.08	0.006	0.896	0.018	-3.048	0.009	-0.127	-0.217	0.007			
34F	2.55	1419	3.15	0.77	1.08	1.88	1.188	0.011	0.075	0.004	0.825	0.018	-3.084	0.010	-0.119	-0.240	0.016			
35A	1.45	1641	3.22	0.52	0.82	1.95	1.184	0.031	0.073	0.012	1.230	0.038	-2.910	0.013	-0.169	-0.218	0.006	-1.16	-1.43	0.23
35B	1.38	1104	3.04	0.59	0.89	1.72	1.225	0.055	0.088	0.009	0.996	0.029	-3.002	0.013	-0.141	-0.218	0.020	-1.10	-1.55	0.17
36C	2.25	1935	3.29	0.71	1.01	2.14	1.176	0.024	0.071	0.009	1.567	0.027	-2.805	0.008	-0.162	-0.235	0.012	-1.04	-1.42	0.13
36D	3.04	1911	3.28	0.88	1.19	2.01	1.200	0.006	0.079	0.002	1.550	0.017	-2.810	0.005	-0.129	-0.242	0.011	-0.81	-1.34	0.13

Notes: For all reactions the initial rate (mM/h) was calculated according to the initial rate law (see text). R* = (column 21 table 1/column 23 table 1)*column 2. SI of different minerals (columns 5, 6 and 7) are calculated as in the text 3.1. D_{Sr} and D_{Mg} are calculated from Usdowski equation (1975). **Columns 16** and **19**: these columns show the measured isotope values of Sr and Ca respectively, uncorrected for the reservoir effect. **Columns 17** and **20**: are the corrected values of columns **16** and **19** respectively as described in the text.

From Fig. 3.6a and b for the Ca isotopes at 12.5 and 25.0 °C as rate of reaction increases $\Delta^{44/40}Ca_{aragonite\text{-}aq}$ tend to become more positive where the slope of the 12.5°C curve tend to be slightly steeper than the one of the 25°C curve. In contrast, the Ca isotope fractionation behavior is opposite at 37.5 °C as R* increases $\Delta^{44/40}Ca_{aragonite\text{-}aq}$ becomes more negative (Fig. 3.6c). Summarizing the results in Fig. 3.6d shows no systematic change of $\Delta^{44/40}Ca_{aragonite\text{-}aq}$ values as function of temperature in the range of 12.5 to 25.0°C on. However at higher temperature at 37.5°C and relatively lower precipitation rates the $\Delta^{44/40}Ca_{aragonite\text{-}aq}$ values tend to be much more positive when compared to the low temperature values.

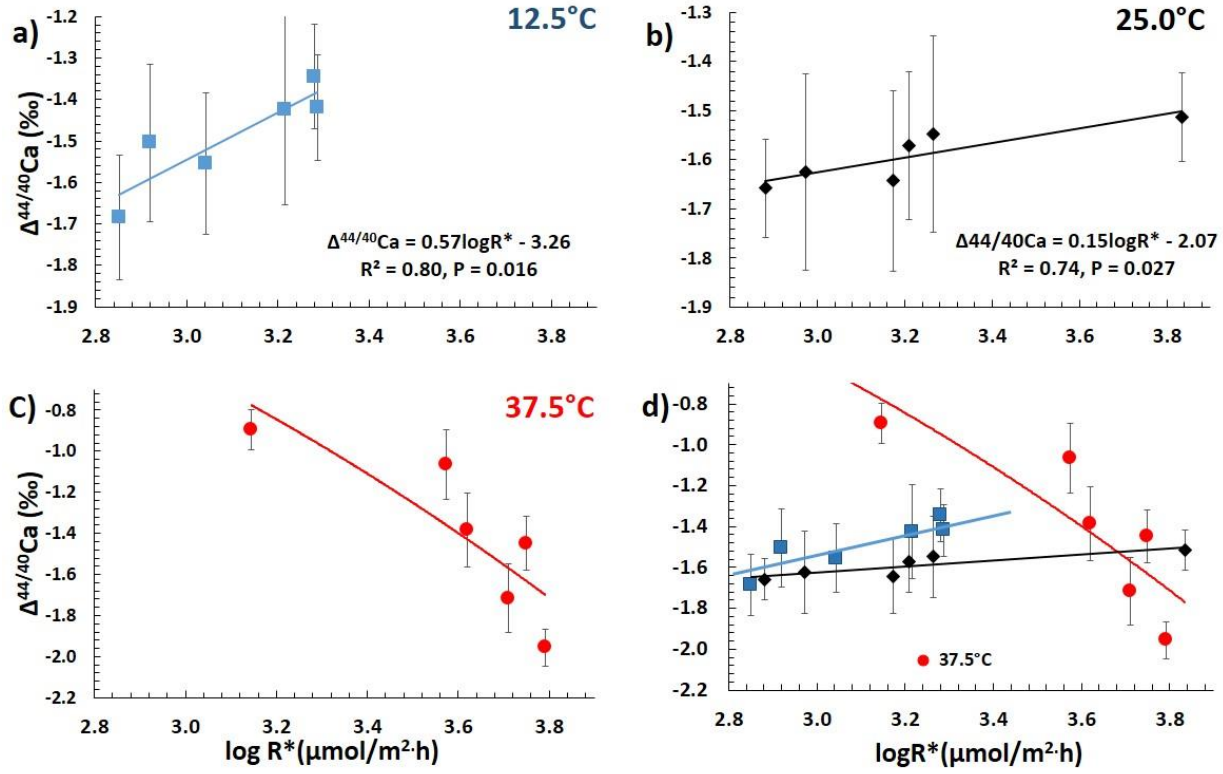

Figure 3.6: These figures shows the $\Delta^{44/40}Ca_{aragonite\text{-}aq}$ as function of log R* at 12.5 (a) and 25.0 °C (b), respectively as rate increase $\Delta^{44/40}Ca_{aragonite\text{-}aq}$ become more positive. Note, that the slope of the 12.5°C curve is steeper than the one of the 25°C curve indicating that the slope of Ca isotope fractionation decreases as a function of temperature. In contrast, at 37.5 °C, as R* increase $\Delta^{44/40}Ca_{aragonite\text{-}aq}$ values become more negative in contrast to the values at lower temperature. Fig 6**d** summarizes the role of temperature. There is no significant effect in the range of 12.5 to 25.0°C. However, increasing the temperature to 37.5°C and at precipitation rates below 3.4 µmol/m^2·h temperature effect becomes more significant. In this interval the lower the temperature is the lower are the $\Delta^{44/40}Ca_{aragonite\text{-}aq}$ values.

3.4. Discussion

3.4.1 Kinetics of aragonite precipitation

Concerning calcite E_a is found to be ~114 kJ/mol in the absence of Mg^{2+} ions (chapter 2), while we found in this study that E_a is ~149 kJ/mol for aragonite formation in the presence of Mg^{2+}-ions in solution (Mg/Ca ~ 3). This means that the presence of ~30 mM of Mg^{2+} ions in the reacting solution diminishes calcite formation by increasing E_a to be higher than at least ~149 kJ/mol, then favoring aragonite to precipitate rather than calcite.

Beside E_a which is the same for all ions most important for the uptake of ions from solution among others is the individual dehydration energy for a trace metal ion to become released from its corresponding aquacomplex. The dehydration energy (Rodriguez-Cruz et al. (1999) Irving and Williams (1953)) is a function of various parameters and decrease in aquatic solutions from Mg (1921 kJ/mol) via Ca (1577 kJ/mol) to Sr (1443 kJ/mol). Following this approach Sr has the highest probability whereas Mg has the least chance to become incorporated into the crystal lattice.

The presence of larger amounts of Mg^{2+-} ions may have chemical consequences because it tends to inhibit calcite nucleation by two roles. The minor one is by increasing the solubility of Mg–calcite and the major factor is due to the increasing Mg–calcite hydrated surface energy (γ), since the nucleation barrier energy is proportional to γ^3. A pristine calcite nuclei show γ-energy of 0.21 J/m^2 (Sun et al (2015)), which is lower than the one of aragonite, 0.28 J/m^2 (Sun et al (2015)) confirming that an Mg depleted solution surface energy favors calcite nucleation. However, increasing the [Mg] : [Ca] ratio in the aqueous solution, will linearly increase γ, reaching 0.35 J/m^2 at equilibrium and ~7% $MgCO_3$ concentration of Mg–calcite in modern seawater which than favors the formation of aragonite. Latter effect of increasing γ may have an effect on the uptake of other trace elements e.g. Sr and the isotope fractionation of Sr and Ca, respectively.

3.4.2 Ion attachment and detachment from an aragonite crystal surface

The surface of a crystal consists of flat regions with terraces and raised partial layers called steps (c.f. Chernov 1961, 1984, 1989). The steps themselves are also incomplete, containing kinks. The kink sites are very important because molecules that attach there make more bonds to neighboring molecules than the ones that attach to the terraces or to flat step edges. Consequently

they are more likely to stick. Conversely, when molecules leave the crystal, they can do so more easily by detaching from kinks than from either complete step edges or from embedded sites in the terraces. As a result, the rate at which ions can be added to a crystal, for a given solute concentration, scales with the kink density. This means that the growth rates of crystals can be altered, among other reasons, by either blocking kink sites or by roughening steps (De Yoreo and Vekilov (2003)).

Accumulation of material from a supersaturated solution expressed as a rate (R*, $\mu mol/m^{2} \cdot h$) occurs because the flux of ions attaching to the crystal (R^*_{attach}) surface exceeds the flux of ions detaching (R^*_{detach}) from the surface. The probability that an ion will detach from the crystal is solely determined by the strength of its bonds to its neighbours. Since the strength of bonding is a function of temperature the total rate from the surface to the solution is independent from the concentration in the crystal but depend on the bonding to its ion neighbours. In contrast, the rate from the solution to the surface is proportional to the solute concentration. The solubility is then the concentration at which the two rates are equal (De Yoreo and Vekilov (2003)) and chemical equilibrium is reached.

The kinetics of the attachment and detachment processes at step edges are determined by the energy barriers seen by the ions. For R^*_{attach} it has been suggested that the barrier to desolvation, i.e., the breaking of bonds to aquacomplexes, is the dominant barrier for the attachment of a complexed trace metal ion to the step (Chernov 1961, 1984).

The primary barrier to detach an ion from a crystal step and limiting R^*_{detach} is its bond to the adjacent ions in the crystal. These barriers are difficult to influence just by altering solution composition because they are controlled by the crystal itself. However, the introduction of distinct impurities that incorporate into the crystal at sufficiently high concentrations can alter R^*_{detach}. It was found that an increase of the Mg concentration in a solution by 20% increases the solubility of calcite from log k_{sp} = - 8.48 to log k_{sp} = -8.08. Latter increasing solubility of the crystal then correspond to an increase in R^*_{detach}. (Davis et al. 2000).

These inferences concerning the effect of Mg impurities in solution on the R^*_{detach} are directly pertinent to our experimental observations here and may reconcile the discrepant observations in trace element partitioning for Sr and Mg for calcite and aragonite as well as for different isotope fractionation behavior in calcite and aragonite to a large extend. Following the mineralogical approach above we infer that R^*_{detach} of aragonite is about 40% higher than the one of calcite

indicated by the higher solubility of aragonite (log k_{sp} = -8.336) relative to calcite (log k_{sp} = -8.48). As a consequence of higher R^*_{detach} values the net R* value of aragonite is expected to be significantly lower than R* of calcite.

Concerning isotope ratios we would expect that the R* - $\Delta^{88/86}$Sr gradient tend to be steeper for calcite than the one for aragonite because R^*_{detach} is expected to be dominated by isotopically light Sr isotopes. Latter flux of isotopically light Sr isotopes from the crystal to the solution (R*detach) then counter balances the flux of light Sr isotopes from the solution to the crystal (R^*_{attach}).

These predictions concerning trace element partitioning and isotope fractionation based on our mineralogical approach is in general accord with our observations concerning trace element partitioning and isotope fractionation and will be discussed in more detail in the sections below.

3.4.3 Strontium and magnesium incorporation into aragonite

Comparing D_{Sr} and D_{Mg} the latter value is about three orders of magnitude lower than the one of Sr (Figs. 3 and 4). Beside the smaller size of the Mg^{2+}-ion relative to the Sr^{2+}-ion presumably this is because of the larger hydration energy of the Mg^{2+}-aquacomplex (1921 kJ/mol) relative to the Sr^{2+}-aquacomplex (1443 kJ/mol). Hence, the probability to overcome E_a and to become incorporated into the crystal is smaller for the Mg^{2+}-ion than for the Sr^{2+}-ion after dehydration. However, with increasing temperature and declining difference between kinetic energy of the ions (E_{Kin}) the energy barrier E_a disproportionally more Ca ions relative to Sr ions will statistically overcome E_a and become eventually incorporated into the crystal. As a consequence D_{Sr} is dropping by about one order of magnitude as a function temperature from 12.5 to 37.5 °C.

There is also a slight effect of temperature to see on D_{Mg} values for all temperatures. Probably, being a non-linear process D_{Sr} sensitivity is higher for $E_{Kin} \sim E_a$ than for D_{Mg} where $E_{Kin} << E_a$ where a slight increase of E_{Kin} is a minor to negligible contribution to E_{kin} in order to overcome E_a.

From Fig. 3.3 it can be seen that variations of R* superimpose the decreasing D_{Sr} trend. For the 12.5 °C data as well at 25 °C (0.005 mmol/mol solution) there is an inverse relationship of the R* - D_{Sr} values. In contrast at the 25 °C (0.01 mmol/mol solution) and the 37.5 °C data there is a positive R* - D_{Sr} relationship. An effect only visible for Sr but not for Mg.

The positive trend between R* and D_{Sr} may be understood to be a consequence of increasing Sr supersaturation (Ω) as a function of increasing R* generating an enhanced uptake of Sr. However, this explanation does not hold for the 12.5 °C data and the 25 °C data (0.005 mmol/mol solution) where an inverse R * - D_{Sr} relationship is observed.

Following our mineralogical approach outlined above we may speculate that the increasing D_{Mg} values and uptake of Mg as a function of R* (Fig. 3.4) into the aragonite crystal causes an increase of the crystal´s solubility and of R^*_{detach} (see discussion in 3.4.2) because the more loosely bound Sr will become released from the crystal lattice disproportionally more than Sr can be gained as a function of R*attach.

Obviously beside the Mg concentration in solution temperature are controlling D_{Sr} values showing about one order of magnitude lower values for 37.5 than for 12.5 °c, respectively. This indicates that the increase of temperature amplifies the effect of Mg to occupy kinks and plateaus of the crystal surface thereby inhibiting the uptake of Sr from the solution. The uptake of Mg is also slightly dropping by about 10% as a function of temperature (from log D_{Mg} -2.9 at 12.5 °C to -3.2 at 37.5 °C). However, this may not reflect the enhanced blocking of kink sites at the crystal surface. The blocking of the crystal kink sites are controlled by absorption- desorption process rather than by the amount of Mg^{2+}-ions to become incorporated (see details in 3.4.2 above).

The temperature controlled decrease in D_{Sr} is superimposed by minor variations as a function of R* where partitioning is changing for the different temperatures. D_{Sr} values are decreasing for 12.5 and 25 °C (0.005 mmol/mol solution), respectively. However, with increasing temperature to 37.5 °C D_{Sr} values increase as a function of R* probably because as a function rate increasing rate favors R*attach and more Sr is incorporated than become released from the crystal.

According to our hypothesis above the change of slope of the R* - D_{Sr} gradient as a function of Sr/Ca ratios as seen for the 25 °C experiment then simply reflects a decline of R^*_{attach} relative to R^*_{detach} marked by relatively more Sr leaving the crystal than Ca ions. For the other temperatures 12.5 °C and 37.5 °C there is no dependency on the Sr/Ca ratio of the initial solution. In the light of our hypothesis this may indicate that any change of the ratio in the initial Sr/Ca ratio does not change the $R^*_{attach}/R^*_{detach}$ ratios. The sensitivity at 25°C for changes in the initial Sr/Ca ratio on the D_{Sr} values may reflect a tipping point where the R* - D_{Sr} gradient reacts sensitive to changes of the trace metal concentrations in solution and the rate.

3.4.4 Calcium and strontium isotope fractionation in aragonite

3.4.4.1 Calcium isotope fractionation

The Ca isotope fractionation in aragonite behaves similar to the one in calcite which was extensively discussed in chapter 2. As for calcite in our aragonite data there is a positive R* - $\Delta^{44/40}Ca_{calcite\text{-}aq}$ gradient for the 12.5 and 25°C data, respectively. However, at 37.5 °C the R* - $\Delta^{44/40}Ca_{calcite\text{-}aq}$ show an inverse behavior. Latter observation was already discussed for calcite and will be briefly repeated here. In addition we will put forward a second hypothesis (Mg blocking hypothesis) in order to account for specific chemical settings for aragonite.

In order to explain the fractionation behavior of Ca we put forward two hypotheses: the first hypothesis, the Ca^{2+}-NH_3 complexation, depends on the temperature dependent Ca to ammonia interaction. In brief we hypothesize that at lower temperatures up to about 25 °C NH_3 complexes with Ca^{2+} to form a Ca^{2+}-NH_3-aquacomplex by a coordinated covalent bonding. The formation constant of this reaction is about 1 (Bjerrum 1941 and Seward 1954) and the extent of complex formation depends on the concentration of ammonia in the aqueous solution. In order to reach a minimum potential energy in the corresponding oscillation potential between Ca^{2+} and NH_3 and hence to reach a more stable bonding the covalent bonding of the Ca^{2+}-NH_3-aquacomplex prefers the isotopically heavy Ca-isotopes ($\Delta E \approx 1/m$). In this case relatively more light Ca isotopes are statistically available to leave the complex to become incorporated into the $CaCO_3$ lattice whereas relatively heavier Ca^{2+}-isotopes remain complexed and dissolved in solution. Hence at a certain relatively low temperature and rate the $\Delta^{44/40}Ca_{calcite\text{-}aq}$ value is low because more light Ca isotopes are available for incorporation into the calcite lattice. Increasing DIC concentration and R*, respectively, will shorten the cross-section and mean free path travel time (Rohlf (1994)) between ions allowing relatively more heavy Ca isotopes to overcome the binding energy of the Ca^{2+}-NH_3-aquacomplex and to become eventually incorporated into the calcite lattice. In this case statistically with increasing rate relative more isotopically heavy Ca^{2+}-ions become available for the incorporation into the crystals lattice. Hence, $\Delta^{44/40}Ca_{aragonite\text{-}aq}$ correlates positively to R*. Further temperature increase to 37.5°C the Ca^{2+}-NH_3-aquacomplex will be completely replaced by a Ca^{2+}-H_2O-aquacomplex substituting the NH_3 molecules completely by H_2O molecules. However, the water molecules are not covalently bond rather form a weak van-der-Waals bonding with the Ca^{2+}-ions. Latter electrostatic bonding cannot be related to an equilibrium type like isotope fractionation process where the heavy isotope is preferred in order

to reach a minimum potential energy. In the absence of a covalent bonding only kinetic isotope fractionation can be observed preferring the light isotopes. Hence, as R* increases more lighter Ca isotopes will be included in aragonite and the $\Delta^{44/40}$Ca values become more negative.

The second hypothesis in order to explain the discrepant behavior of Ca isotope fractionation at 12.5 and 25°C compared to 37.5 °C depends on the impurity effect of Mg as described above in section 3.4.2. We infer that at lower temperatures at 12.5 and 25 °C R^*_{detach} favors the release of light Ca isotopes to a much larger extend when compared to R^*_{attach}. With increasing temperature and a tipping point around 25 °C disproportionally more lighter Ca isotopes are associated with R^*_{attach} when compared to R^*_{detach}. In the latter case relatively more lighter Ca isotopes (40Ca) are incorporated than leaving the crystal as a function of R*. In contrast for the lower temperatures there is a slight higher loss of lighter Ca isotopes than gain from the solution. As seen from Fig. 3.6d there is hardly a gradient visible which indicates that the R*attach and R*detach of light isotopes may be close to each other when temperature approaches to 25 °C.

Both processes "Ca^{2+}-NH_3 complexation" and the "Mg^{2+} impurity effect" as described above may be favored in our experimental setup. The effect of Ca^{2+}-NH_3 complexation on $\Delta^{44/40}$Ca as a function of R* is similar in aragonite and calcite (chapter 2) whereas the Mg^{2+}-impurity effect is only interfering with the aragonite precipitation because Mg was completely absent in our calcite experiment. The relative contribution of the two effects "Ca^{2+}-NH_3 complexation" and the "Mg^{2+}-blocking" affect can be further tested when aragonite is precipitated in the absence of ammonia. Then in the case of aragonite any change of sign in the $\Delta^{44/40}$Ca-precipitation rate can be attributed to the Mg^{2+} blocking effect.

3.4.4.2 Strontium isotope fractionation

Similar to the observation in calcite we see a kinetic type of Sr isotope fractionation for all temperatures where isotope fractionation increases and more lighter Sr isotope are taken up as a function of R*. Obviously NH_3 complexation doesn't have any influence on the Sr isotope fractionation. Probably because of its lower ionic potential based on the larger ionic radius (Sr^{2+}~132 pm; Ca^{2+} ~114 pm) solvation of Sr with water molecules forming a Sr^{2+}-H_2O-aquacomplex is more dominant than covalent bindings and forming of a Sr^{2+}-NH_3-aquacomplex during solvation. This is supported by earlier observations that Sr is not complexing with most ligands due its lower ionization potential when compared to Ca (Irving and Williams (1953)). In

this case Sr isotope fractionation favors only kinetic fractionation as it is observed for Ca at 37.5 °C.

3.5. Comparison of element partitioning and isotope fractionation in aragonite and calcite

Concerning the trace element uptake and isotope fractionation in calcite and aragonite there are similarities but also large differences. Similarities concern the isotope fractionation behavior of Ca isotopes during precipitation of calcite and aragonite and their dependencies on the type of complexation in the solution. Whereas differences in trace element partitioning for Sr (D_{Sr}) and isotope fractionation ($\Delta^{88/86}Sr_{calcite\text{-}aq}$) are caused by the absence of Mg during calcite precipitation but of its presence during aragonite precipitation.

3.5.1 Calcium isotope fractionation in calcite and aragonite

The pure Ca fluxes (µmol/h) are indistinguishable for calcite and aragonite, respectively. However, because of the much larger specific surface of aragonite (~267 m^2/mol) when compared to calcite (~59 m^2/mol) the accumulation rate (µmol/ m^2·h) for aragonite becomes smaller. From Fig. 3.7. it can be seen that Ca isotope fractionation for all temperatures and rates as well as independent from either Ca^{2+}-NH_3- or Ca^{2+}-H_2O–complexation is indistinguishable for the two $CaCO_3$ polymorphs calcite and aragonite.

There is hardly any $\Delta^{44/40}$Ca value above -1.5 ‰ for the 12.5 and 25°C data for both calcite and aragonite. Whereas more than half of the 37.5 °C data show values above -1.5 ‰ up to about -0.6 ‰. Beside the change in the direction of the Ca isotope fractionation (see discussion in 3.4.4.1 above!) the stronger covalent Ca^{2+}-NH_3- complexation is corresponding to lower $\Delta^{44/40}$Ca values because only light (e.g. ^{40}Ca) ions can disproportionally be desolvalted from Ca^{2+}-NH_3-complexation. In this regard a value of -1.5 ‰ may correspond to a certain threshold value for the dissociation energy. Obviously the dissociation energy for the Ca^{2+}-NH_3-complexation is higher than the one of the Ca^{2+}-H_2O–complex where $\Delta^{44/40}$Ca values of up to -0.6 ‰ can be seen.

A major implication of this observation is that the direction of the Ca isotope fractionation as well as the amount is independent of the mineralogy. Fractionation depends on the type of bonding and on R*. Obviously the dependency on R* is much more sensitive for the weak Ca^{2+}-H_2O-aquacomplex in contrast to the strongly bound Ca^{2+}-NH_3-complex.

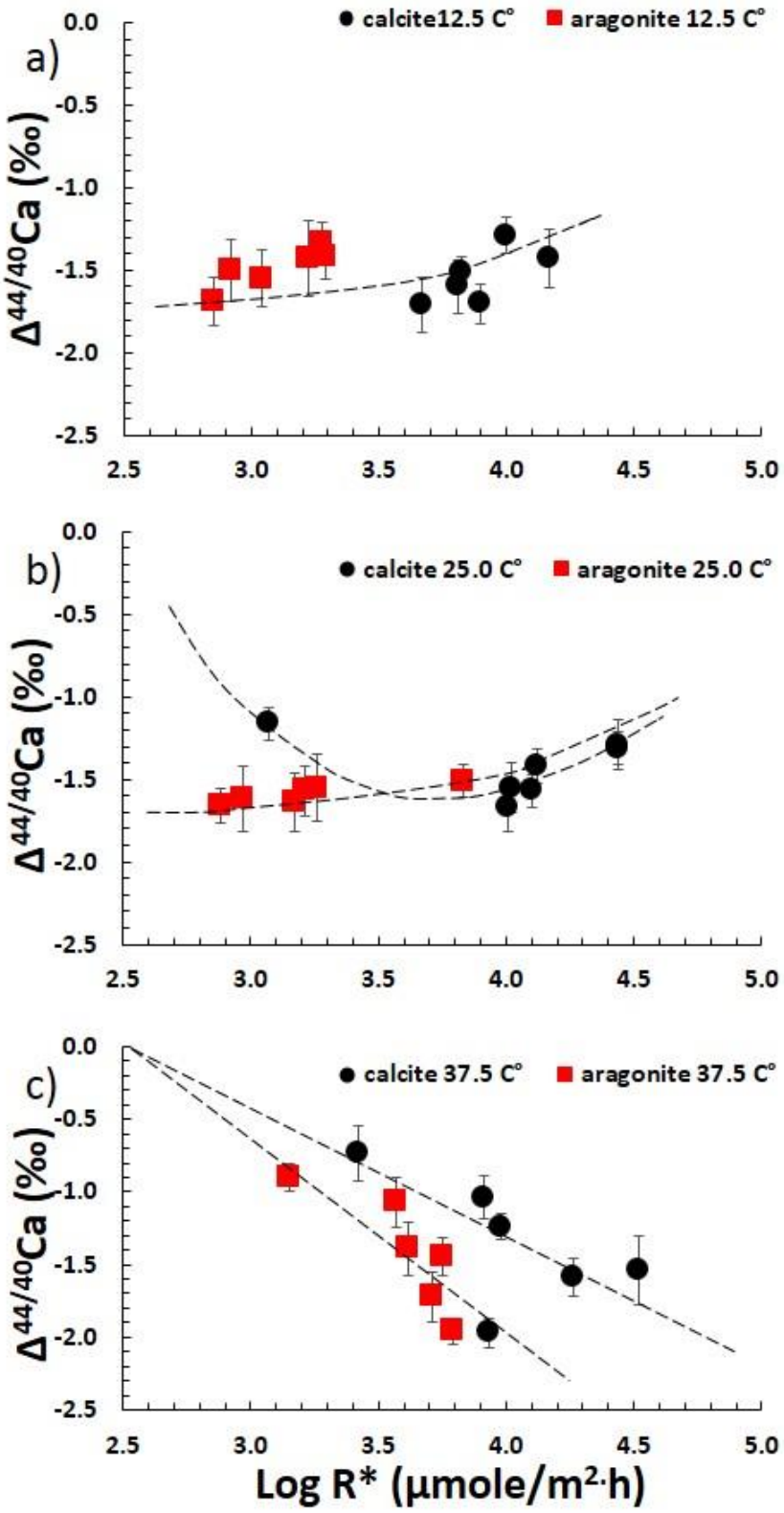

Figure 3.7: In Fig 3.7a and b it can be seen that calcite and aragonite values show indistinguishable $\Delta^{44/40}$Ca values for different R* being lower for aragonite but higher for calcite. For both calcite and

aragonite Ca fractionation behavior changes at 37.5 °C (Fig. 3.7c) again with $\Delta^{44/40}$Ca values lower for aragonite than for calcite.

3.5.2 Strontium isotope fractionation in calcite and aragonite

Strontium isotope fractionation in calcite and aragonite differs in their respective R* - $\Delta^{88/86}Sr_{calcite\text{-}aq}$ gradients which are much steeper for calcite than for aragonite (Fig. 3.8a). The shallow R*- $\Delta^{88/86}$Sr gradients for aragonite as well as the strong temperature dependency of D_{Sr} (see discussion in 3.4.3) may be associated to the impurity effect associated with the presence of Mg in solution.

The presence of Mg increases aragonite solubility and R^*_{detach} of Sr characterized by the enrichment of lighter Sr isotopes. Latter flux is counter balanced by R^*_{attach} also marked by lighter Sr isotopes. As a consequence the amount of Sr isotope fractionation is significantly smaller (~ -0.16 to -0.25) for aragonite than for calcite (-0.11 to -0.36). In addition, the restricted range of Sr fractionation in aragonite is associated with lower R* values when compared to calcite due to the counter balancing effects of R^*_{attach} and R^*_{detach}, respectively.

The similarities and differences in Sr partitioning and isotope fractionation is one more time emphasized in Fig. 3.8b. The larger spread of $\Delta^{88/86}Sr_{calcite\text{-}aq}$ values are associated with lower D_{Sr} values for calcite and the considerable lower spread of the $\Delta^{88/86}Sr_{calcite\text{-}aq}$ values are associated with higher D_{Sr} values for aragonite. The D_{Sr} and $\Delta^{88/86}Sr_{calcite\text{-}aq}$ values for calcite are strongly correlated because only the kinetic effect R* is influencing both the uptake of Sr and the Sr isotope fractionation. Therefore low precipitation rates are associated with low D_{Sr} values and smaller amounts (more positive values) of Sr isotope fractionation. Whereas high precipitation rates are related to larger D_{Sr} values and higher amounts (more negative values) of Sr isotope fractionation. This relationship between R*, D_{Sr} and $\Delta^{88/86}Sr_{calcite\text{-}aq}$ in calcite is independent of temperature.

The situation is different for the uptake of Sr in aragonite. Here we see a significant influence of temperature with lower D_{Sr} values associated with higher temperatures and higher D_{Sr} values associated to lower temperatures. In contrast to calcite the spread of the $\Delta^{88/86}Sr_{aragonite\text{-}aq}$ values are much smaller when compared to the calcite data. Both observations can be attributed to the impurity effect of Mg which causes temperature controlled solubility for aragonite associated with in an increasing loss of Sr as function of temperature. The smaller spread in the $\Delta^{88/86}Sr_{aragonite\text{-}aq}$ values reflect the counterbalancing effect of R*attach and R*detach as discussed above in this section. In contrast to calcite there is a general inverse R* - $\Delta^{88/86}Sr_{calcite\text{-}aq}$

relationship but an ambivalent relationship to D_{Sr}, positive for 25 (0.1 mmol/solution) and 37.5 °C but inverse for the 12.5 and 25 °C (0.05 mmol/mol solution). The contradictionary behavior of Sr at 25 °C may presumably reflect a tipping point value where R*attach gets higher than R*detach as a function temperature.

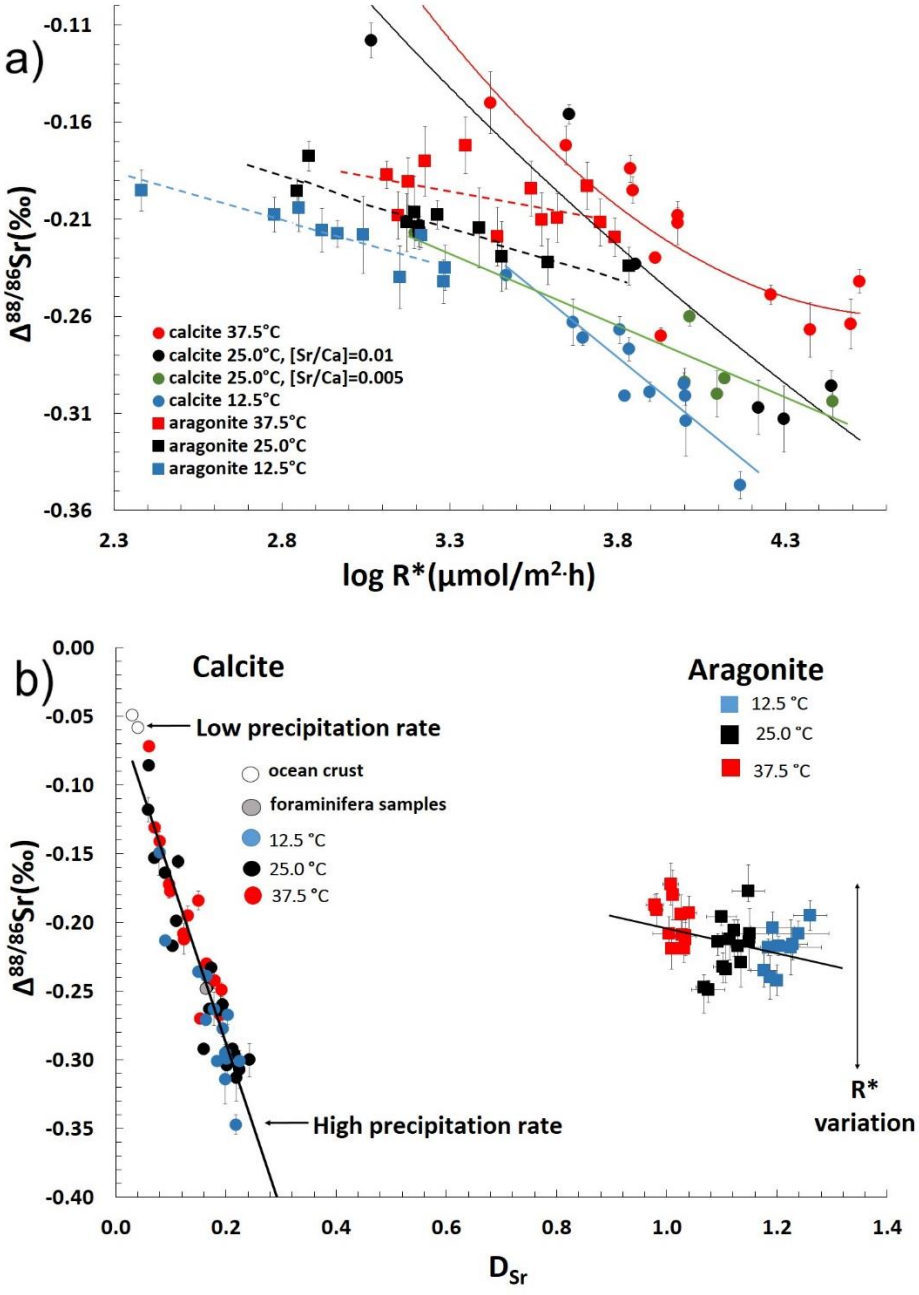

Figure 3.8: Comparison between aragonite and calcite. Solid curves represent calcite, while dashed curves represent aragonite. The values shown in this plot combine the data from this study and our earlier study on calcite (chapter 2). (**a**) This diagram shows that all $\Delta^{88/86}Sr$ values (for both calcite and aragonite) become more negative as a function of increasing R*. However the rate effect is larger in calcite as seen from the steepness of the corresponding curves.

(**b**) The linear correlations of $\Delta^{88/86}Sr$ and D_{Sr} for calcite it is dependent only on R* and is independent of temperature. For aragonite $\Delta^{88/86}Sr$ values are much less sensitive to R* than to temperature because the Mg^{2+} blocking effect on the Sr ions and their isotope composition (see text). In contrast to calcite the D_{Sr} - $\Delta^{88/86}Sr$ values correlation depend on temperature.

3.6. Implications

(a) The D_{Sr} - $\Delta^{88/86}Sr_{calcite\text{-}aq}$ relationship may be applied in paleo proxy research and applied as self-consistent criteria for diagenesis. This is because independent from the adjacent environmental conditions all primary Sr element and isotope ratios have plot along the calcite or the aragonite array.

(b) The strong dependency of the $\Delta^{44/40}Ca_{calcite\text{-}aq}$ value on complexation in solution may be used to better constrain metal complexation in aquatic solution.

(c) Also Ca- and Sr isotope fractionation may be used to examine the blocking effect of Mg impurities in much more detail.

3.7. Summary and Conclusions

- The rate law (order of reaction) is similar for both calcite and aragonite when precipitation is occurring under the same chemical conditions and experimental setup.
- Although there are similarities concerning the D_{Sr}-temperature relationship between calcite and aragonite the uptake of Sr into aragonite as a function of R* is completely different from the uptake in calcite.
- In aragonite R* is much less significant and the D_{Sr}-precipitation – R* relationship is changing sign as a function of temperature above ≥25 °C as a function of both temperature and initial Sr/Ca ratios. Probably this reflects the Mg^{2+}-blocking and the enhanced release of crystal lattice bound Sr. Latter effect disappears as a function of rising temperature and the incorporation of relatively more Sr from the fluid.
- The effect of R* on $\Delta^{88/86}Sr$ values is smaller in aragonite compared with calcite because of the Mg^{2+} blocking effect.
- The $\Delta^{44/40}Ca_{aragonite\text{-}aq}$ fractionation as function of R* follows the same temperature controlled pattern in both aragonite and calcite.

APPENDIX:

1. Correction for Isotope fractionation due to the Reservoir effect

The isotope composition of an aquatic reservoir with respect to Ca and Sr will change when a significant amount of Ca and Sr is precipitating as solid $CaCO_3$. This has to be corrected for:

Isotope fractionation (I) $\alpha_{pr} = R_p/R_r$

where p and r are the product and the reactant respectively and R is the abundance of the heavy isotope; R = heavy isotope/ light isotope

While (II) : $\Delta \approx (\alpha - 1)*1000$

Rearranged to (III): $\alpha \approx (\frac{\Delta}{1000} + 1)$

Substituting Eq. (I) in Eq. (III) results in (IV): $R_p/R_r = (\frac{\Delta}{1000} + 1)$

The eq. 3.1.17 from Zeebe and Wolf-Gladrow, 2003 accounts for the Rayleigh distillation effect:

(V) $R_p/R_r = (f^{\alpha} -1)/(f - 1)$; f is the fraction of metal ions remaining in solution.

Equations (V) and (IV) result in: $(\frac{\Delta}{1000} + 1) = (f^{\alpha} -1)/(f - 1)$

Rearrange to (VII): $f^{\alpha} = \frac{\Delta f}{1000} + f - \frac{\Delta}{1000}$

Equation (VII) can be rewritten to (VIII): $\alpha \ln f = \ln [\frac{\Delta f}{1000} + f - \frac{\Delta}{1000}]$

Eq. (VIII) is then arranged to Eq. 7 as in the the text: $\alpha_{corrected} = \left(ln\left[\frac{\Delta f}{1000} + f - \left(\frac{\Delta}{1000}\right)\right]\right) / lnf$

2. K_a of ammonium ion and DIC calculations

Total alkalinity (TA, see eq. a1) was measured from neutralization titration with 0.02N HCl at different intervals of time during the course of precipitation for some reactions. We found that TA did not increase more than 10% from the value at the precipitation point until the end of the reaction. We therefore determined TA at the end of all the reactions and adopted this values for further calculations.

(a1) $TA = [NH_3] + [HCO_3^-] + 2[CO_3^{2-}]$

$[NH_3]$ in our solutions at different results is calculated following Lemarchand et al. 2004:

(a2) $[NH3] = \frac{[Cl^-]+TA-2[M^{2+}]}{\frac{[H^+]}{Ka}+1}$

where $[M^{2+}]$ is the concentration of metal divalent ions in the solution, $[Cl^-]$ is the concentration of chloride ions, $[H^+]$ calculated from pH values at the end of each experiment and K_a is the ammonium acid dissociation constant.

The acid dissociation constant (pK_a) of ammonium chloride (eq. a3) equals the pH of the half neutralized mother solution, because at half neutralization the concentrations of ammonia species are equal and K_a equals $[H^+]$. Measured values of pK_a at different temperatures are shown in table A.

(a3) $[NH_4^+]_{(aq)} \rightleftharpoons NH_{3\,(aq)} + H^+_{(aq)}$

By plotting pH versus 1/T (Fig. A) we can calculate pK_a at any temperature as well as the apparent enthalpy of ionization of ammonium which calculated to be about +51kJ/mol.

Table A**:** Acid dissociation constant (pK_a) of ammonium chloride as function of temperature.

Temperature ^oC	**Temperature ^oK**	**1/T ($^oK^{-1}$)**	**pH = pK_a**
5.3	278.45	0.003591	10.130
11.4	284.55	0.003514	9.915
21.4	294.55	0.003395	9.611
30.7	303.85	0.003291	9.335
39.0	312.15	0.003204	9.095

Note: The pH values at different temperatures of half neutralized mother solution for calcite: $K_a = [NH_3].[H^+]/[NH_4^+]$, at half neutralization $[NH_3] = [NH_4^+]$ and so $K_a = [H^+]$ and pK_a = pH. Using van't Hoff equation: - ln $K_a = [\Delta H/RT] + C$; or pK_a = pH = $[\Delta H/2.303RT] + C$, where R is the gas content = 8.314 J/mol. Kelvin, T is the temperature in Kelvin and °C is constant.

$[CO_3^{2-}]$ in our solutions also calculated following Lemarchand et al. (2004): (eq.a4).

(a4) $[CO_3^{2-}] = \frac{TA-[NH_3]}{\frac{[H^+]}{K2}+2}$

Where K_2 is the second dissociation constant of carbonic acid and calculated following in Millero (1995): (eq.a5)

(a5) $\ln K_2 = -0.84 - 3741.13/T - 1.44 \ln(T) + (-0.13 - 24.41/T)S^{0.5} + 0.12S - 0.01S^{1.5}$

where T is the temperature in Kelvin and S is the salinity of the solution as determined at the end of all the reactions.

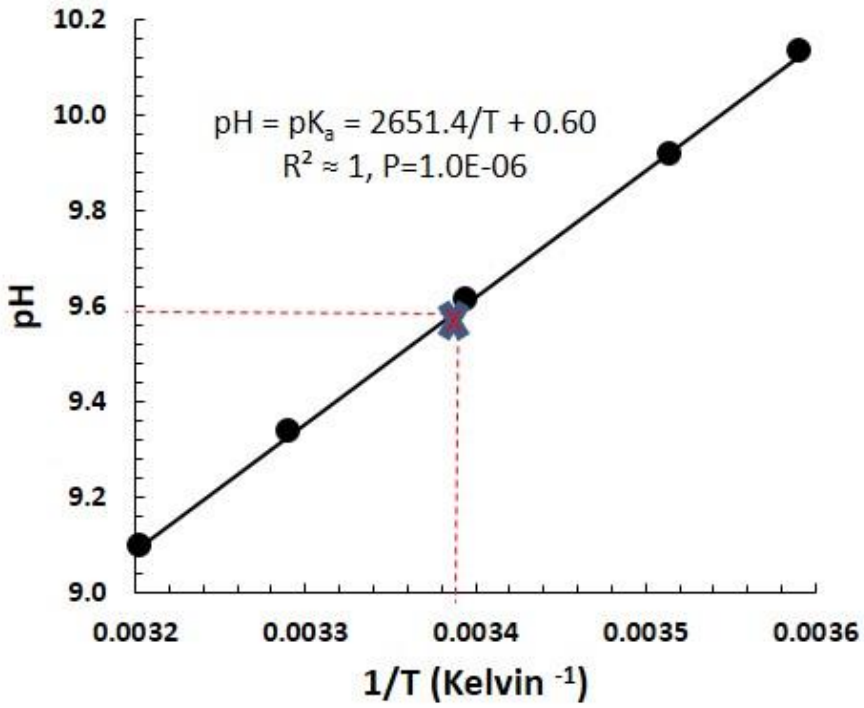

Figure A**:** pH of half neutralized mother solution versus different 1/temperatures (^{o}K).
For example, from the upper figure at 22 °C (295.15K corresponding to 0.00339 1/°K),
pH = pK$_a$ = 9.59±0.07.

3. Saturation indexes with respect to calcite, amorphous calcium carbonate (ACC) and strontianite ($SrCO_3$).

Saturation state Ω = $[Me^{2+}][CO_3^{2-}]$/Ksp Millero 1995, where $Me^{2+}$is either Ca or Sr. Saturation index (SI) = log Ω. Ksp of calcite is calculated as function of temperature at salinity 32 as in Millero 1995. Ksp of ACC is determined as in Clarkson et al. 1992 and Ksp of strontianite is determined as in Busenberg et al. 1984 are shown in table B.

Table B: Ksp values of calcite, ACC and $SrCO_3$ as function of temperature and salinity

T/°C	Ksp $_{calcite}$* 10^7	Ksp$_{ACC}$ * 10^7	Ksp$_{SrCO3}$ * 10^{10}
37.5	3.72	6.17	4.98
25.0	3.74	9.09	5.36
12.5	3.85	13.85	5.24

4. R* using equation 20.

Table C: Estimated R* using equation 20 for samples precipitated at 25°C versus measured R* values.

Sample reaction	log [CO_3^{2-}] (mM)	Log R(μmol/m^2·h) calculated as in Lemarchand et al. (2004)	log R(μmol/m^2·h) measured in this study
43C	0.09	6.55	4.44
43D	0.27	7.16	4.00
44A	-0.04	6.12	4.44
44B	0.12	6.64	4.12
45C	-0.33	5.14	4.30
45D	-0.30	5.23	4.01
46E	-0.39	4.95	4.22
46F	-0.49	4.59	4.10
2	-0.55	4.39	3.07
3	-0.19	5.59	3.66
4	-0.82	3.49	3.20
7	-1.40	2.25	4.02
8	-1.70	1.43	3.85

Notes: Equation used by Lemarchand et al. to calculate rate is $\log R^* = n_2 \log([CO_3^{2-}]) + \log k_f$, where for samples 43C to 4: $n_2 = 3.34$ and $\log k_f = 6.24$. For samples 7 and 8: $n_2 = 2.73$ and $\log k_f = 6.07$.

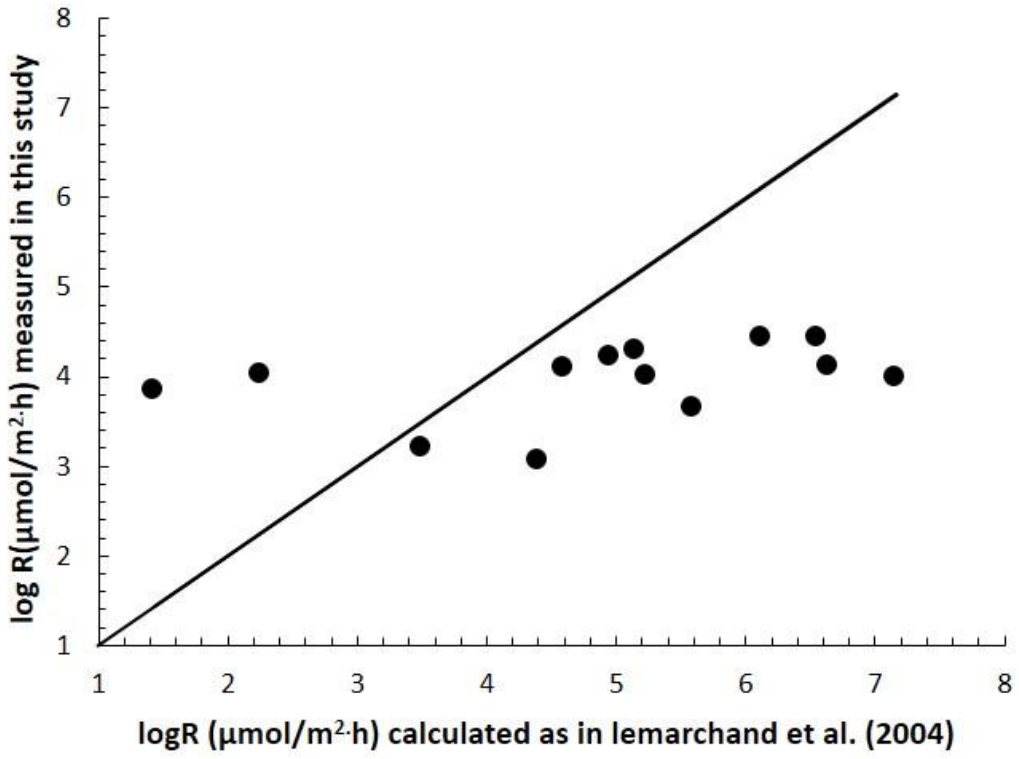

Figure B**:** Measured R* (µmol/m^{2}·h) using initial rate method versus estimated R* using equation 20 which was adopted earlier by Lemarchand et al. (2004) to estimate precipitation rate of their calcite products.

5. Determination of Dsr by graphic method

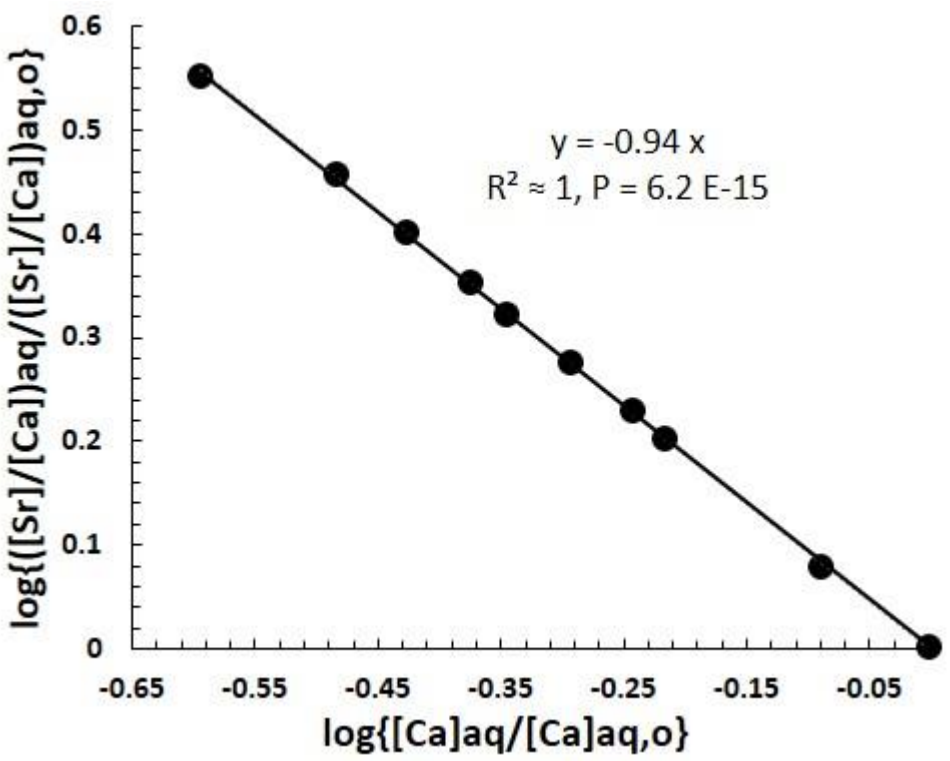

Figure C: Determination of D_{Sr} value of sample reaction 2 at 25.0°C graphically by plotting of $\log\{[Ca]_{aq}/[Ca]_{aq,o}\}$ versus $\log\{([Sr]/[Ca])_{aq}/([Sr]/[Ca])_{aq,o}\}$. Slope of this curve equals D_{Sr} -1. So D_{Sr} = 0.06 which is very close to (0.059) the value calculated by (eq. 21) as shown in table 5. This figure is a validation of using the Usdowski equation to our system of precipitation reactions to calculate $D_{Sr.}$

Chapter 4

SUMMARY AND OUTLOOK

4.1 Summery

The order of reaction is exactly the same for both calcite and aragonite when precipitation is occurring under the same chemical conditions and experimental setup. It is 1 with respect to Ca^{2+} ions. However with respect to DIC is temperature dependent, decreasing from 3 via 2 to 1 as temperature increases from 12.5 via 25 to 37.5 °C, respectively. The presence of Mg^{2+}-ions in solution (Mg/Ca ~ 3) inhibit calcite formation by increasing E_a to be higher than at least ~149 kJ/mol, as result only pure metastable aragonite is precipitate rather than calcite. The precipitation rates of calcite tend to be higher than those of aragonite for two main reasons: (1) the specific surface area of aragonite is much higher (~ 2.67 m^2/g) than that of calcite (~0.59 m^2/g), (2) increasing Mg^{2+}-concentrations are causative for increasing the material flux back (R^*_{detach}) from the crystal to the solution to a large extent. The later effect not only affect aragonite precipitation rate but also affecting Sr incorporation and Sr isotopic fractionation between aragonite and aqueous solution. Additionally, it may also be responsible for the observed Ca isotopic fractionation behavior as function of precipitation rate at different temperatures.

The Ca isotope fractionation in aragonite behaves similar to the one in Calcite. At 12.5 and 25.0 °C as rate of reaction increases $\Delta^{44/40}Ca_{aragonite\text{-}aq}$ tend to become more positive. In contrast, the Ca isotope fractionation behavior is opposite at 37.5 °C as R* increases $\Delta^{44/40}Ca_{aragonite\text{-}aq}$ becomes more negative. Two hypotheses are presented to explain the discrepant behavior of Ca isotopic fractionation: (1) at lower temperatures up to about 25 °C NH_3 complexes with Ca^{2+} to form a Ca^{2+}-NH_3-aquacomplex by a coordinated covalent bonding, as result of this interaction $\Delta^{44/40}Ca$ increase as R* increases. With increasing temperature to 37.5°C the Ca^{2+}-NH_3-aquacomplex will be completely replaced by a Ca^{2+}-H_2O-aquacomplex substituting the NH_3 molecules completely by H_2O molecules, the water molecules are not covalently bond rather form a weak van-der-Waals bonding with the Ca^{2+}-ions. In the absence of a covalent bonding only kinetic isotope fractionation can be observed preferring the light isotopes for incorporation. Hence, as R* increases more lighter Ca isotopes will be included in aragonite and the $\Delta^{44/40}Ca$

values become more negative. This hypothesis is applicable for both polymorphs of $CaCO_3$. The second hypothesis can only explain the discrepant behavior of $\Delta^{44/40}Ca$ as function of R* in aragonite, since in case of precipitating calcite Mg^{2+} ions are simply not present.

In the case of aragonite it is argued that at lower temperatures at 12.5 and 25 °C R^*_{detach} favors the release of light Ca isotopes to a much large extent when compared to R^*_{attach} and as consequence $\Delta^{44/40}Ca$ become more positive with increasing R*. With increasing temperature and a tipping point around 25 °C disproportionally more lighter Ca isotopes are associated with R^*_{attach} when compared to R^*_{detach} as result of that $\Delta^{44/40}Ca$ become more negative with increasing R*. A major implication of this observation is that the $\Delta^{44/40}Ca_{calcite\text{-}aq}$ values may be used to determine the type of metal complexation in aquatic solution.

Concerning Sr isotope fractionation ($\Delta^{88/86}Sr$), it is similar for both calcite and aragonite. Since Sr^{2+} ions are larger than Ca^{2+} (Sr^{2+}~132 pm; Ca^{2+} ~114 pm) Sr has a lower ionic potential and as result Sr^{2+}-NH_3-aquacomplex formation is much less to occur at any temperature in aqueous solution. In the absence of covalent bonding Sr isotope fractionation favours kinetic fractionation only. For both polymorphs of $CaCO_3$ and at any temperature, as R* increases $\Delta^{88/86}Sr$ become more negative. At constant R* as temperature decreases $\Delta^{88/86}Sr$ become also more negative. However rate effect on $\Delta^{88/86}Sr$ is larger in calcite when compared with aragonite. This is due to the impurity effect associated with the presence of Mg in solution. We would expect that the R* - $\Delta^{88/86}Sr$ gradient tend to be steeper for calcite than the one for aragonite because R^*_{detach} is expected to be dominated by isotopically light Sr isotopes. Latter flux of isotopically light Sr isotopes from the crystal to the solution (R^*_{detach}) then counter balances the flux of light Sr isotopes from the solution to the crystal (R^*_{attach}). As a consequence the amount of Sr isotope fractionation is significantly smaller ($\Delta^{88/86}Sr$ ~ -0.16 to -0.25) for aragonite than for calcite ($\Delta^{88/86}Sr$ ~ -0.11 to -0.36), respectively.

In calcite D_{Sr} increases with increasing R* and also increases with decreasing temperature. However rate effect is more significant than temperature effect. On the other hand in aragonite as temperature decreases D_{Sr} increases when compared to the effect of temperature in calcite. However R* effect in aragonite is less significant. At 12.5°C as R* increases D_{Sr} values decrease without any dependency on the initial $([Sr]/[Ca]_{0,aq})$-ratio in the reacting solution. While at 25.0°C a discrepant behavior of D_{Sr} values can be observed. At a $([Sr]/[Ca]_{0,aq})$ initial ratio of

0.01 D_{Sr} values tend to increase as a function of rate. In contrast when the initial ($[Sr]/[Ca]_{0,aq}$) ratio is 0.005 mmol/mol D_{Sr} values tend to decrease. At 37.5°C as R* increases D_{Sr} values increase without any significant effect of the initial ($[Sr]/[Ca]_{0,aq}$) ratio. At 37.5°C increasing Sr supersaturation (Ω) as a function of increasing R* generating an enhanced uptake of Sr. However, this explanation does not hold for the 12.5 °C since increasing R* will also increases uptake of Mg into the aragonite crystal causes an increase of the crystal´s solubility and of R^*_{detach} because the more loosely bound Sr will become released from the crystal lattice disproportionally more Sr can be gained as a function of R^*_{attach}. The sensitivity at 25°C for changes in the initial Sr/Ca ratio on the D_{Sr} values may reflect a tipping point where the R* - D_{Sr} gradient reacts sensitive to changes of the trace metal concentrations in solution and the rate.

Comparing D_{Sr} and D_{Mg} the latter value is about three orders of magnitude lower than the one of Sr. Beside the smaller size of the Mg^{2+}-ion relative to the Sr^{2+}-ion which means more energy strain needed for including Mg^{2+} in aragonite crystal lattice, more energy is needed to desolvate Mg^{2+} ions, because of the larger hydration energy of the Mg^{2+}-aquacomplex (1921 kJ/mol) relative to the Sr^{2+}-aquacomplex (1443 kJ/mol). Hence, the probability to overcome E_a and to become incorporated into the crystal is smaller for the Mg^{2+}-ion than for the Sr^{2+}-ion after dehydration. However D_{Mg} values increase with increasing R* but decreases as temperature increase.

The D_{Sr} - $\Delta^{88/86}Sr$ relationship is an important tool to reconstruct precipitation rate of calcite (inorganic and of biogenic origin) and to reconstruct precipitation temperature of inorganic aragonite and may be applied in paleo proxy research as criteria for diagenesis of $CaCO_3$.

4.2 Outlook

In future work we will use the same chemical setup to

1. Dissolve different polymorphs of $CaCO_3$ (inorganic and biogenic) in both seawater and pure water as function of increasing pCO_2 in the atmosphere. We will investigate the rate of dissolution, pH at equilibrium and the isotopic composition of partially dissolved $CaCO_3$ and compare it with the initial conditions to verify the degree of isotopic fractionation.

2. Precipitate strontianite ($SrCO_3$) at different temperatures and precipitation rate to see how these factors will affect Sr isotope composition in $SrCO_3$. Comparing these results with Sr isotope composition in calcite and aragonite may be a useful tool to decide whether Sr is actually incorporated into $CaCO_3$ or precipitated independently as $SrCO_3$.

We also plan to precipitate aragonite and calcite from seawater using the seeded growth techniques, while maintaining pH and concentration of reactants (calcium, bicarbonate, and carbonate ions) constant during the crystal growth reaction. The kinetics of crystallization will be studied over a wide range of supersaturation and temperature. Trace element incorporation and isotopic composition then will be compared with what we already did.

Acknowledgements

First I would like to thank Prof. Dr. Anton Eisenhauer for supervision of my thesis and his support during the last three years. I acknowledge Prof. Dr. Klaus Wallmann as second supervisor. The "Deutsche Forschungsgemeinschaft, (DFG)" provided funding through the TRION project (Ei272/30-2)". I want to say a special thank to Ana Kolevica for laboratory help and support in the design of the experiment. I also would like to thank Florian Böhm for helping me a lot during this time and had always an open door to discuss results or any problems. Also thanks to Volker Liebetrau, Nicolas Glock, Bettina Domeyer, Anke Bleyer and Regina Surberg. Prof. Dr. Mutaz Al-Qutob from the Al-Quds University in AbuDies, Palestinian Authority, is acknowledged for his general support of my work. Finely I thank my family especially my wife "Samia Alkhatib" for her contineous support.

References

Aizenberg J., Lambert G., Addadi L., and Weiner S. (1996) Stabilization of Amorphous Calcium Carbonate by Specialized Macromolecules in Biological and Synthetic Precipitates. Advanced Materials, Vol. 8. No. 3, 222-225.

Aizenberg J., Lambert G., Weiner S. and Addadi L. (2002) Factors Involved in the Formation of Amorphous and Crystalline Calcium Carbonate: A Study of an Ascidian Skeleton. J. AM. CHEM. SOC., Vol. 124, No. 1, 32-39.

Andersson M. P., Rodriguez-Blanco J. D. and Stipp S. L. S. (2016) Is bicarbonate stable in and on the calcite surface? Geochimica et Cosmochimica Acta 176, 198–205.

Anthony J. W., Bideaux R. A., Bladh K. W. and Nichols M. C., ed. (2003). Handbook of Mineralogy. V (Borates, Carbonates, Sulfates). Chantilly, VA, US: Mineralogical Society of America.

Atkins P. and De Paulla J. (2006) Atkins, Physical Chemistry.8th Edition, W.H. Freeman and company, New York. P 798.

Baker P.A., Gieskes J.M. and Elderfield H. (1982) Diagenesis of carbonates in deep sea sediments—evidence from Sr/Ca ratios and interstitial dissolved Sr data: Journal of Sedimentary. Petrology 52, 71–82.

Banner J. L. (1995) Application of the trace element and isotope geochemistry of strontium to studies of carbonate diagenesis. Sedimentology 42, 805–824.

Banner J. L. and Hanson G. H. (1990) Calculation of simultaneous isotopic and trace element variations during water–rock interaction with applications to carbonate diagenesis: Geochimica et Cosmochimica Acta 54, 3123–3137.

Beck J. W., Edwards R. L., Ito E., Taylor F., W. Recy J., Rougerie F., Joannot P. and Henin C. (1992) Sea-surface temperature from coral skeletal strontium calcium ratios. Science257 (5070), 644–647.

Benson S., Lennard C., Maynard F. and Roux C. (2006) Forensic applications of isotope ratio mass spectrometry—A review. Forensic Science International 157, 1–22.

Berner R. A. (2004) The Phanerozoic carbon cycle: CO_2 and O_2: Oxford University Press (in press).

Bischoff J. L., Fitzpatrick J. A., Rosenbauer R. J. (1992). "The solubility and stabilization of ikaite ($CaCO_3.6H_2O$) from 0° to 25 °C". Journal of Geology 101: 21–33.

Bjerrum J. (1941) Metal Ammine Formation in Aqueous Solutions. P. Haase and Son, Copenhagen, P. 147.

Böhm F., Eisenhauer A., Tang J., Dietzel M., Krabbenhöft A.,Kisakürek B. and Horn C. (2012) Strontium isotope fractionation of planktic foraminifera and inorganic calcite. Geochim. Cosmochim. Acta 93, 300-314.

Böhm F., Gussone N., Eisenhauer A., Dullo W.-C., Reynaud S. and Paytan A. (2006) Calcium isotope fractionation in modern scleractinian corals. Geochim. Cosmochim. Acta 70, 4452–4462.

Brand U., Logan A., Hiller N. and Richardson J. (2003) Geochemistry of modern brachiopods: applications and implications for oceanography and paleocenanography. Chem. Geol. 198, 305–334.

Brown S. J. and Elderfield H. (1996) Variations in Mg/Ca and Sr/Ca ratios of planktonic foraminifera caused by postdepositional dissolution: Evidence of shallow Mg-dependent dissolution. Paleoceanography, Vol. 11, No. 5, 543-551.

Burton E. A. and Walter L. M. (1987) Relative precipitation rates of aragonite and Mg calcite from seawater: Temperature or carbonate ion control ?.Geology 15, 111-114.

Busenberg E., Plummer L. N. and Paker V. B. (1984) The solubility of strontianite ($SrCO_3$) in CO_2-HO_2 solutions between 2 and 91°C the association constants of $SrHCO_3^+$(aq) and $SrCO_3^0$(aq) between 5 and 80°C and an evaluation of the thermodynamic properties of Sr^{2+} (aq) and $SrCO_3$ (cr) at 25°C and 1 atm total pressure. Geochim. Cosmochim. Acta 48, 2021-2035.

Chave K. E. (1954) Aspects of the biogeochemistry of magnesium 1. Calcareous marine organisms. Journal of Geology 62, 266-283.

Chernov A. A. (1961) The spiral growth of crystals. Sov Phys Uspekhi 4:116-148.

Chernov A. A. (1984) Modern Crystallography III: Crystal Growth. Springer, Berlin

Chernov A. A. (1989) Formation of crystals in solutions. Contemp Phys 30:251-276.
Clarkson J. R., Price T. J. and Adams C. J (1992) Role of Metastable Phases in the Spontaneous Precipitation of Calcium Carbonate. J. CHEM. SOC. FARADAY TRANS, 88(2), 243-249
Criss R.E, (1999) Principles of Stable Isotope Distribution, Oxford University Press.
Crowley T. J. (1983) Calcium-carbonate preservation patterns in the central North Atlantic during the last 150,000 years. Marine Geology, Vol. 51, issues 1-2, 1-14.
Curti E. (1997) Coprecipitation of radionuclides: basic concepts, literature review and first applications. PSI-Bericht Nr. 10–97.
Davis K. J., Dove P. M. and De Yoreo J. J. (2000) The Role of Mg· as an Impurity in Calcite Growth. Science, 1134-1137.
De Kanel J. and Morse J. W. (1979) A simple technique for surface area determination. J. Phys. E: Sci. Instrum. 12, 272-273.
Dekens P. S., Lea D. W., Pak D. K. and Spero H. J. (2002) Core top calibration of Mg/Ca in tropical foraminifera: Refining paleotemperature estimation. Geochemistry Geophysics Geosystems.Vol 3, No. 4, 1-29.
DePaolo D. J. (2011) Surface kinetic model for isotopic and trace element fractionation during precipitation of calcite from aqueous solutions. Geochim. Cosmochim. Acta 75, 1039–1056.
De Villiers S., Shen G. T. and Nelson B. K. (1994) The Sr/Ca temperature relationship in coralline aragonite—influence of variability in (Sr/Ca) seawater and skeletal growth-parameters. Geochim. Cosmochim. Acta 58(1), 197–208.
De Yoreo, J. J. and Vekilov P. G. (2003). Principles of crystal nucleation and growth. Reviews in mineralogy and geochemistry. 57-93.
Dietzel M., Gussone N. and Eisenhauer A. (2004) Precipitation of aragonite by membrane diffusion of gaseous CO_2 and the coprecipitation of Sr^{2+} and Ba^{2+} (10° to 50°C). *Chem. Geol*. 203**,** 139–151.
Elderfield H., Bertram C. J. and Erez J. (1996) A biomineralization model for the incorporation of trace elements into foraminiferal calcium carbonate. Earth and Planetary Science Letters 142, 409-423.
Enmar R., Stein M., Bar-Matthews M., Sass E., Katz A. and Lazar B. (2000) Diagenesis in live corals from the Gulf of Aqaba. I. The effect on paleo-oceanography tracers. Geochim. Cosmochim. Acta 64(18), 3123–3132.
Fantle M. S. and Higgins J. (2014) The effects of diagenesis and dolomitization on Ca and Mg isotopes in marine platform carbonates: Implications for the geochemical cycles of Ca and Mg. Geochim. Cosmochim. Acta 142, 458-481.
Farrell J. W., and Prell W. L. (1989) Climatic change and CaCO3 preservation: An 800,000 year bathymetric Reconstruction from the central equatorial Pacific Ocean, Paleoceanography. Vol. 4, issue 4, 447–466.
Füchtbauer H. and Hardie L. A. (1976) Experimentally determined homogenous distribution coefficient for precipitated magnesian calcites: Application to marine carbonate cements. Geological Society of American Abstract with Programs 8, 877.
Gabitov R. I. (2013) Growth-rate induced disequilibrium of oxygen isotopes in aragonite: An in situ study. Chemical Geology 268-275.
Gabitov R. I., Gaetani G. A., Watson E. B., Cohen A. L. and Ehrlich H. L. (2008) Experimental determination of growth rate effect on U^{6+} and Mg^{2+} partitioning between aragonite and fluid at elevated U^{6+} concentration. Geochim. Cosmochim. Acta 72, 4058–4068.
Gabitov R. I., Sadekov A. and Leinweber A. (2014) Crystal growth rate effect on Mg/Ca and Sr/Ca partitioning between calcite and fluid: An in situ approach. Chemical Geology 367, 70–82.
Gaetani G. A. and Cohen A. L. (2006) Element partitioning during precipitation of aragonite from seawater: A framework for understanding paleoproxies. Geochimica et Cosmochimica Acta 70, 4617-4634.
Gaetani G A., Cohen A. L., Wang Z. and Crusius J. (2011) Rayleigh-based, multi-element coral thermometry: A biomineralization approach to developing climate proxies. Geochim. Cosmochim. Acta 75, 1920–1932.

Gagan M. k., Ayliffe L. K., Hoplry D., Cali J. A., Mortimer G. E., Chapell J., McCulloch M. T. and Head M. J. (1998) Temperature and surface ocean water balance of the mid-Holocene tropical western Pacific. Science 279, 1014–1018.
Garrels R.M and Christ C.L. (1965) Solutions, Minerals and Equilibria, Freeman, Cooper and Co.
Gauldie, R.W., 1993. Polymorphic crystalline structure of fish otoliths. Journal of Morphology 218, 1–28.
Given R. K. and Wilkinson B. H. (1985) Kinetic control of morphology, composition, and mineralogy of abiotic sedimentary carbonates. Journal of Sedimentary Petrology 55, 109-119.
Goldstein S. L. and Hemming S. R. (2003) Long-lived Isotopic Tracers in Oceanography, Paleoceanography, and Ice-sheet Dynamics. Treatise on Geochemistry Vol. 6, No 17, 453-489.
Gruzensky P. M (1967) Growth of calcite crystals. In Crystal Growth, Conference Proceedings of the International Conference on Crystal Growth (1966: Boston MA) (ed. H. Steffen Peiser), Supplement to Journal of Physics and Chemistry of Solids S: 365 Suppl. 1. Pergamon Press, New York.
Gussone N., Böhm F., Eisenhauer A., Dietzel M., Heuser A.,Teichert B. M. A., Reitner J.,Worheide G. and Dullo W. C.(2005) Calcium isotope fractionation in calcite and aragonite.Geochim. Cosmochim. Acta 69(18), 4485–4494.
Gussone N., Eisenhauer A., Heuser A., Dietzel M., Bock B., Böhm F., Spero H. J., Lea D. W., Bijma J. and Nägler T. F. (2003) Model for kinetic effects on calcium isotope fractionation ($\delta^{44}Ca$) in inorganic aragonite and cultured planktonic foraminifera. *Geochim. Cosmochim. Acta* 67**,** 1375–1382.
Gutjahr A., Dabringhaus H. and Lacmann R. (1996) Studies of the growth and dissolution kinetics of $CaCO_3$ polymorphs calcite and aragonite I. Growth and dissolution rates in water. Journal of Crystal Growth 158, 296-309.
Hardie L. A. (1996) Secular variation in seawater chemistry: An explanation for the coupled secular variation in the mineralogies of marine limestones and potash evaporites over the past 600 m.y. Geology, Vol. 24, No. 3, 279-283.
Hathorne Ed. C., Gagnon A., Felis T., et al. (2013) Interlaboratory study for coral Sr/Ca and other element/Ca ratio measurements. G^3 Geochemistry Geophysics Geosystems, Vol. 14, No. 9, 3730-3750.
Hemming N. G., Reeder R. J. and Hanson G. N. (1995) Mineral-fluid and isotopic fractionation of boron in synthetic calcium carbonate. Geochim. Cosmochim. Acta 59**,** 371–379.
Heuser A., Eisenhauer A., Böhm F., Wallmann K., Gussone N., Pearson P. N., Nägler T. F. and Dullo1 W.-C.(2005) Calcium isotope ($\delta^{44/40}Ca$) variations of Neogene planktonic foraminifera. Paleoceanography, Vol. 20, PA2013, 1-13.
Heuser A., Eisenhauer A., Gussone N., Bock B., Hansen B. T. and Nägler T. F. (2002) Measurement of calcium isotopes ($\delta^{44}Ca$) using a multicollector TIMS technique. Int. J. Mass Spectrom. 220, 387–399.
Holland H. D., Borcsik M., Munoz J. and Oxburgh U. M. (1963) The co-precipitation of Sr^{+2} with aragonite and of Ca^{+2} with strontianite between 90 and 100°C. Geochim. Cosmochim. Aeta 27, 957-977.
Huang y. and Fairchild I. J. (2001) Partitioning of Sr^{2+} and Mg^{2+} into calcite under karst-analogue experimental conditions. Geochim. Cosmochim. Acta Vol. 65, No. 1, 47–62
Humphrey J.D. and Howell R. P. (1999) Effect of differential stress on strontium partitioning in calcite. J. Sediment. Res. 69, 208–215.
Immenhauser A., Nägler T. F., Steuber T. and Hippler D. (2005) A critical assessment of mollusk $^{18}O/^{16}O$, Mg/Ca, and $^{44}Ca/^{40}Ca$ ratios as proxies for Cretaceous seawater temperature seasonality. Palaeogeogr. Palaeoclim. Palaeoecol. 215, 221–237.
Irving H. and Williams R. J. P. (1953) The stability of transition metal complexes. Journal of the chemical society 3192-3210.
Jacobson R.L., and Usdowski H.E. (1976) Partitioning of Sr^{2+} between calcite, dolomite, and liquids: an experimental study under high temperature diagenetic conditions, and a model for the prediction of mineral pairs for geothermometry. Contributions to Mineralogy and Petrology 59, 171–185.
Katz A., Sass E., Starinsky A. and Holland H.D. (1972) Strontium behavior in the aragonite– calcite transformation: An experimental study at 40–988C: Geochim. Cosmochim. Acta 36, 481–496.
Kazmierczak T.F., Tomson M. B. and Nancollas G.H. (1982) Crystal Growth of Calcium Carbonate. A Controlled Composition Kinetic Study.J. phys. Chem., 86(1), 103-107.

Kellya S., Heatonb K. and Jurian Hoogewerffa J. (2005). Tracing the geographical origin of food: The application of multi-element and multi-isotope analysis Trends in Food Science & Technology 16, 555–567.
Kim S-T., Gebbinck C. K., Mucci A. and Coplen T. B. (2014) Oxygen isotope systematics in the aragonite–CO_2–H_2O–NaCl system up to 0.7 mol/kg ionic strength at 25 °C. Geochimica et Cosmochimica Acta 137, 147–158.
Kinsman D. J. J. and Holland H. D. (1969) The coprecipitation of cations with $CaCO_3$- IV. The coprecipitation of Sr^{2+} with aragonite between 16 and 96 °C. Geochim. Cosmochim. Acta 33, 1–17.
Koch, P. L. (2007). Isotopic study of the biology of modern and fossil vertebrates. *Stable* isotopes in ecology and environmental science, 2, 99-154.
Koutsoukos P. G. and Kontoyannis C. G. (1984) Precipitation of Calcium Carbonate in aqueous solutions. J. Chem. Soc., Faraday Trans. 1, 80, 1181-1192.
Krabbenhöft A., Fietzke J., Eisenhauer A., Liebetrau V., Böhm F. and Vollstaedt H. (2009) Determination of radiogenic and stable strontium isotope ratios (87Sr/86Sr; d88/86Sr) by thermal ionization mass spectrometry applying an 87Sr/84Sr double spike. J. Anal. At. Spectrom. 24, 1267–1271.
Langmuir D. (1997) Aqueous Environmental Geochemistry. Prentice, Hall.
Lea D. W., Mashiotta T. A. and Spero H. J. (1999) Controls on magnesium and strontium uptake in planktonic foraminifera determined by live culturing. Geochim. Cosmochim. Acta 63, 2369–2379.
Leeder M. R. (1982) Sedimentology Process and Product. Chapman & Hall, London.
Lemarchand D., Wasserburg G. J. and Papanastassiou D. A. (2004) Rate-controlled calcium isotope fractionation in synthetic calcite. Geochim. Cosmochim. Acta 68, 4665–4678.
Lopez O., Zuddas P. and Faivre D. (2009) The influence of temperature and seawater composition on calcite crystal growth mechanisms and kinetics: Implications for Mg incorporation in calcite lattice. Geochim. Cosmochim. Acta 73, 337-347.
Lorens R. B. (1981) Sr, Cd, Mn and Co distribution coefficients in calcite as a function of calcite precipitation rate. Geochim. Cosmochim. Acta 45, 553-561.
Lowenstam H. A. and Weiner S. (1989) On Biomineralization; Oxford University Press: New York.
Malone M. J. and Baker P. A. (1999) Temperature dependence of the strontium distribution coefficient in calcite: an experimental study from 40 to 200°C and application to natural diagenetic calcites. J. Sediment. Res. 69, 216–223.
Marland, G. (1975). "The stability of $CaCO_3.6H_2O$ (ikaite)". Geochimica et Cosmochimica Acta 39: 83–91.
McCrea J. M. (1950) On the isotope chemistry of carbonates and a paleotemperature scale. J. Chem. Phys. 18, 849–857.
Michener R. and Lathja K. (eds) (2007) Stable isotopes in ecology and environmental science. 2nd ed. Blackwell, London.
Millero F. J. (1995) Thermodynamics of the carbon dioxide system in the oceans. Geochim. Cosmochim. Acta 59**,** 661–677.
Milliman J. D. (1993) Production and accumulation of calcium carbonate in the ocean: Budget of a nonsteady state. Global Biogeochemical Cycles, Vol. 7, No. 4, 715-957.
Morse, J.W. and Bender, M.L. (1990) Partition coefficients in calcite: examination of factors influencing the validity of experimental results and their application to natural systems. Chemical Geology 82, 265–277.
Morse J. W. and Mackenzie F. T. (1990) Geochemistry of Sedimentary Carbonates. Elsevier, Amsterdam.
Morse J. W., Arvidson R. S. and, and Lüttge A. (2007) Calcium Carbonate Formation and Dissolution. Chem. Rev. 107, 342-381.
Morse, J. W.; Wang, Q.; Tsio, M. Y. (1997) *Geology 25*, 85.
Mucci, A. (1987) Influence of temperature on the composition of magnesian calcite overgrowths precipitated from seawater Geochim. Cosmochim. Acta 51, 1977-1984.

Mucci A. and Morse J. W. (1983) The incorporation of Mg and Sr into calcite overgrowths: influences of growth rate and solution composition. Geochim. Cosmochim. Acta 47, 217-233.
Nägler T. F., Eisenhauer A., Müller A., Hemleben C. and Kramers J. (2000) The $\delta^{44}Ca$ temperature calibration on fossil and cultured Globigerinoides sacculifer: new tool for reconstruction of past sea surface temperatures. Geochem. Geophys. Geosyst. 1, 2000GC000091.
Nancollas G. H and Reddy M. M. (1971) The crystallization of calcium carbonate. II. Calcite growth mechanism. Journal of Colloid and Interface Science. Volume 37, Issue 4, 824–830.
Nehrke, G., Reichart, G.J., Van Cappellen, P. Meile, C. and Bijma, J. (2007) Dependence of calcite growth rate and Sr partitioning on solution stoichiometry: non-Kossel crystal growth. Geochim. Cosmochim. Acta 71, 2240–2249.
Newsome S. D., Clementz M. T. and Koch P. (2010) Using stable isotope biogeochemistry to study marine mammal ecology. Marine Mammal Science, Vol. 26, No. 3, 509-572.
Niedermayr A., Köhler S. J. and Dietzel M. (2013) Impacts of aqueous carbonate accumulation rate, magnesium and polyaspartic acid on calcium carbonate formation (6–40 °C). Chemical Geology 340, 105-120.
Nielsen L. C., DePaolo D. J. and De Yoreo J. J. (2012) Self-consistent ion-by-ion growth model for kinetic isotopic fractionation during calcite precipitation. Geochim. Cosmochim. Acta 86, 166-181.
Ortega R., Maire R., Deve`s G and Quinif Y(2005) High-resolution mapping of uranium and other trace elements in recrystallized aragonite–calcite speleothems from caves in the Pyrenees (France): Implication for U-series dating. Earth and Planetary Science Letters 237, 911 – 923.
Paquette J. and Reeder R. J. (1990) New type of compositional zoning in calcite: insights into crystal-growth mechanisms. Geology 18**,** 1244–1247.
Paquette J. and Reeder R. J. (1995) Relationship between surface structure, growth mechanism, and trace element incorporation in calcite. Geochim. Cosmochim. Acta 59**,** 735–749.
Petrou A. L. and Terzidaki A. (2014) Calcium carbonate and calcium sulfate precipitation, crystallization and dissolution: Evidence for the activated steps and the mechanisms from the enthalpy and entropy of activation values. Chemical Geology 381, 144-153.
Plummer, L.N., Busenberg, E., 1982. The solubilities of calcite, aragonite and vaterite in CO_2–H_2O solutions between 0 and 90 °C, and an evaluation of the aqueous model for the system $CaCO_3$–CO_2–H_2O. Geochimica et Cosmochimica Acta 46, 1011–1040.
Brecevic L. and Nielsen A. (1989) Solubility of amoprphous calcium carbonate. *J. Cryst. Growth 98*, 504-510.
Radha A. V., Forbes T. Z., Killian C. E., Gilbert P. U. and Navrotsky A. (2010) Transformation and crystallization energetics of synthetic and biogenic amorphous calcium carbonate. Proc Natl Acad Sci USA 107 (38):16438–16443.
Richter F. M. and Liang Y. (1993) The rate and consequence of Sr diagenesis in deep-sea carbonates. Earth Planet. Sci. Lett. 117, 553–565.
Rodriguez-Cruz S. E. Jockusch R. A. and Williams E. R. (1999) Binding Energies of Hexahydrated Alkaline Earth Metal Ions, $M^{2+}(H_2O)_6$, M = Mg, Ca, Sr, Ba: Evidence of Isomeric Structures for Magnesium, *J. Am. Chem. Soc.*, 1999, *121* (9), 1986–1987.
Rohlf, James William (1994) Modern Physics from alpha to Z^0, Wiley.
Romanek C. S., Morse J. W. and Grossman E. L. (2011) Aragonite Kinetics in Dilute Solutions. Aquat. Geochem 17, 339-356.
Rosenthal Y., Boyle E. A. and Slowey N. (1997) Temperature control on the incorporation of magnesium, strontium, fluorine, and cadmium into benthic foraminiferal shells from Little Bahama Bank: prospects for thermocline paleoceanography. Geochim. Cosmochim. Acta 61, 3633–3643.
Russell W. A., Papanastassiou D. A. and Tombrello T. A. (1978) Ca isotope fractionation on the Earth and other solar system materials. Geochim. Cosmochim. Acta 42**,** 1075–1090.
Scherer M. and Seitz H. (1980) Rare-earth element distribution in Holocene and Pleistocene corals and their distribution during diagenesis. *Chem. Geol.* 28**,** 279–289.

Schlager W. and James N. P. (1978) Low-magnesium calcite limestones forming at the deep-sea floor, Tongue of the Ocean, Bahamas. Sedimentology 25, 675-702.
Seward R. P. (1954) The Complexing of Hydrazine with Calcium Ion as Determined by Distribution Measurements. Journal of the American Chemical Society. Issue 19. Vol. 76, 4850-4852.
Sime N. G., De La Rocha C. L. and Galy A. (2005) Negligible temperature dependence of calcium isotope fractionation in 12 species of planktonic foraminifera. Earth Planet. Sci. Lett. 232, 51–66.
Smith S. V., Buddemeier R. W., Redalje R. C. and Houck J. E. (1979) Strontium-calcium thermometry in coral skeletons. Science 204, 404–407.
Stoessell R.K., Klimentidis R. E. and Prezbindowski D. R. (1987) Dedolomitization of Na– Ca–Cl brines from 100 to 200 °C at 300 bars. Geochim. Cosmochim. Acta 51, 847–856.
Stoll H. M. and Schrag D. P. (2000) Coccolith Sr/Ca as a new indicator of coccolithophorid calcification and growth rate. Geochem., Geophys., Geosystems. 1, 1–24.
Stoll H. M., Klaas C. M., Probert I., Encinar J. R. and Alonso J. I. G. (2002a) Calcification rate and temperature effects on Sr partitioning in coccoliths of multiple species of coccolithophorids in culture. Global Planet. Change 34, 153–171.
Stoll H. M., Rosenthal Y. and Falkowski P. (2002b) Climate proxies from Sr/Ca of coccolith calicte: calibrations from continuous culture of Emiliania huxleyi. Geochim. Cosmochim. Acta 66, 927–936.
Sun W., Jayaraman S., Chen W., Persson K. A. and Ceder G. (2015) Nucleation of metastable aragonite $CaCO_3$ in seawater. Applied Physical Sciences, Vol. 112, No. 11, 3199-3204.
Tang J., Köhler S. J. and Dietzel M. (2008a) Sr^{2+}/Ca^{2+} and $^{44}Ca/^{40}Ca$ fractionation during inorganic calcite formation: I. Sr incorporation. Geochim. Cosmochim. Acta 72, 3718–3732.
Tang J., Dietzel M. Böhm, F., Köhler S. J. and Eisenhauer A. (2008b) Sr^{2+}/Ca^{2+} and $^{44}Ca/^{40}Ca$ fractionation during inorganic calcite formation: II. Ca isotopes. Geochim. Cosmochim. Acta 72, 3733–3745.
Tang J., Niedermayr A., Köhler S .J., Böhm F., Kisakürek B., Eisenhauer A. and Dietzel M. (2012) Sr^{2+}/Ca^{2+} and $^{44}Ca/^{40}Ca$ fractionation during inorganic calcite formation: III. Impact of salinity/ionic strength. Geochim. Cosmochim. Acta 77, 432–443.
Teng H. H., Dove P. M. and DeYoreo J. J. (2000) Kinetics of calcite growth: surface processes and relationships to macroscopic rate laws. Geochim. Cosmochim. Acta 13, 2255–2266.
Tesoriro A. J. and Pankow J. F. (1996) Solid solution partitioning of Sr^{2+}, Ba^{2+} and Cd^{2+} to calcite. Geochimica et Cosmochimica Acta. Vol 60, No. 6, 1053-1063.
Turnbull A.G. (1973) A thermochemical study of vaterite. Geochimica et Cosmochimica Acta vol. 37, 1593-1601.
Usdowski E., Michaelis J., Böttcher M. E. and Hoefs J. (1991) Factors for the oxygen isotope equilibrium fractionation between aqueous and gaseous CO2, carbonic acid, bicarbonate, carbonate, and water (19 °C). Int. J. Res. Phys. Chem. Chem. Phys. 170, 237–249.
Usdowski H. E. (1975) Fraktionierung der Spurenelemente bei der Kristallisation. Springer-Verlag, Berlin, Heidelberg, 104 pp.
Vollstaedt, H., Eisenhauer A., Wallmann K., Böhm F., Fietzke J., Liebetrau V., Krabbenhöft A., Farkaš J., Tomašových A., Raddatz J. and Veizer J. (2014) The Phanerozoic $\delta^{88/86}Sr$ record of seawater: New constraints on past changes in oceanic carbonate fluxes. Geochim. Cosmochim. Acta, Volume 128, 249-265.
Watkins J. M., Nielsen L. C., Ryerson F. J. and DePaolo D. J. (2013) The influence of kinetics on the oxygen isotope composition of calciumcarbonate. Earth and Planetary Science Letters 375, 349-360.
Watson E .B. (2004) A conceptual model for near-surface kinetic controls on the trace element and stable isotope composition of abiogenic calcite crystals. Geochim. Cosmochim. Acta 68, 1473–1488.
Weber J. N. (1973) Incorporation of strontium into reef coral skeletal carbonate. Geochimica et Cosmochimica Acta 37 (9), 2173–2190.
Weber J. N. and Woodhead P. M. (1970) Carbon and oxygen isotope fractionation in skeletal carbonate of reef-building corals. Chem. Geol. 6, 93–117.

Weber J. N. and Woodhead P. M. (1972) Temperature dependence of oxygen-18 concentration in reef coral carbonates. J. Geophys. Res. 77, 463–473.
Weinbauer M. G. and Velimirov B. (1995) Calcium, Magnesium and strontium concentrations in the calcite sclerites of Mediterranean gorgonians (Coelenterata: Octocorallia). Estuar. Coast. Shelf Sci. 40, 87–104.
Wiechers H. N. S., Sturrock P. and Marais G. v. R. (1975) Calcium carbonate crystallization kinetics, Water Research, Volume 9, Issue 9, 835–845.
Zeebe R. E. (1999) An explanation of the effect of seawater carbonate concentration on foraminiferal oxygen isotopes. Geochim. Cosmochim. Acta 63, 2001–2007.
Zeebe R. E. (2005) Reply to the comment by P. Deines on ‘‘An explanation of the effect of seawater carbonate concentration on foraminiferal oxygen isotopes,” by R.E. Zeebe (1991). Cosmochim. Acta 69, 789–790.
Zeebe R. E. and Wolf-Gladrow D. (2003) CO_2 in seawater, kinetics, isotopes. Elsevier Oceangraphy Series, 65.
Zuddas P. and Mucci A. (1994) Kinetics of calcite precipitation from seawater: I. A classical kinetics descriptions for strong electrolyte solutions. Geochim. Cosmochim. Acta 58, 4353–4362.
Zuddas P. and Mucci A. (1998) Kinetics of calcite precipitation from seawater: II. The influence of the ionic strength. Geochim. Cosmochim. Acta 62, 757–766.